Norwegian University
of Life Sciences

Master's Thesis 2020 60 ECTS
Faculty of Chemistry, Biotechnology and Food science

Purification and Characterization of "Chitin binding protein D" from *P. aeruginosa*

Ole Golten
Master of science, Biotechnology

Purification and characterization of “Chitin binding protein D” from *P. aeruginosa*

Masters Thesis

By

Ole Golten

Protein Engineering and Proteomics Group

Faculty of Chemistry, Biotechnology and Food science

Norwegian University of Life Sciences

Ås

Acknowledgments

The research presented in this study was performed in the Protein Engineering and Proteomics group at the Faculty of Chemistry, Biotechnology and Food science, supervised by prof. Gustav Vaaje-Kolstad, Dr. Fatemeh Askarian and Dr. Magnus Øverlie Arntzen.

Firstly, I would like to thank my main supervisor prof. Gustav Vaaje-Kolstad for great feedback throughout my master period. I have greatly appreciated the guidance and our scientific discussions which has assisted this current work, but also encouraged my passion for science by allowing me to challenge myself.

Secondly, I would like to thank my co-supervisor Dr. Fatemeh Askarian for always taking the time to help and encourage me in the laboratory by guiding me and greatly expanding my laboratory knowledge. I have cherished our cooperation. In addition, I would like to thank my co-supervisor Magnus Øverlie Arntzen for helping me navigate the complexities of the proteomics discipline and guiding me in proteomics experimental design and analysis. Also, always being present for a conversation.

I would also like to thank all the members of the PEP group for the great group spirit and willingness to help. A special thanks to laboratory manager Anne Cathrine Bunæs for always being cheerfully present to help and answer questions.

Finally, I would like to thank my friends and family for supporting me through the five years at Ås concluding in this degree. A special thanks to my significant other Malin Berglund for encouraging and holding out with me during our master thesis quarantine.

Ole Golten
June 2020, Ås

Abstract

Pseudomonas aeruginosa is an opportunistic gram-negative pathogen and widespread environmental bacterium. The increasing antibiotic resistance and mounting difficulty in treating infections has warranted an increase in research performed on *P. aeruginosa.* The threat of *P. aeruginosa* as a pathogen has resulted in several healthcare organizations such as the CDC and WHO to actively monitor infections. *P. aeruginosa* was discovered as early as 1862, however, the complex regulatory network and wide range of infection mechanisms still allows *P. aeruginosa* to be investigated and novel breakthroughs are still being made. The bacterium is still surrounded by enigma and investigation of new antimicrobial reagents is of critical priority. Understanding the infection mechanisms and virulence factors of *P. aeruginosa* will aid in identifying new antimicrobial agents.

The main objective of this study was to characterise a secreted protein and theorized virulence factor named Chitin binding protein D (CbpD). CbpD is a 43 kDa protein secreted as a 39 kDa protein by *P. aeruginosa*. The biological function of CbpD is not deduced, however, CbpD is secreted together with several known virulence factors. It is therefore near standing to identify CbpD as a virulence factor, however, there is no functional evidence linking CbpD to virulence. Furthermore, the recent discovery of the LPMO enzyme class shows that CbpD contains the conserved features of AA10 LPMO class. Intriguingly, LPMOs are predominantly known for their role in biomass degradation.

The secondary objective of this study was investigating post-translational modifications on CbpD. Recent proteomic studies have investigated the bacteriological post-translational modifications of *P. aeruginosa*. Several modifications have been observed during large scale proteomic analysis. However, the relevance of these modifications remains unknown. During this study, attempts in understating the role of the modifications were made by creating mutant protein variants.

In conclusion, purification protocols were established to allow the investigation of CbpD with traditional biochemical analysis in addition to proteomics analysis of CbpD. The research in this study has investigated a chitin utilization hypothesis, protein melting temperature, substrate affinity, structure elucidation and PTM analysis. This study represents a step forward in understanding CbpD. However, the biological role of CbpD remains unclear and must be further analysed to increase our knowledge of this secreted protein and LPMOs in general.

Sammendrag

Pseudomonas aeruginosa er en opportunistisk gram-negative patogen og utbredt bakterie funnet i naturen. Den økende antibiotika resistensen og stigende vanskeligheten forbundet med å behandle infeksjoner rettferdiggjør etterspørselen for økt forskning på *P. aeruginosa.* Trusselen forbundet med *P. aeruginosa* som en patogen har resultert i at flere helseorganisasjoner som CDC og WHO aktivt observerer infeksjoner. *P. aeruginosa* var først oppdaget så tidlig som 1862, men det komplekse regulatoriske nettverket og bredden av infeksjons mekanismer tillater fortsatt ny forsking og gjennombrudd. Bakterien er fortsatt omringet av hodebry og forskning av nye antimikrobielle reagenser er av kritisk prioritet. Å forstå infeksjons mekanismen og virulens faktorene til *P. aeruginosa* vil hjelpe i å identifisere nye antimikrobielle reagenser.

Hovedmålet med denne studien var å karakterisere et sekretert protein og hypotetisk virulens faktor med navnet Chitin binding protein D (CbpD). CbpD er et 43 kDa protein sekretet som et 39 kDa protein av *P. aeruginosa.* Den biologiske funksjonen til CbpD er ikke forstått, men, CbpD er sekretert sammen med kjente virulens faktorer. Det er derfor nærstående å tenke at CbpD er en virulens faktor, men, det foreligger ikke bevis for å støtte den hypotesen. Dessuten, har CbpD nylig blitt assosiert AA10 LPMO enzym klasse. LPMOer er enzymer som i all hovedsak er kjent for sin rolle i nedbrytning av biomasse.

Sekundær målet med denne studien var å investigere post translasjonell modifikasjoner på CbpD. Nylig gjennomført proteomikk studier har identifisert bakteriologiske modifikasjoner på proteiner i *P. aeruginosa.* Relevansen for disse modifikasjonene er fremdeles ukjent. I løpet av denne studien vil den biologiske funksjonen av modifikasjoner bli undersøkt ved å lage mutanter.

For å konkludere, rense protokoller var etablert for å gjennomføre tradisjonelle biokjemiske karakteriseringer i tillegg til proteomikk analyse av CbpD. Forskningen i denne studien ser på en kitin utnyttelse hypotese, protein smeltepunkt analyse, substrat affinitet, struktur analyse og PTM analyse. Denne studien representerer et steg videre i å forstå CbpD. Den biologiske funksjonen forblir ukjent og må bli analysert videre for å øke vår forståelse av dette sekreterte proteinet og LPMOer.

Abbreviations

LPMO	Lytic Polysaccharide Monooxygenases
AA	Amino acid
ddH_2O	Double distilled water
EtOH	Ethanol
MeOH	Methanol
PMF	Peptide mass fingerprinting
PTM	Post-translational modifications
MALDI-TOF	Matrix assisted desorption ionization
LC	Liquid chromatography
MS	Mass spectrometry
IMAC	Immobilized metal affinity chromatography
HIC	Hydrophobic interaction chromatography
SEC	Size exclusion chromatography
IEX	Ion exchange
HPLC	High performance liquid chromatography
His-Tag	Histidine fusion tag
LB	Lysogeny Broth
TB	Terrific Broth
BHI	Brain Heart Infusion
DTT	Dithiotheriol
TFA	Trifluroacetic acid
IAA	Iodoacetamide
AmBic	Ammonium carbonate
MST	Microscale thermophoresis
PMSF	Phenylmethylsulphonyl fluoride
Tm	Melting point
GH	Glycoside Hydrolase
CBM	Carbohydrate binding module
CAZy	Carbohydrate active enzyme database
CFU	Colony forming units
Bp	Base pairs
Da	Dalton
Ppm	Parts per million
GlcNac	N-acetyl glucosamine
nm	Nano meter
PCR	Polymerase chain reaction
v/v	Volume per volume
w/v	Weight per volume
rpm	Revolutions per minute
g	Relative centrifugal force

Table of contents

1 Introduction

1.1 Aim

The function of the putative lytic polysaccharide monooxygenase of *Pseudomonas aeruginosa*, CbpD, is not known, despite the existence of many studies describing the biochemical properties of this protein. Due to the classification of CbpD as an LPMO, it is conceivable that the protein may be involved in chitin degradation. On the other hand, CbpD has also been linked to a role in virulence. The primary aim of this study was therefore to purify full length and truncated variants of the protein, investigate its activity towards chitin and its putative role in chitin degradation by *P. aeruginosa*. The secondary aim was to confirm the presence of post-translational modifications of CbpD and investigate their functional importance.

1.2 *Pseudomonas aeruginosa*

P. aeruginosa was first observed by the pharmacologist Carle Gessard in 1862. While investigating the blue-green puss of infected wounds, a rod-shaped bacterium was identified and initially named *Bacillus pyocyanes* based on the blue-green tint (Gessard, 1984). Later the name was altered to *P. aeruginosa* descending from the Latin word “aerugo” translating to the blue-green rust of copper (Villavicencio, 1998). Interestingly, even though *P. aeruginosa* was identified as early as 1862, few cases of infection were identified in the early 20th century (Stanley, 1947). *P. aeruginosa* is commonly referred to as an ubiquitous opportunistic bacterium, and can be found in a wide array of environments (Green et al., 1974). The bacterium is a well-known versatile pathogen which can exploit several environmental niches, e.g. distilled water and on several inanimate hospital surfaces (Favero et al., 1971), due to its ability to utilize different nutrient sources (Williams & Worsey, 1976). As a widespread environmental bacterium, studies have shown that *P. aeruginosa* can be introduced into hospitals and ingested from fresh vegetables (Correa et al., 1991; Kominos et al., 1972). However, healthy humans are seldomly infected, mainly once the host immune systems are compromised, infections are observed. This phenotype has led to the classification as an opportunistic bacterium (Botzenhart & Döring, 1993). A significant breakthrough in understanding *P. aeruginosa* as both a

widespread environmental bacterium, and an opportunistic pathogen was unlocked when Stover et al. sequenced the *P. aeruginosa* strain PAO1 genome in 2000. The genome sequence revealed evidence of several small paralogous gene families with specific functions, suggesting a broad genetic ability which can explain the environmental versatility (Stover et al., 2000). In addition, the genome encodes almost 300 cytoplasmic membrane transport systems, with almost 2/3 involved in uptake of nutrients and other macromolecules, which is consistent with the observed environmental adaptability (Stover et al., 2000).

P. aeruginosa infections are observed either as acute or chronic, the latter arises in immunocompromised hosts, while acute cases are often related to trauma victims experiencing large epithelial layer deterioration (e.g. burn victims). On the other hand, chronic infections are often pre-existing immunocompromising conditions e.g. cystic fibrosis (Botzenhart & Döring, 1993; Gellatly & Hancock, 2013; Hardalo & Edberg, 1997; Lyczak et al., 2000). Infections caused by *P. aeruginosa* have been notoriously difficult to treat, since *P. aeruginosa* has shown resistance to a wide range of antibiotics and antimicrobial agents. The main reasons of resistance in this bacterium, is a result of different factors including, I) The cell wall has a low permeability to antimicrobial agents, II) *P. aeruginosa* contains a broad arsenal of genetically encoded resistance mechanisms, III) Mutations in the chromosome have resulted in resistance genes, IV) An ability to obtain new resistance genes from the environment (e.g. through horizontal gene transfer) (Lambert, 2002). Antibiotic resistance has become a major challenge, and an increasing focus in healthcare research. The intrinsic resistance of *P. aeruginosa* to antibiotics has resulted in the recent classification as a priority pathogen for research and development, addressing the growing resistance against known antibiotics (WHO, 2017).

1.2.1 Pathogenicity

P. aeruginosa is regarded as both a widespread environmental bacterium and pathogen. We are in daily contact with *P. aeruginosa*; however, most often, *P. aeruginosa* infections are not observed in healthy individuals. Recent studies tallying the amount of healthcare associated (HCA) infections from 2015-2017 rank *P. aeruginosa* as the fourth most common HCA pathogenic infection in the United States (Weiner-Lastinger et al., 2020). Novel methods for addressing *P. aeruginosa* virulence is required. However, the infection mechanisms must be understood to establish new treatments. Complicating matters further, pathogen-host

interactions are difficult to study, since infected individuals often have a plethora of prior healthcare complications obscuring the pathogenic contribution of *P. aeruginosa*.

The immune system is tasked with protecting the host against pathogens and is comprised of both physical barriers (e.g. the epithelial layer) and immune responses. In order to establish an infection, the pathogen must circumvent the immune system. *P. aeruginosa* is regarded as a virulent pathogen, which is generally defined as the ability to infect a host organism. The ability to infect is mediated by proteins and molecules which aid in establishing infections. These proteins and molecules are regarded as virulence factors.

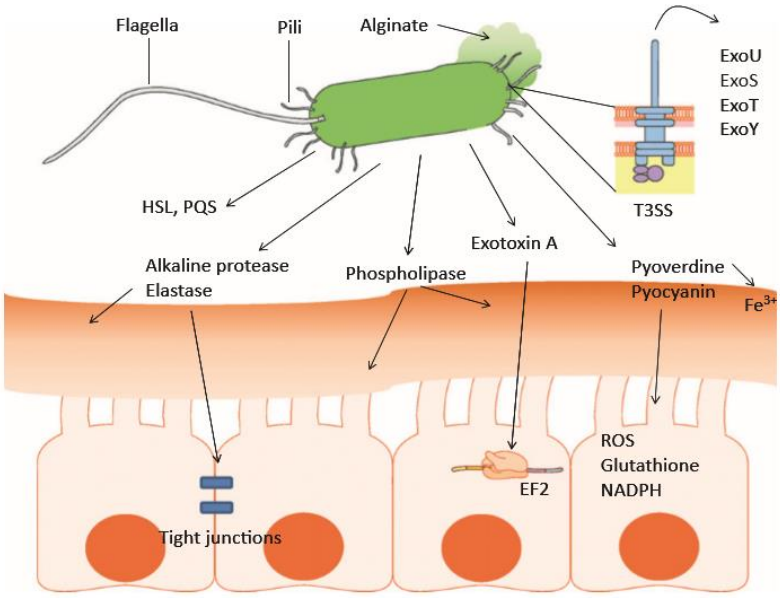

Figure 1-1. Illustration of P. aeruginosa in an infection context*. This illustration shows a summary of some virulence factors secreted by P. aeruginosa (green) and how they target different host cell locations, in this image epithelial cells (orange). The arrows indicate secreted virulence factor and show examples of virulence factor targets. Flagella and pili are used for adhesion to the epithelial cells, which in turn allows the Type 3 Secretion System (T3SS) to inject toxins into the cell. The flagella and pili adhesion also allow for alginate secretion which aids biofilm formation. Figure source: (Gellatly & Hancock, 2013)*

P. aeruginosa contains several secretion systems and mechanisms deploying virulence factors which are important during infections as seen in **Figure 1-1**. Interestingly, *P. aeruginosa* contains five out of the six commonly known secretion systems. As reviewed by (Bleves et al., 2010; Gellatly & Hancock, 2013; Hardalo & Edberg, 1997; Liu, 1974; Lyczak et al., 2000). *P. aeruginosa* is able to regulate several virulence factors through a phenomenon referred to as "quorum sensing". This regulatory network is regulated by external stress factors and cell density. Regulation is achieved by autoinducer signalling molecules produced by *P. aeruginosa*. Each bacterium produces a basal level of autoinducers. However, once the cell density increases and an autoinducer concentration threshold is reached, cell receptor binding initiates a quorum sensing response (Lee & Zhang, 2015; Pesci et al., 1997). The ability to use

quorum sensing allows *P. aeruginosa* to alter the regulatory pathways as a response to environmental cues. During an infection setting *P. aeruginosa* can respond to immune system defences by secreting virulence factors, and/or establishing biofilms (Lee & Zhang, 2015). Biofilm formation is a common trait employed by bacteria serving as a protective layer. The bacteria are suspended in a self-produced alginate, protecting the bacteria from antibiotics, antimicrobial reagents and some immune system responses (Høiby et al., 2010).

The extracellular virulence factors are secreted through the T1SS, T2SS, T3SS, T5SS and T6SS, the aim of this study restricts the scope, and only the T2SS will be described further. The T2SS secretes proteins through the outer membrane and is a conserved mechanism amongst gram-negative bacteria. However, *P. aeruginosa* is a unique case when considering the diversity of exoproteins secreted (Filloux et al., 1990). Among the secreted proteins there are several well characterized virulence factors, such as proteases, lipases and toxins. Proteases such as the elastases LasB and LasA have been shown to degrade collagen and the disruption of basement membranes, which are important physical barriers normally inhibiting bacterial infections (Bejarano et al., 1989). The T2SS also secretes phospholipase C known to target cell membrane glycolipids and secrete Exotoxin A which is linked to the lethality of *P. aeruginosa* infections. (Gellatly & Hancock, 2013; Liu, 1974; Lyczak et al., 2000) Interestingly, the T2SS is also known to secrete a protein named “Chitin binding protein D” (CbpD) (Jindra Folders, 2000). CbpD is a suggested virulence factor by many (Gaviard et al., 2019; Jindra Folders, 2000; Ouidir et al., 2014) However, not much is known about this protein.

1.3 Chitin Binding Protein D (CbpD)

Chitin binding protein D (CbpD) is a 43 kDa protein that was firstly characterized as a secreted proteolytic enzyme with staphylolytic capabilities (Burke & Pattee, 1967). Further investigation and characterization of this staphylolytic enzyme, proposed that the protein was secreted as a 30 kDa serine protease which was processed to an active 23 kDa enzyme named LasD (Park & Galloway, 1995). Further on, the 23 kDa active LasD protease was linked to virulence since it was secreted together with other known virulence related proteases such as LasA and LasB. In addition, the proposed function of the enzyme was to process the protease pro-LasA to the active LasA protease (Park & Galloway, 1998). However, LasD showed no sequence homology with other known proteases, and the closed homologs are characterised chitin binding proteins

(Jindra Folders, 2000). Further investigation of LasD showed that the protein binds colloidal chitin, protecting LasD from proteolytic enzymes. When protected from proteases, LasD was revealed as a 43 kDa protein without proteolytic or staphylolytic capabilities, resulting in changing the name from LasD to CbpD (Jindra Folders, 2000). For several years, CbpD was annotated as LasD a staphylolytic protease related to virulence, resulting in the real functionality left uncharacterized.

The function of the protein is still not clear; however, the protein is secreted through a type II secretion system together with several other known virulence factors, which are well characterized. Such as LasB, LasA and alkaline phosphatase, which raises the question if CbpD is a virulence factor for *P. aeruginosa.* CbpD is transferred across the inner membrane, mediated by a signal peptide through the sec translocon. The signal peptide is cleaved of and finally secreted as a 39 kDa protein. The T2SS secretes the proteins from the periplasm across the outer membrane, the secretion machinery is still enigmatic and how the T2SS recruits the proteins and the secretion mechanism is unknown (Michel-Souzy et al., 2018). Interestingly, the closest homolog of CbpD is the characterized virulence factor, N-acetylglucosamine binding protein A (GbpA) which mediates the colonization of *Vibrio cholerae* on different host surfaces (Kirn et al., 2005). Recent attempts on the characterization of CbpD have been performed as a part of understanding the post-translational modifications of *P. aeruginosa*. CbpD contains several modifications, and with a proteomic focus and approach, lysine modifications and S/T/Y phosphorylation's have been identified (Gaviard et al., 2019). In addition, high throughput proteomic analysis of the *P. aeruginosa* proteome has identified CbpD as phosphorylated (Ouidir et al., 2014) and acetylated (Ouidir et al., 2015). However, these studies have focused on identifying modifications and not investigating the biological functions associated with the characterized PTMs. Furthermore, the LasD/CbpD misunderstanding still lingers in the literature, and Gaviard et al. 2019 study CbpD under the impression that CbpD is a 23 kDa protein with staphylolytic capabilities. Even though this was disproven by Folders et al. 2000. Investigating CbpD in the light of PTMs with the focus on a secreted 39 kDa protein will increase the understating of this enigmatic protein. Attempting to characterize the biological functions of CbpD will prove valuable for understanding a possible role in virulence.

The function of CbpD is elusive since it is known to bind chitin, indicating a role in chitin degradation, but also is classified as a virulence factor by many. The CbpD sequence is classified as an auxiliary activity family 10 (AA10) lytic polysaccharide monooxygenase

(LPMO) by the Carbohydrate Active Enzyme database (CAZy; (Levasseur et al., 2013)). LPMOs are mostly known for their important roles in degradation of recalcitrant biomass such as chitin and cellulose, but some (as the already described CbpD and GbpA, are also related to virulence). LPMOs is a recently discovered protein family and is still an emerging field.

1.4 Lytic Polysaccharide monooxygenase (LPMO)

Degradation of crystalline carbohydrates is an important hurdle in biomass conversion, and a key challenge in industrial utilization of recalcitrant biomasses, by degrading polysaccharides to monosaccharides (Horn et al., 2012). Previously, degradation of polysaccharide carbohydrates such as chitin and cellulose has mainly focused on enzymes such as cellulases and chitinases. These enzymes cleave glyosidic bonds on the carbohydrate chain (endo-) or on the chain terminus (exo-). However, as early as 1950, the hypothesis of cellulose degradation requiring two steps dubbed the C_1-C_x system was formed. Firstly, accessing the polymeric chains in the crystalline structure (C_1), secondly, degradation of the polysaccharide chain to smaller oligomers and monomers (C_x) (Reese et al., 1950). However, this system was not revisited before 1994, when Din et al. showed that a carbohydrate binding module (CBM) could synergistically increase the substrate availability for endoglucanases, resulting in the increase of soluble monosaccharides (Din et al., 1994). Recent discoveries in 2005 by Vaaje-Kolstad et al. exhibited how the non-catalytic protein CBP21 from *Serratia marcescens* containing a CBM33 protein family, synergistically increased the degradation of β-chitin in concert with different chitinases (Vaaje-Kolstad et al., 2005a). The same year, Vaaje-Kolstad et al. solved the crystal structure of CBP21, revealing a flat surface containing several hydrophilic amino acids mediating chitin binding (Vaaje-Kolstad et al., 2005b). However, as recent as 2010, 60 years after introducing the hypothesis of the C_1-C_x system by Reese et al. Major breakthroughs by Vaaje-Kolstad et al. presented the C_1 mechanism which released the polysaccharides from the crystalline structure, in fact was enzymatic. Presenting that CBP21 is an oxidative enzyme that could cleave the glyosidic bonds in crystalline chitin. The enzymatic reaction required a divalent metal ion, an external electron donor and molecular oxygen (Vaaje-Kolstad et al., 2010). Initial confusion surrounding which divalent ion was present in the active site was solved the following year. Quinlan et al. presented that a homologous protein from *Thermococcus aurantiacus* in the GH61 family, in fact was a copper dependant enzyme. This homologous

protein could oxidize and cleave cellulose directly without the synergetic combination of cellulases (Quinlan et al., 2011). The same year, Forsberg et al. presented proteins in the homologous CBM33 family also could directly cleave crystalline cellulose (Forsberg et al., 2011).

The emergence of novel enzymes containing GH61 and CBM33 families retaining the ability to oxidatively cleave glyosidic bonds, resulted in the formation of the name, Lytic Polysaccharide MonoOxygenase (LPMO) by Horn et al and colleagues (Horn et al., 2012). In addition, these novel enzymes showed that their classification in Glycoside Hydrolases and Carbohydrate Binding Module protein families was outdated. These breakthroughs led to a reorganization in the manually curated Carbohydrate Active enZyme database (CAZy). The addition of Axillary Activity (AA) classes incorporating GH61 and CBM33 protein families in respectively, AA9 and AA10 protein families. The potential ability to mediate the access of crystalline carbohydrates is stipulated as the criteria for integration in the AA protein families (Levasseur et al., 2013). Recently, several new AA classes have been added, totalling 9 AA classes and 6 LPMO families. These classes include lignin active enzymes, even though lignin is not a carbohydrate, lignin is found together with cellulose and degradation of both is important in biomass conversion (http://www.cazy.org/Auxiliary-Activities.htmL).

LPMOs are classified in the AA 9, 10, 11, 13, and 14 families which are divided by substrate specificity, phylogenetic origin or LPMO regioselectivity. This study will be dedicated to an AA10 LMPO, previously being classified in the CBM33 protein family. AA10 LPMOs have been shown to cleave both chitin (Aachmann et al., 2012; Vaaje-Kolstad et al., 2010) and cellulose (Forsberg et al., 2011; Forsberg, Zarah et al., 2014), in addition they can be found in fungi, bacteria and virus.

1.4.1 LPMOs related to virulence

As previously noted, most studies on LPMOs are related to biomass degradation. However, several LPMOs have been coupled to their role in virulence. Since the LPMO class of enzymes is recently discovered, the scope of their biological function remains enigmatic. Virulence factors aid a pathogen in establishing an infection. GbpA of *Vibrio cholerae* is an LPMO known to bind the N-acetylglucosamaine monomer (GlcNac) present as modifications on glycoproteins found on intestinal epithelial cells. GbpA binding to the intestinal epithelial cells

mediates the colonization of *V. cholerae* which in turn causes the disease cholera (Kirn et al., 2005). Furthermore, the pathogen *Enterococcus faecalis* is able to establish bloodstream and organ infections also contains an LPMO. The *Efa*CBM33A LPMO is shown to be upregulated during growth in blood (Vebø et al., 2009). There are several LPMOs suggested as virulence factors, however, few have been experimentally tested.

1.4.2 LPMO structure

LPMOs that are classified in the CAZy database show a great sequence diversity, however, the LPMO active site motif is highly conserved throughout LMPO families. The active site contains two histidine residues referred to as the histidine brace, and are responsible for coordinating the divalent copper ion (Quinlan et al., 2011). The histidine brace is the only LPMO motif which is totally conserved throughout the LPMO families. The cooper coordination utilizes three nitrogen groups on the two histidine's to coordinate the copper atom. In addition to the conserved histidine brace, a conserved other shell containing a glutamate in all chitin and cellulose C1 oxidizing LPMO10s or glutamine found in the equivalent positions for all other LPMOs (Vaaje-Kolstad et al., 2017). The specific role of the glutamate and glutamine is still uncertain, however, the catalytic importance has been described (Vaaje-Kolstad et al., 2005a). Recently, NMR structure has purposed that the glutamate and glutamine residue coordinates oxygen species (O'Dell et al., 2017). Furthermore, buried in the hydrophobic core of the enzyme, an aromatic amino acid of either tyrosine in AA9 or phenylalanine in AA10 has been purposed to take part in the LPMO mechanism as a potential electron transfer system within the enzyme (Frandsen et al., 2016).

The LPMO structure contains a flat surface area mediating crystalline polysaccharide binding. The binding is facilitated by several hydrophilic amino acids firstly described by Vaaje-Kolstad et al in 2005 when solving the structure of CBP21 (Vaaje-Kolstad et al., 2005b). These findings varied from other known chitin active enzymes, since the substrate binding surface was flat, and not the typical cleft or groove.

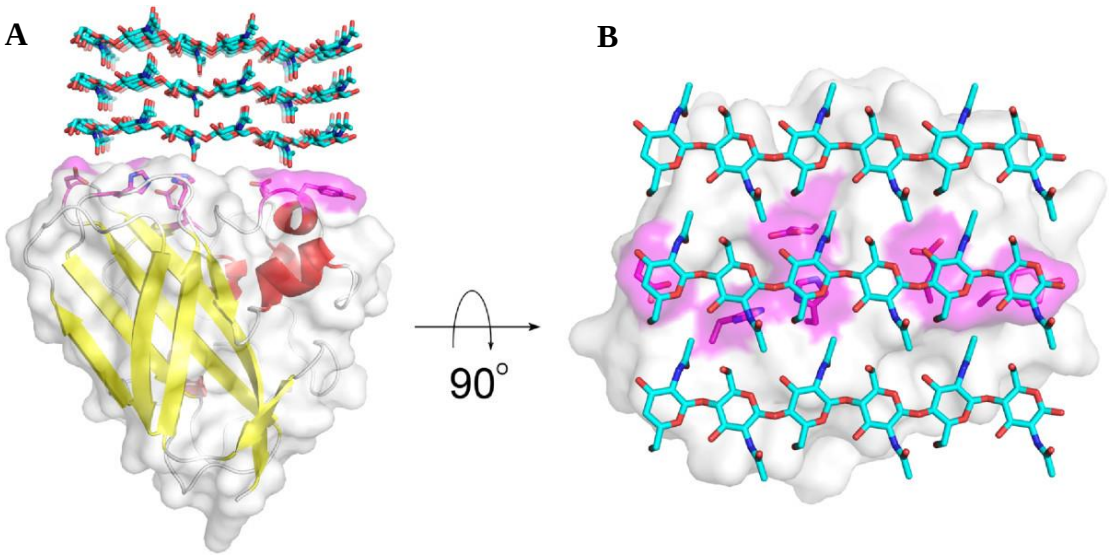

Figure 1-2: Artistic illustration showing how CBP21 from S. marcescens might bind to the crystalline chitin structure. *Panel A shows how the flat structure of the enzyme allows binding on the substrate surface, in addition the hydrophilic amino acids (shown in pink) which influence the binding ability of CBP21 to chitin. In panel B the hydrophilic surface amino acids are shown from above. The histidine brace and aromatic tyrosine is visualized as cartoon sticks. The figure is retrieved from (Vaaje-Kolstad et al., 2010).*

The crystal structure of CBP21 shown in **Figure 1-2** also purposed a structural motif comprised of a fibronectin type III like domain comprised of a β-sandwich containing a three and four stranded β-sheet (Vaaje-Kolstad et al., 2005b). Later crystal structures and computational data show that the LPMO domains contain either seven or eight β-strands and the major structural diversity is located in the loop between β-strand one and three on the core β-sandwich named loop 2 (L2)(Wu et al., 2013). The structural diversity within the L2 section has been linked to substrate regioselectivity (Forsberg, Z. et al., 2014).

1.4.3 LPMO mechanism

The initial LPMO mechanism was first described in 2010 by Vaaje-Kolstad et al. when presenting incorporation of $^{18}O_2$ on the oxidized site in the form of an aldonic acid during C1 oxidation (Vaaje-Kolstad et al., 2010). After the pivotal discovery of the C1 mechanism, additional oxidization sites were debated, leading to the discovery of a C4 LPMO reaction of soluble cello-oligosaccharides by Isaksen et al. in 2014 (Isaksen et al., 2014). The reaction mechanism using oxygen as a co substrate led to the classification of the enzyme as a monooxygenase, however recent discoveries have shown that hydrogen peroxide (H_2O_2) also can be used as a co substrate (Bissaro et al., 2017).

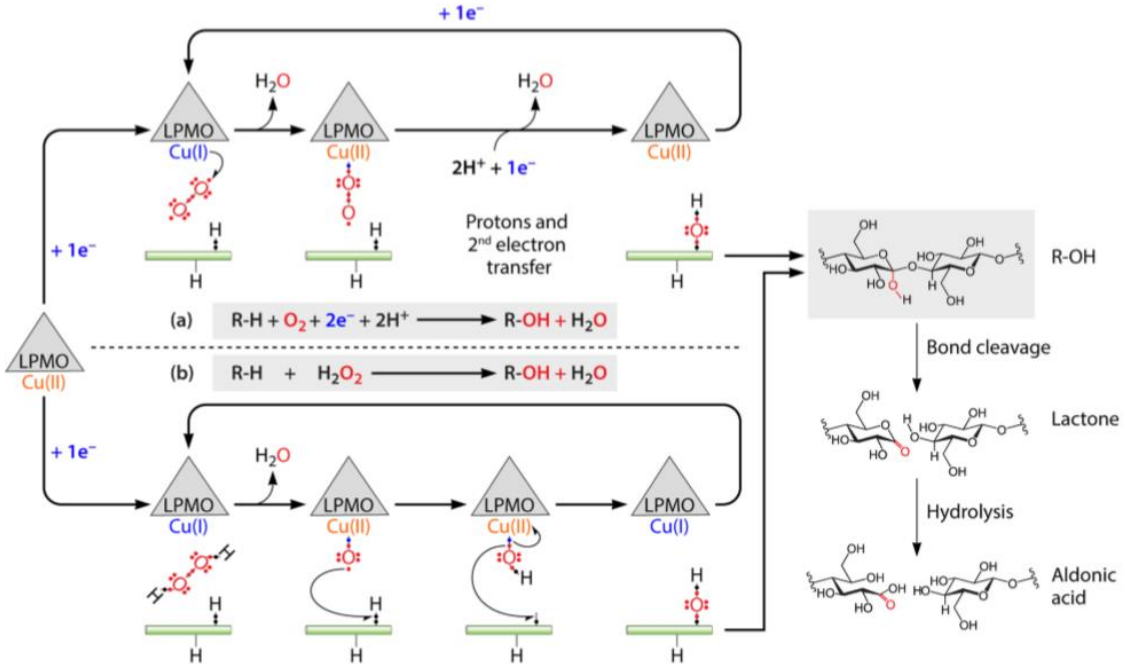

Figure 1-3: Schematic illustration of the LPMO mechanism utilizing both O_2 and H_2O_2 as co-substrates. *The LPMO enzyme is illustrated as the grey triangles with the redox state annotated below the enzyme. The crystalline polymeric structure is illustrated as the green bar with the exposed C1 hydrogen atom. The illustration shows a C1 oxidation with both oxygen (A) and hydrogen peroxide (B) as co-substrate. Electrons are illustrated as $1e^-$ in blue, whilst protons are illustrated as H^+ .The figure is retrieved from (Bissaro et al., 2018).*

Enigma still surrounds the LPMO mechanism, studies suggest that the co-substrate is either oxygen or hydrogen peroxide. However, which of the co-substrate is physiologically relevant remains unclear (Eijsink et al., 2019; Hangasky et al., 2018). The LPMO mechanism with oxygen as co-substrate requires an initial priming reaction followed by utilizing a second electron and proton transfer (**Figure 1-3**; panel A). After the reaction cycle is completed the LPMO requires a new priming reaction. The source of the additional electrons is still unclear. However, it is theorized that the enzyme can contribute the electrons through a potential redox pathway mediated by the tyrosine or phenylalanine residues in the active site (Frandsen et al., 2016). When the LPMO reaction is performed with hydrogen peroxide as the co-substrate, the initial priming still occurs. However, the second transfer of electron and proton are not necessary (**Figure 1-3**; panel B). In addition, after the reaction cycle is completed, the LPMO remains reduced and does not require a new priming reaction (Bissaro et al., 2017).

1.5 Chitin and enzymatic chitin degradation

Chitin is one of the world's most abundant biomasses, comprised of β-1,4-linked N-acetylglucosamine monomers to create a physically and chemically robust biopolymer (**Figure 1-4**), N-acetyl glucosamine monomers are rotated 180 degrees allowing the β-1-4 linkage (Muzzarelli et al., 1986). Chitin is observed in crystalline structures as α, β or γ – chitin. α-chitin crystalline structure is composed of anti-parallel chains creating strong intermolecular hydrogen bonding and α-chitin is therefore the most stable chitin allomorph. β-chitin is composed of parallel chains, with fewer intramolecular hydrogen bonds compared to α-chitin and is therefore not as stable and prone to swelling. The last, γ-chitin is as mix of both anti-parallel and parallel chains (Kurita, 2001).

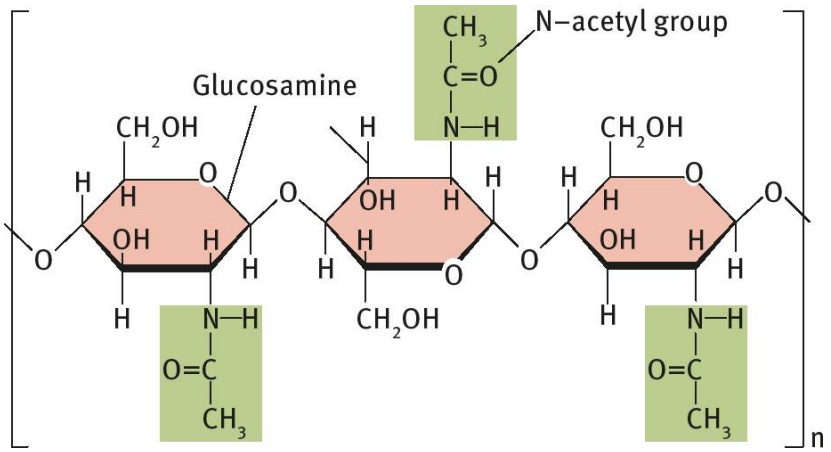

Figure 1-4: Illustration of the chitin chain comprised of N-acetylglucosamine monomers. *This image shows the repeat unit of the chitin polymer. The chitin backbone illustrates with the peach coloured glucosamine monomers. Each monomer is rotated 180° to facilitate the β-1,4 linkage. The N-acetyl group is illustrated in the green rectangles. Figure source: (Nathalie, 2016).*

Chitin occurs in nature as crystalline formations creating strength and structural components for arthropods and in the cell walls of fungi and yeast (Rinaudo, 2006). The crystalline structure creates mechanical strength, which results in difficulties degrading chitin. However, nature does not accumulate chitin as microorganisms have evolved efficient enzymatic systems to degrade the polysaccharide. These enzymatic systems include enzymes such as chitinases, LPMOs and β-N-hexosaminidases. Effective chitin degrading organisms often contain several chitinases which work in concert together with LPMOs and β-N-hex amidases. *Serratia marcescens* is a highly efficient chitin degrading organism which contains three chitinases and an LPMO. A series of experiments showed that the presence of chitinases and a LPMO was important for full utilization of the chitin substrate (Vaaje-Kolstad et al., 2005a). In addition, chitin degradation of soluble chitooligomers is aided by β-N-hexoamidases.

1.5.1 Chitin degradation by *P. aeruginosa*

The chitin degradation performed by *P. aeruginosa* remains enigmatic. During the initial characterization of CbpD, binding affinity towards chitin was observed and colonies cultivated on chitin supplemented agar plates showed degradation of chitin (Jindra Folders, 2000). However, during the aforementioned cultivation experiment *P. aeruginosa* cells with CbpD deleted also presented degradation of chitin, leading to the observation of a chitinase named ChiC (Folders et al., 2001). *P. aeruginosa* contains both a chitin binding LPMO and a chitinase, however, the biological role of these chitin active enzymes remains unknown. Several have shown that *P. aeruginosa* is not able to utilize chitin as the sole carbon source (Jagmann et al., 2010; Jindra Folders, 2000) However, *P. aeruginosa* has been reported to grow on the chitin monomer GlcNac. In addition, *P. aeruginosa* was shown to grow parasitically in co-cultures with the chitin degrading bacteria *Aeromonas hydrophilia* (Jagmann et al., 2010). Additionally, CbpD and ChiC are both regulated by quorum sensing pathways (Folders et al., 2001; Hentzer et al., 2003) increasing the enigma surrounding the biological function of CbpD and a purposed role in chitin degradation.

1.6 Post-translational modifications (PTMs)

An intriguing feature of CbpD is the prevalence of several post-translational modifications (Gaviard et al., 2019; Ouidir et al., 2014; Ouidir et al., 2015). Post-translation modifications are protein modifications that occur either during or after protein synthesis. These modifications include addition or removal of covalently bound groups and cleavages in the peptide chain such as removing signal peptides. PTMs in eukaryotic cells are well characterized and have established roles in both gene regulation and signalling cascades. For example, histone modifications create a combinatorial modification code of methylation, acetylation and ubiquitylation which regulates the transcription of DNA in the nucleus (Allfrey et al., 1964; Turner, 2000). In addition, eukaryotic protein phosphorylation show functions such as regulating loss/gain of function in cell signalling and protein-protein interactions (Cohen, 2002; Graves & Krebs, 1999).

Recently, the field of prokaryotic protein modifications has been emerging and proving important for regulating biological functions. The understanding that one gene may result in several gene products (i.e. post-translational modifications) with different biological functions

has led to coining the term "protein species" (Jeffery, 2016). Modifications on *P. aeruginosa* have been attempted linked to pathogenicity, and phospho-peptides of known virulence factors have been observed (Ravichandran et al., 2009). However, biological functions of virulence mediated PTMs is still unclear. Further characterization of the phospho-proteome of *P. aeruginosa*, reveals several S/T/Y phosphorylation's are prevalent and detected in a variety of cell functions (Ouidir et al., 2014). In addition, the acetylome of *P. aeruginosa* further presents the occurrence of acetylation in several cell functions (Ouidir et al., 2015). A recent review summarizing PTMs in *P. aeruginosa* presents a wide variety of different PTMs distributed across several cellular functions. Among these cellular functions, some virulence factors are shown to be multi-modified containing different modifications (Gaviard et al., 2018). However, proteomic articles often present large datasets containing observed modifications but do not investigate their biological relevance. In-depth proteomic analysis of CbpD has been performed with the focus of identifying PTMs presented in (**Figure 1-5**). However, the biological function is still uncharacterized (Gaviard et al., 2019).

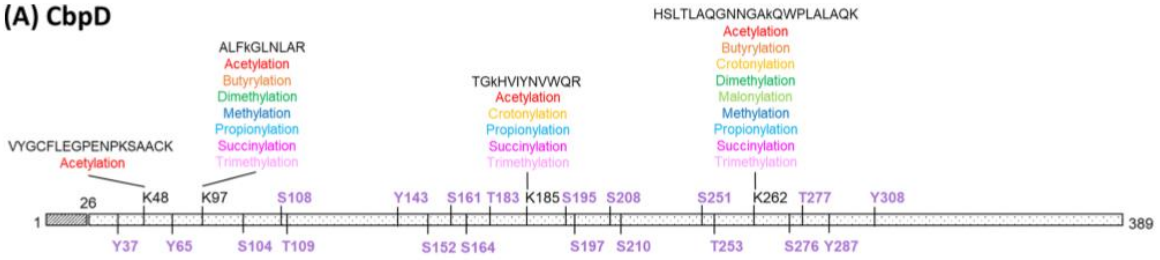

Figure 1-5: Observed PTMs on the CbpD amino acid sequence. *This figure shows the PTMs observed on CbpD, the residues in purple are S/T/Y phosphorylations while the modified lysine (K) residues are shown in black. The PTMs are stated above the lysine residue with the peptide sequence stated in black. The amino acid sequence is presented from 1-389 and the signal peptide is illustrated in grey (residue 1-26). Figure source:(Gaviard et al., 2019).*

Further understanding the biological role of PTMs on CbpD will be attempted during this study, using high accuracy mass spectrometry-based proteomics.

1.7 Proteomics

Mass spectrometry-based proteomics is an indispensable tool, allowing researchers to investigate cell protein expression in the regards of protein sequence, post-translational modifications and protein-protein interactions. Full genome sequencing has allowed advancement in the proteomic analysis by facilitating database searches. The basics in mass

spectrometry include an ionizing source creating ionized analytes, a mass analyser detecting mass-to-charge ratio (m/z) and a detector quantifying the number of ions. There is a wide range of different methods and equipment in this expanding field as briefly introduced in **Figure 1-6**. However, this study utilized Matrix Assisted Laser Desorption/Ionization – Time Of Flight (MALDI-TOF) and ElectroSpray Ionization (ESI) instrumentation and the accompanying software.

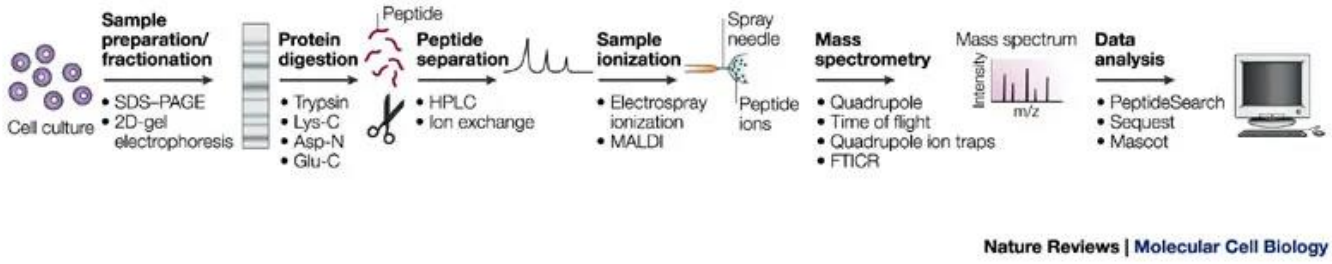

Figure 1-6: Schematic illustration of ESI and MALDI-TOF mass spectrometry workflows. *This image shows examples of workflows utilized in mass spectrometry. The choice of workflow is dependent on the individual research question. The main steps in the workflow are highlighted in bold, whilst some options are listed in bullet points beneath the arrows. Figure source: (Steen & Mann, 2004).*

The proteomics approach is dependent on the research question and the biological system being investigated. Bottom up proteomics is based on the digestion of proteins to peptides and subsequently identifying the proteins by the peptides present. Sequence specific proteases allows the digestion of full-length protein to peptides, enabling bottom up proteomics. However, the peptide length varies based on amino acid sequence and protease choice, which may cause loss of data. Protein digestion can be carried out by several proteases with a variable degree of selectivity. An industry standard is the selective serine protease, trypsin, which is a stable protease with a high degree of selectively, cleaving after lysine or arginine residues (Olsen et al., 2004). This selectivity often creates peptides of suitable length of MS analysis; therefore, trypsin is often the first attempted protease. Individual augmentation depending on protein sequence is often needed, and several other selective proteases are available. Less selective proteases create short overlapping peptides which increase the complexity in peptide sample mixtures resulting in intricate data analysis. In addition, short peptides often don't contain basic residues and will therefore not ionize and evade detection by MS. Therefore, less selective proteases are often disregarded.

Decreasing the complexity of protein samples is performed by separation of the peptides present. Depending on the peptide composition and separation requirements, different methods are available. Utilization of a correct gradient for the peptide sample is crucial to receive a high analytical resolution. Elution of the peptides forces the solutes through a needle held at a large electrical potential compared to the MS intake, resulting in vaporization of the solvent and ionization of the peptide. The peptide ions freed from solvent and charged are manipulated by an electric field transferring the peptides into the system. The ionized peptides are manipulated by the electric currents in the MS which is held a constant vacuum. LC-MS systems utilize several different methods for analysing peptides (Steen & Mann, 2004). During this study, proteomic analysis was performed using the an orbitrap MS introduced later in the theory section.

1.8 Wet lab theory

1.8.1 Immobilized Metal Affinity Chromatography (IMAC)

IMAC purification is based on metal ions suspended in the stationary phase interacting with the molecules of interest. Elution of the analyte is performed by changing the buffer conditions to weaken the affinity towards the ligand. IMAC columns are constructed using a polymeric matrix creating a support system for the metal ions, a chelating agent that coordinates the metal ion to the matrix and the metal ion its self (Porath, 1992).

IMAC purification is performed with recombinant proteins containing a fusion tag that provides affinity towards the IMAC column material. There are several different tags used for purification of crude protein samples, in this study poly histidine tags were used during purification of recombinant protein samples. Metal ions can form bonds with the imidazole groups of histidine amino acids (Porath et al., 1975). Poly histidine tags can have a variety of lengths between 2-10 histidine amino acids on the C or N-terminal side of the protein (Ford et al., 1991).

Elution is performed by changing the buffer conditions by either adjusting pH or the buffer content for competitive elution. The histidine amino acid contains an imidazole group which is a general base when unprotonated and a general acid when protonated. The imidazole group has a pKa of 6, when operating at pH above 6 the imidazole group is negatively charged and binds to the metal cation in the IMAC column. Lowering the pH will create a weaker affinity and protonating the imidazole group resulting in elution. Competitive elution uses the competition between pure imidazole against the histidine tag. Pure imidazole has a greater affinity towards the metal ion resulting in the elution of the protein.

1.8.2 Hydrophobic Interaction Chromatography (HIC)

Hydrophobic interaction chromatography separates proteins based on the hydrophobicity of the surface proteins. A polymeric matrix consisting of beads coated with a hydrophobic compound created a grid structure allowing the sample to flow through the column. Selection of the column depends on the protein properties often by using HIC column selection kits. The role of water is important in the reversible binding of protein to the column. Water as a polar substance is not able to interact with the hydrophobic compounds on the beads, creating a highly ordered shell of water molecules known as surface tension around the hydrophobic compound. Hydrophobic residues are drawn to the hydrophobic compounds because it is thermodynamically favourable with less ordered water molecules by increasing the entropy (Shepard & Tiselius, 1949).

Salts are added to promote hydrophobic interactions, salt choice depends on which hydrophobic species are present. The reversible interactions allow protein separation by lowering the salt concentration in the buffer, resulting in lower affinity to the column and elution of the protein (Melander et al., 1984). Different distribution of hydrophobic surface amino acids results in fractionation during purification. Purification is performed with four general steps, column equilibration, sample application and washing, elution and regeneration. Column equilibration is executed using a starting buffer containing a high concentration of salt. To ensure protein interactions with the column “salting on” is performed by adjusting the sample to the same salt concentration as the start buffer. Elution is performed using a gradient and lowering the concentration of salt. However, in some cases the addition of hydrophobic molecules is required

to elute excessively hydrophobic proteins. The added hydrophobic molecules will bind competitively, resulting in the elution of protein from the column material.

1.8.3 Ion Exchange Chromatography (IEX)

Ion Exchange separates proteins based on the net surface charge, which is influenced by several factors, such as pH, the amount of charged amino acids and the distribution of charges. These factors are unique to the protein, and selection based on ionic interactions can result in either pure protein fractions or reduce the contaminations. The columns are comprised of a polymeric matrix of beads bound to either a cation or anion depending of the selectivity for the protein of interest. There are several IEX columns available, and choosing the column suited for the research purpose is important in obtaining the desired selection. The protein pI is important during IEX purification, using tools such as the Protparam tool on ExPASy (https://web.expasy.org/protparam/) the theoretical pI can be deduced. The pH of the buffer system will alter the affinity of the protein to the column, if the pH is above the pI, the protein will bind to cation columns while if the pH is below the pI the protein will bind to anion columns. However, the theoretical pI is only based on the amino acid sequence depending on the amount of charged residues, the residue location will also affect the affinity and must be taken into account while optimizing.

The general steps in IEX purification start with column equilibration using a buffer of low ionic strength before applying the sample. Proteins containing a charge will bind to the column. Washing with the same low ionic strength buffer removes non-specific protein binding. Finally, elution is performed by increasing the ionic strength of the buffer (e.g. salts), resulting in displacement of the proteins bound to the column. The retention time will depend on the physiochemical properties of the protein (Kopaciewicz et al., 1983).

1.8.4 Size Exclusion Chromatography (SEC)

Size exclusion chromatography, also referred to as gel filtration, utilizes a resin of inert porous beads that should not interact with the injected samples. The pore size of the resin may vary for

the experimental setup; however, the general principles apply for all SEC columns. Purification is isocratic, allowing the same buffer for equilibration to be used for elution. During sample application, lower molecular weight molecules can enter the porous beads, while larger molecules flow around the beads. Separation of the molecules is dependent on their size, larger molecules will travel shorter distances and elute faster, while smaller molecules can enter the porous cavities and increase the travel time. A UV monitor allows detection of eluted products in a chromatogram where protein fractions are collected. Since the same buffer for equilibrium and elution is used, SEC purification is ideal for sensitive proteins by ensuring a stable buffer system (Kuga, 1981). Furthermore, since the elution is based on size alone, buffer components from the initial protein sample will elute at the end of the elution, resulting in buffer exchange.

1.8.5 Robotized gas sampling robot

The cell viability of *P. aeruginosa* was determined using traditional methods such as OD_{600} and CFU. However, in certain testing conditions these were not applicable. Therefore, the use of a robotized gas sampling robot to monitor the carbon dioxide and oxygen concentration was performed. The growth of *P. aeruginosa* could be determined by the metabolism, allowing the use of media not suitable in OD_{600} and CFU methods. The Nitrogen group at NMBU have themselves created a system which they have called the robotized incubation system for monitoring gases illustrated in (**Figure 1-7**).

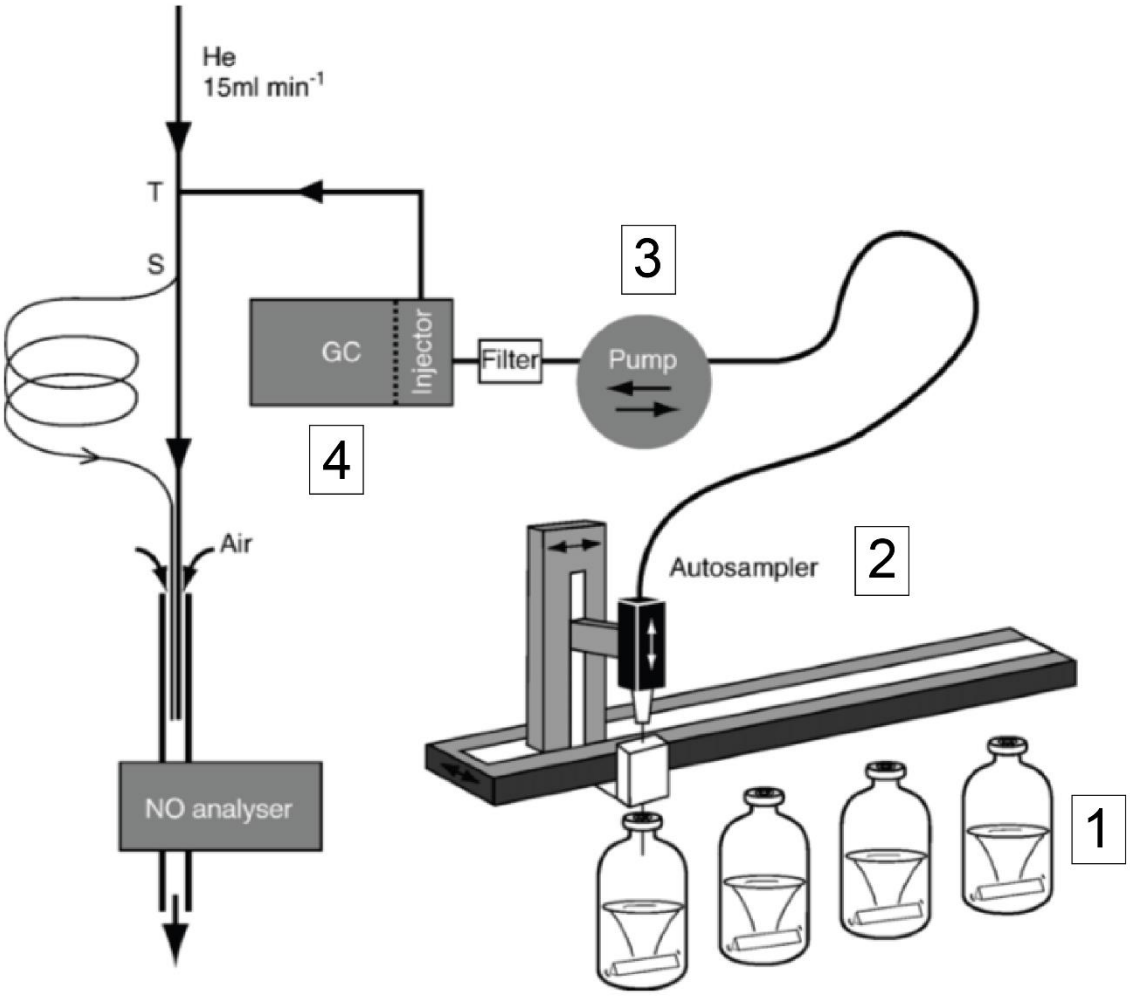

Figure 1-7 Illustration of the robotized incubation system for monitoring gases. *This image shows the schematic of the gas measuring system. The serum flasks (1) contain the bacterial culture and is sealed and crimped with butyl septa. Gas samples are retrieved with an autosampler (2) which pierces the septum. The pump (3) retrieves the sample before changing direction and returning the same amount of He to ensure the headspace volume is constant. The gas sample is the analysed using gas chromatography (4). NO was not analysed during these experiments and not present on our setup.*

The system is not available commercially and is made by the Nitrogen group. In addition, the software used to analyse the data is created and maintained by the Nitrogen group using python scripts. Flasks, cultures and magnets are all prepared under sterile conditions and the use of a water bath and magnet stirrer allows incubation with agitation (**Figure 1-7**; 1). The autosampler is controlled by a python script, which dictates sampling routines. In addition, the script ensures that the needle never pierces the same position twice, lowering the risk for gas leakage (**Figure 1-7**; 2). Furthermore, all connections have been rigorously tested for gas leakage and is accounted for during sample analysis, controls are also present during analysis to verify if leakages occur. A peristaltic pump allows the retrieval of gas samples; however, the bi-directional pump also returns the same volume of helium to ensure the volume of gas

(headspace) remains constant. The retrieved sample is measured with gas chromatography allowing the quantification of CO_2, O_2 and CH_4. If NO is of interest, the gas sample continues through a NO analyser. Quantification of gasses is performed by adding gas standards of known concentrations for CO_2, O_2 and CH_4. The system and rigorous quality testing are explained in the publication which first introduced the system (Molstad et al., 2007).

1.8.6 High Performance Liquid Chromatography (HPLC)

High Performance Liquid Chromatography (HPLC) separates mixed analytes by utilizing a mobile phase moving analytes through the chromatographic system which are retained by a stationary. The mobile phase is comprised of a buffer system which depends on which analysis is performed. Separation is achieved by the interactions between the analytes and column material in the stationary phase. The separation resolution can be optimized by employing elution gradients by increasing the elution buffer in the buffer system. However, depending on which analytes are analysed and the necessity for separation, the choice of column, gradient and buffer system is tailored for each experiment. Quantification of products is performed with a detector, often UV-based if analyte absorbs light at UV- wavelengths, enabling the quantification of the separated analytes.

1.8.6.1 Hydrophilic Interaction Chromatography (HILIC)

HILIC is a general HPLC method for distinguishing polar analytes based on their hydrophobicity. HILIC is performed by utilizing a hydrophilic strong cation exchange (SCX) stationary phase and hydrophobic organic mobile phase (Alpert, 1990). During HILIC analysis the mobile phase is comprised of an acetonitrile layer and a water layer, the latter is adsorbed to the stationary phase. During analysis the injected analytes will distribute throughout the acetonitrile and water gradient according to the polarity of the analyte. Increasing the percentage of acetonitrile will decrease the stationary water layer retaining the polar analytes, resulting in elution (Alpert, 1990; Buszewski & Noga, 2012). In addition to the acetonitrile and

water partitioning, hydrogen bonding will also affect the retention to the stationary phase (Berthod et al., 1998).

1.8.6.2 Reverse Phase Chromatography (RPC)

Reverse phase chromatography is a general chromatographic method utilized in several chromatographic systems, among them HPLC. The method is based on the use of a hydrophobic stationary phase. Depending on the column choice, the hydrophobic stationary phase is often comprised of carbon alkyl groups. During RPC analysis, the hydrophobic analytes in the mobile phase adhere to the stationary phase. Thereafter, elution is performed by decreasing the polarity in the mobile phase, resulting in elution of the molecules from least to most hydrophobic. RPC was used during this study to separate peptides during LC-MS analysis (Neue, 2007).

1.8.7 Mass Spectrometry

1.8.7.1 Electrospray ionization mass spectrometry (ESI-MS)

The Q-Exactive (Thermo Scientific) system contains a quadrupole mass selector coupled with an orbitrap mass detector generating high resolution spectra.

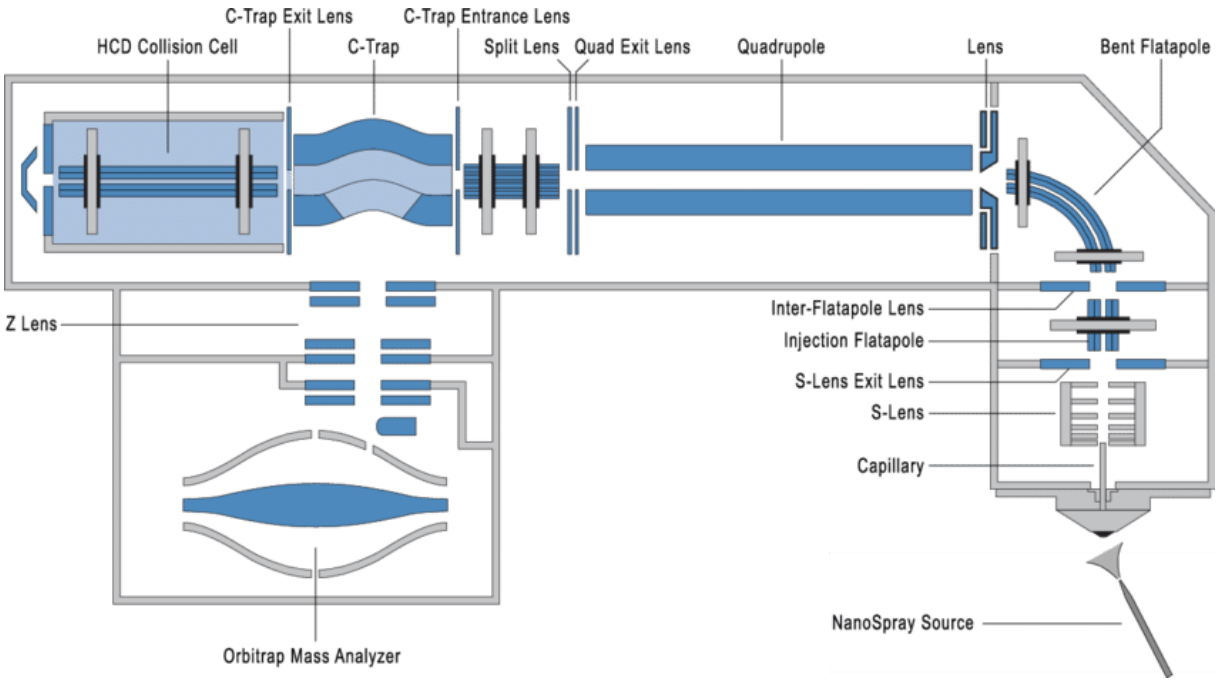

Figure 1-8: Schematic illustration of the Thermo Scientific Q-Exactive mass spectrometer. *This image shows an illustration of the Q-Exactive MS. The nano spay source is the HPLC eluent needle. All the components are named with corresponding to arrows. Figure source:(Michalski et al., 2011)*

The schematic in **Figure 1-8** show the internal compartments of the Q-Exactive which is an Electrospray ionization (ESI) system. The ions are transferred into the system by forcing the HPLC eluent through a needle held at a high electric potential. This potential will create electrostatically dispersed droplets. Once dispersed, the solvents in the droplets vaporises, creating ionized and charged ions which can enter the MS (Steen & Mann, 2004). The dispersed ions are centred by electronic lenses before entering the quadrupole mass selector. During full scan mode, the quadrupole does not select ions and they travel into the ion trap called C-trap (**Figure 1-8**; C-trap) which rapidly reduces the velocity and collects the ions in packets, before analysing the mass using the orbitrap. In tandem MS mode also referred to as MS/MS, the quadrupole selects the masses of interest which travel into the HCD collision cell performing collision induced fragmentation (CID) of the ions (**Figure 1-8**; HCD collision cell). Fragmentation is induced by collisions between peptides and an inert gas (e.g. nitrogen) causing breakage of the peptides along the amide bond. The breakage creates new ions which are referred to as (b-ion) if the charge is retained on the amino terminal, or (y-ion) if the charge is retained on the carboxyl terminal of the peptide. These fragments are transferred back to the C-trap which packets the fragments before analysing the mass using the orbitrap detector. The mass analyser for both full scan MS and tandem MS is the orbitrap detector. The ions are

manipulated by electronic fields to harmonically oscillate around a central coil in the orbitrap detector. The oscillation frequency, after Fourier transformation, corresponds to mass-over-charge allowing the determination of mass at high resolution (Makarov, 2000).

The spectra which are generated by the MS show mass-over-charge (m/z). As the amino acid sequence may dictate the charge state of the peptides, the determination of charge states is performed by analysing the isotope profile of the peptides. Since 1% of carbon on Earth is ^{13}C a peptide is likely to have one or several ^{13}C incorporated in its structure. Hence, the isotope pattern will show several peaks reflecting peptides containing only ^{12}Cs, and peptides containing one or more ^{13}Cs; the distance between the peaks will reveal the charge state. The mass difference is approximately 1 Da, resulting in the m/z being (1/1, 1/2 or 1/3) for charges 1-3. Depending on charge state, this will conceptualize as 1, 0.5 or 0.33 Da in mass difference in the isotope profile. After MS analysis, the data is extracted as a mass list of the full scan and fragments (Aebersold & Mann, 2003).

1.8.7.2 MALDI-TOF MS

MALDI-TOF mass spectrometry utilizes a laser to ionize macromolecules embedded in a dry substrate matrix (Karas & Hillenkamp, 1988; Tanaka et al., 1988). The matrix substrate, containing an organic solvent, is mixed with the analyte and dried to a microcrystalline matrix suspending the analytes (Vorm et al., 1994). The choice of matrix substrate is dependent on which macromolecules are analysed. Ionization of the analytes is achieved by a powerful nitrogen laser irradiating the analytes in a vacuum chamber and accelerating the ions through an electric field to the same kinetic energy (**Figure 1-9**). Since the ions are traveling in a vacuum for a set distance, the travel time will be proportional to the mass-over-charge (Steen & Mann, 2004).

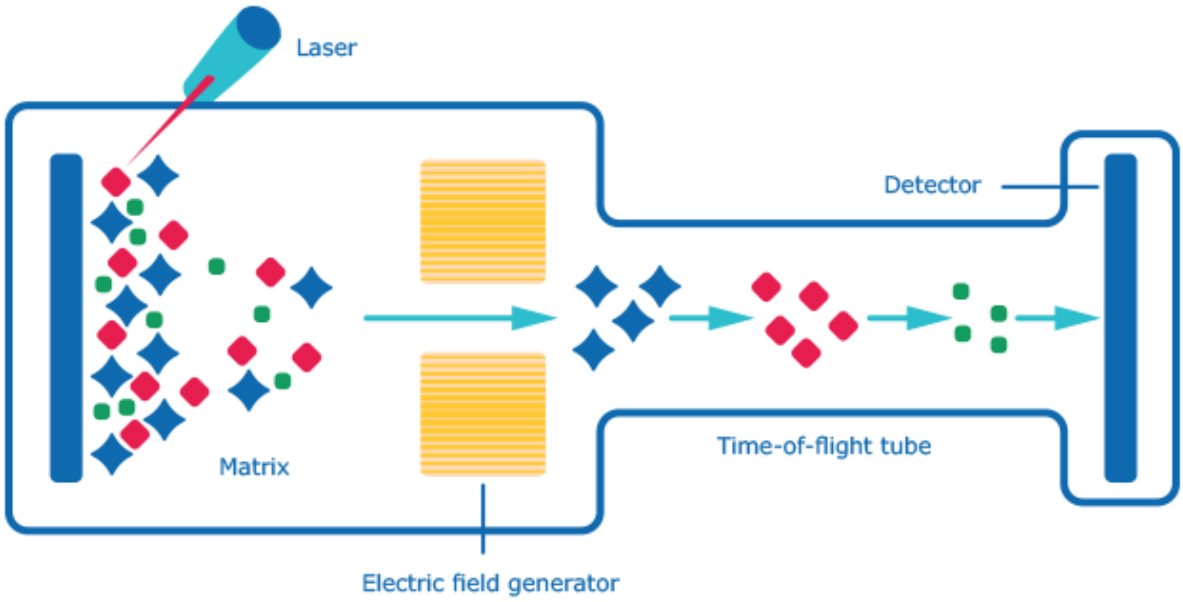

Figure 1-9: Schematic illustration of the general MALDI-TOF MS components. *This illustration shows the basic system components in the MALDI-TOF-MS. The analytes are suspended in a matrix on the target plate which are ionized by a laser allowing the charged ions to travel through an electric field which accelerates the ions to the same kinetic energy. The ions are allowed to "fly freely" through the Time-Of-Flight (TOF) tube and are separated based on mass in a vacuum before being detected. Since the ions are travelling in a vacuum, the mass can be determined by the time the ions use to travel in the free drift tube. Figure source: https://www.sigmaaldrich.com/technical-documents/articles/biology/custom-dna-oligos-qc-analysis-by-mass-spectrometry.html*

The ions travel through a free drift tube in vacuum before being registered on the detector, since the ions are accelerated to the same kinetic energy the smaller ions will travel faster than larger ions, this separation will translate into m/z data. After MALDI-TOF analysis, the results are extracted as mass lists.

1.8.7.3 PTM profiling

The data output from both MALDI-TOF and ESI LC-MS are in the form of mass lists, each mass can be linked to a peptide or a fragment of a peptide. Using different algorithms and database searches the peptides can be identified to the protein of origin. In general terms, there are three main categories for identifying proteins. I) Peptide-mass finger printing (PMF) is often applied to MALDI-TOF spectra. Tryptic digestion of a given protein will lead to a set of peptide masses that are almost unique to that given protein, MALDI spectra typically contain all ionizable peptides from a single protein and a set of observed peptide masses can therefore be used to identify the protein; hence, the name fingerprint. MALDI-TOF analysis of peptides is often performed on simpler protein samples requiring less data analysis. Therefore, peptide

fingerprinting is commonly used by comparing theoretically digested peptides with the mass spectrum obtained (Pappin et al., 1993). II) Probability based proteomics approach using theoretical fragment spectra generated from the amino sequence of peptides in the database and comparing them to the observed peaks. A statistical method creates a score which represents the significance of the match (Perkins et al., 1999). III) *De-novo* sequencing of proteins, i.e. deducing the sequence directly from spectra. The two abovementioned methods are both based on the use of databases, which limit the proteomics discipline to sequenced genomes. *De-novo* sequencing has proven to be difficult since tandem MS sequence information often is incomplete and contains intervening peaks. Lack of data creates issues when attempting to safely identify the entire amino acid sequence. However, several of the above mentioned search methods are used together in data analysis such as i.e. MaxQuant (Cox & Mann, 2008).

Adding to the complexity of peptide analysis, post-translational modifications (PTMs) occur on several proteins. These modifications can be either adding, removing or modifying groups on the amino acid residues. As mentioned above, there are several biological functions for PTMs, however, challenges in confidently identifying modifications limits the research in this field. PTMs are generally not considered during large scale proteomics analysis containing large amounts of proteins. The reason being that large scale proteomics analysis often generates low sequence coverage, resulting in PTMs remaining un-discovered (Steen & Mann, 2004). There are several enrichment methods which allow the pinpointed research of specific modifications. Extraction of these modifications from large cell lysates include methods such as PTM specific antibodies, two-dimensional electrophoresis (2DE) and chromatographic methods retaining the selected modifications (Mann & Jensen, 2003). Protein phosphorylation exemplifies several of the challenges in PTM identification. Such as, low stochiometric concentrations, tightly regulated protein modification pathways, variation in phospho-sites and phosphatases removing phosphorylation's (Mann et al., 2002). These factors contribute to the challenge of identifying and characterizing peptides containing PTMs. However, to increase the chances of success in detecting modifications, analysis of purified proteins is possible, albeit a luxury limited to a few biological systems.

PTM profiling of a single protein is easier to achieve than for a protein mix due to the deceased peptide complexity in the samples. Peptide mass fingerprinting using MALDI-TOF is possible by amending the database to search for digested peptides with a change in mass corresponding to specific modifications. However, the combinatorial searches against several PTMs will create vast searches with unrealistic search times, limiting the ability to identify the PTMs. LC-

MS using full scan and tandem MS modes will result in high resolution spectra allowing a detailed characterization of fragment ions, lowering the combinatorial possibilities and increasing the chances of identifying modified peptides. This is further aided by the separation with enrichment strategies. However, enrichment is not flawless either, the introduction of new sample handling steps increases the chances of error. In addition, enrichment can introduce bias in data analysis creating issues of quantification. Further increasing the complexity of PTM analysis is encountered with labile modifications such as phosphorylated serine and threonine modifications, which may be lost in CID fragmentation (Zhou et al., 2001).

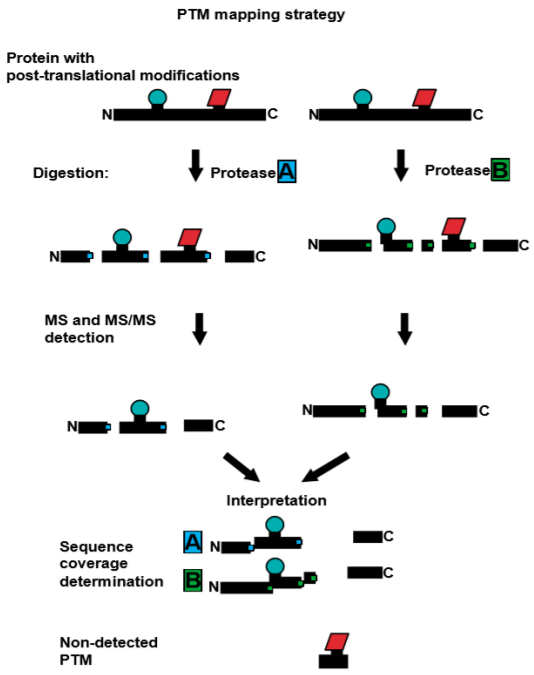

Figure 1-10 Schematic illustration of a general PTM mapping strategy using two proteases. *This image shows a general strategy to increase the sequence coverage. The amino acid sequence and protease choice will determine the sequence coverage and PTM available for detection. Figure source:(Mann & Jensen, 2003).*

PTM profiling has the highest success rate when starting with high concentrations of pure protein. As illustrated in (**Figure 1-10**), low sequence coverage may result in modifications remaining un-identified, the use of two proteases minimizes this. Search software has traditionally not been conditioned to search for PTMs, therefore new algorithms and software have been established. With the expanding field of mass spectrometry, PTM identification strategies have become simpler. While the feat of quantifying PTMs still remains challenging for many sample types and PTMs, new software have been designed for unbiased quantification of thousands of PTMs in large-scale proteomics analyses, i.e. non-enriched samples (Humphrey et al., 2018).

During this study, PEAKS Studio was used due to its many features aiding research in the proteomics discipline. The key features are *de novo* sequencing, database search, PTM analysis and mutation searches. PEAKS is unique compared to other search engines as it performs built-in *de-novo* sequencing of the MS/MS data (Ma et al., 2003). In addition to standard database searching combining *de-novo* deduced sequences (Zhang et al., 2012). A False Discovery Rate (FDR) on protein identification is determined by creating a decoy database of shuffled proteins, with both forward and reverse shuffling. The determined FDR allows filtering of peptides to ensure that only confidently identified peptides are annotated. PEAKS PTM is an integrated module which allows the investigation of post-translational modifications on proteins. The software uses two methods during the search, peptide pairs and PTM rareness. The low stochiometric concentration of modifications results in both modified and un-modified peptides being present. The modified and unmodified peptide together is called a peptide pair. Peptides both with and without modification identified from several MS/MS spectra are rewarded in the algorithm. The PTM rareness will also be regarded by the algorithm and commonly known PTMs are rated with a higher confidence score (Han et al., 2011). Confidently scoring PTMs, was performed with the software specific Ascore method which is a probability based method scoring the peptide spectral matches (PSM) based on the peptide intensity and site determining MS/MS fragments (Beausoleil et al., 2006).

2 Materials

2.1 Laboratory equipment

Table 1: Laboratory equipment used during the master thesis.

Category	**Equipment**	**Supplier**
Instruments	Agilent 1290	Agilent Technologies
	Äkta Purifier	GE Healthcare
	Äkta Start	GE Healthcare
	BioPhotometer D30	Eppendorf
	Cell density meter, Ultrospec 10	Biochrom
	CP-4900	Varian
	Microfluidizer	Siemens
	Mosquito® Crystal Nanolitre	SPT Labtech
	NanoDrop™ One	Thermo Scientific
	Q-Exactive	Thermo Scientific
	Rotator, Multi RS-60	Biosan
	Thermal cycler, SimpliAmp	Thermo Scientific
	ThermoMixer™ C	Eppendorf
	UltiMate™ 3000 RSLC nano system	Thermo Scientific
	UltraFlextreme	Bruker
Equipment	µCuvette®	Eppendorf
	Bench top UV Transilluminator	UVP
	Boiling water bath, SBB Aqua 5 plus	Grant
	Criterion™ Cell	Bio-Rad
	Gel Doc™ EZ imager	Bio-Rad
	Gene pulser II	Bio-Rad
	Incubator 37°C	Termaks
	Incubator 37°C, New Brunswick™ Scientific Innova 44	Eppendorf
	Injection needle LC 0.7 mm	GE Healthcare

	Magnet Stirrer, RCT Basic	IKA
	Microwave oven, MD142	Whirlpool
	Mill-Q® Direct water purification system, Direct 16	Merck
	Mini-PROTEAN® Tetra cell	Bio-Rad
	pH 913	Metrohm
	PowerPac™ 300	Bio-Rad
	PowerPac™ Basic power supply	Bio-Rad
	Pulscontroller plus	Bio-Rad
	Rainin™ Liquidator	Mettler Toledo
	Rock Imager®	Formulatrix
	Safe 2020 Laminar flow workbench	Thermo Scientific
	Scale, Entris Satorious	VWR
	Ultrasonic waterbath XUBA	Grant
	Vortex, MS 3 basic	IKA
	Waterbath 22-65°C, Julabo 5A	Julabo
Centrifuges	Allegra X-30R	Beckmann Coulter
	Avanti J25-s	Beckmann Coulter
	Benchtop Centrifuge 5418R	Eppendorf
	Plate spin II	Kubota
	Vacufuge plus	Eppendorf
	20 mm Aluminium crimp cap	Supleco
	20 mm Butyl stopper	Supleco
Disposables	Assorted glassware	
	CellStar™ Tubes, 15 and 50 mL	Greiner Bio-One
	Criterion™ IEF Precast gels	Bio-Rad
	CryoPure tubes, 1.8 mL	Sarstedt
	Culture tubes, 13 mL	Sarstedt
	Eppendorf tubes, 1.5 and 2.0 mL	Axygen
	MicroAmp™ Adhesive film	Applied Biosystems
	MicroAmp™ Optical 96-well reaction plate	Applied Biosystems
	Mini-PROTEAN Precast Gels	Bio-Rad

	Nunc™ 96 well microtiter plates	Thermo Scientific
	PCR tubes, 0.2 mL	Axygen
	Petri dishes, 9 cm	Heger
	Pipette tips	VWR
	Protein LoBind, 2.0 mL	Eppendorf
	Proteomics pipette tips, epTIPS™ Low-retention	Eppendorf
	Semi-Micro Cuvette	Brand
	Stericup® 0.22 µM filter unit	Merck
	Syringes, 10 and 1 mL	BD Plastipak
	UVette®	Eppendorf
Columns	150 mm BEH amide 1.7µm column	Aquity
	Acclaim™PepMap™ 100 C18 column	Thermo Scientific
	HiLoad 16/600 Superdex	GE Healthcare
	HisTrap HP, 5 mL	GE Healthcare
	HiTrap Phenyl FF, 5 mL	GE Healthcare
	Hitrap Q FF, 5 mL	GE Healthcare

2.2 Chemicals

Table 2. An overview of chemicals and corresponding supplier utilized during this study.

Chemical	**Supplier**
10x Tris-Glycine-SDS	Bio Rad
2,5 Dihydroxybenzoic acid (DHB)	Sigma
50x TAE Electrophoresis Buffer	Thermo Scientific
5x Phusion buffer	NEB
Acetic acid Glacial	VWR
Acetonitrile	Honeywell
α-Cyano-4-hydroxycinnamic acid (HCAA)	Bruker

Agar powder	VWR
Ammonium bicarbonate	Sigma
Ammonium Sulphate	Merck
Ampicillin disodium salt	Sigma
Antifoam 204	Sigma
Ascorbic Acid	Sigma
Bacto Tryptone	BD
Bacto yeast extract	BD
BenchMark™ protein ladder	Invitrogen
Beta-glycerophosphate	Sigma
Bio Rad protein assay	Bio Rad
Brain Heart Infusion	Oxoid
Calcium Chloride	Sigma
Calf intestine alkaline phosphatase	Invitrogen
Carbenicillin disodium salt	Alfa Aesar
Cathode buffer 10x	Bio Rad
Complete Mini EDTA free protease inhibitors	Roche
Coomassie G-250	Bio Rad
Copper Sulphate	VWR
Cut Smart Buffer	NEB
D- (+)- Saccharose	Sigma
D- (+)-Glucose anhydrous	VWR
Dipotassium hydrogen phosphate	VWR
Dithiothreitol (DTT)	Sigma
DNase 1	Thermo Scientific
dNTP mix	NEB
Ethanol Absolute	VWR
Ethylenediaminetetraacetic acid (EDTA)	Merck
Gel Loading Dye purple	NEB
Glycerol 85%	Merck
Hydrochloric acid	VWR
IEF Anode buffer 10x	Bio rad
IEF standards 4.45-9.6	Bio Rad

Imidazole	Sigma
Iodoacetamide (IAA)	Sigma
Isopropanol	VWR
Isopropyl 1 Thio -b - D Galactopyranoside (IPTG)	Sigma
Kanamycin monosulphate	Sigma
Chlorin	Orkla
KpNI - HF	NEB
L- (+)-Arabinose	Sigma
Lysozyme	Sigma
M9 minimal salts 2x	Gibco
Magnesium Chloride Hexahydrate	Merck
Methanol	Honeywell
Nupage reducing agent	Novex
Nupage sample buffer	Novex
peqGREEN DNA/RNA Dye	peqlab
Phenylmethylsulphonyl fluoride (PMSF)	Sigma
Phosphate buffered saline	Sigma
PhosSTOP Easypack	Roche
Phusion polymerase	NEB
Poly (Ethylene) Glycol 20 000	Sigma
Poly (Ethylene) Glycol 8000	Sigma
Potassium dihydrogen phosphate	Sigma
Quick Load 100bp	NEB
Quick load 1Kb	NEB
RedTaq 2x Master	VWR
S.O.C Medium	Invitrogen
Sbf1 - HF	NEB
SeaKem LE Agarose	Lonza
Sodium Acetate Trihydrate	Sigma
Sodium Chloride	VWR
Sodium Fluoride	Sigma
Sodium orthovanadate	Sigma
Sodium pyrophosphate	Sigma

Sypro orange dye 1000x	Thermo Scientific
Trifluoric acid (TFA)	Flukka
TrizmaBase	Sigma
UREA	Sigma
β-Chitin extracted from squid pen	France Chitin

2.3 Kits

Table 3 An overview of kits utilized during this study with the corresponding supplier.

Kit	**Supplier**
Nucleospin® Gel and PCR Clean-Up	Machery-Nagel
GeneJet Plasmid Midiprep	Thermo Scientific
JSCG+ Crystallization kit	Hampton research
Salt Rx™ HT Crystallization kit	Hampton research
Index™ Crystallization kit	Hampton research
PEG/Ion™ HT Crystallization kit	Hampton research
WIZARD™ Crystallization kit	Molecular dimensions
Monolith His-Tag labelling Kit RED-tris-NTA	Nano temper technologies
In-Fusion® HD Cloning kit	Takara Bio

2.4 Primers

Table 4: Primers used during the project with name, sequence and comments describing their placement.

Name	**Sequence 5'-3'**	**Comments**
CbpD-OutC-FW	GCGGCCTTTGCCTGCCTCTACCGG	Placed on the insert for primary screening and sequencing

CbpD-IntC-Rev	TGGCCTTGTACGAACTGGAA	Placed on the insert for primary screening and sequencing
AraC_FW_Confirmation	TTTTCACCACCCCCTGACCGCGA	pGM931 Plasmid, primary screening
CbpD-KpnI-His_FW	GTTTCTCCATGGTACCGGCTGCG CTTCCTCAAGGGC	Cloning rCbpD$_{PA}$ (Carrying C-terminal His-Tag) and its promoter within pGM931 plasmid
CbpD-Sbf1-His_Rev	AGAGTCGACCTGGCAGGTCAATG GTGATGATGGTGCGCCAGCAGGGTC	Cloning rCbpD$_{PA}$ (Carrying C-terminal His-Tag) and its promoter within pGM931 plasmid

2.5 Proteins and Enzymes

Table 5:Overview of proteins used throughout this study with plasmid, production organism and additional comments.

Name	**Plasmid**	**Antibiotics**	**Production organism**	**Comments**
rCbpD$_{PA}$	pGM931	Carbenicillin	*P. aeruginosa* PA14	Full length enzyme, C-terminal 6x-His-Tag
rCbpD$_{PA}$ Lys	pGM931	Carbenicillin	*P. aeruginosa* PA14	Full length enzyme, K48R, K97R, K166R, K185R, K262R mutated to R, C-terminal 6x-His-Tag
rCbpD$_{PA}$ Native	pGM931	Carbenicillin	*P. aeruginosa* PA14	Full length enzyme, no His-Tag
rCbpD$_{EC}$	pNIC-CH	Kanamycin	BL STAR 21	Full length enzyme, C-terminal 6x-His-Tag
rCbpD$_{EC}$ M1	pNIC-CH	Kanamycin	BL STAR 21	AA10 LPMO module, C-terminal 6x-His-Tag

$rCbpD_{EC}$ M2+M3	Pet-28a	Kanamycin	BL STAR 21	Modules 2 and 3 (M2, M3), N-terminal 6x-His-Tag

3 Methods

3.1 Prepared media, buffers and solutions

3.1.1 Media

Media	**Contents**
LB	10 g Bacto tryptone 5 g Bacto yeast extract 10 g Sodium chloride (NaCl) The dry ingredients were weighed out, placed in a 1000 mL beaker and dissolved in 800 mL ddH_2O using a magnet stirrer. After dissolving the ingredients, the volume was adjusted to 1000 mL before transferring the media to a 1000 mL blue cork bottle and autoclaved at 121°C for 15 minutes.
TB Stock 1.1x	12 g Bacto tryptone 24 g Bacto yeast extract 4 mL Glycerol The dry ingredients were weighed out, placed in a 1000 mL beaker and dissolved in 800 mL ddH_2O using a magnet stirrer. After dissolving, 4 mL of glycerol was added before adjusting the volume to 900 mL, yielding a TB stock solution at 1.1x concentration. After dissolving the 1.1x media was transferred to a 1000 mL blue cork bottle and autoclaved at 121°C for 15 minutes. TB stock media was diluted to 1x as described in section **3.7.4.**
BHI	37 g Brain Heart Infusion Dissolved and autoclaved in the same manner as LB medium.

M9 Minimal salt (2x)	25.6 g Sodium phosphate dibasic heptahydrate (95.5 mM) 6 g Monopotassium phosphate (44.09 mM) 1 g Sodium chloride (17.1 mM) 2 g Ammonium chloride (37.4 mM) M9 Minimal salt (2x) was bought as sterile media from Gibco.

3.1.2 Stock solutions

Stock solutions of common buffer and media ingredients were prepared to save time in buffer preparation. Weighing steps were performed on an analytical weight. After mixing and dissolving the buffer ingredients, the solutions were filter sterilized using Stericup 0.22 µM vacuum filter system (Merck).

Stock solutions	**Contents**
Trizma base hydrochloric acid (Tris-HCl) 1M	121.14 g Trizma base After weighing, the salt was transferred to a 1000 mL beaker and dissolved in 800 mL ddH_2O using a magnet stirrer. The pH was adjusted using 37% hydrochloric acid (HCl) and measured using a 913-pH meter. After confirming the correct pH, the buffer was transferred to a 1000 mL graduated flask before adjusting the final volume to 1000 mL. Sterilization was achieved by passing the buffer through a 0.22 µM filter.
Imidazole (2 M)	136.15 g Imidazole After weighing, the salt was transferred to a 1000 mL graduated flask before dissolving in 800 mL ddH_2O using a magnet stirrer. Once fully dissolved, the volume was

	adjusted to 1000 mL. Sterilization was achieved by passing the buffer through a 0.22 µM filter.
Sodium Chloride (NaCl) 5 M	146.1 g NaCl After weighing, the salt was transferred to a 500 mL graduated flask and dissolved in 400 mL using a magnet stirrer. Once fully dissolved the volume was adjusted to 500 mL. Sterilization was achieved by passing the buffer through a 0.22 µM filter.
Phenylmethylsulphonyl fluoride (PMSF) 50 mM	2.18 g PMSF After weighing the salt was transferred to a 250 mL graduated flask and dissolved in 200 mL Isopropanol using a magnet stirrer. Once fully dissolved the volume was adjusted to 250 mL. Sterilization was achieved by passing the buffer through a 0.22 µM filter.
Magnesium Chloride ($MgCl_2$) 20mM	0.476 g $MgCl_2$ After weighing the salt was transferred to a 250 mL graduated flask and dissolved in 200 mL ddH_2O using a magnet stirrer. Once fully dissolved the volume was adjusted to 250 mL. Sterilization was achieved by passing the buffer through a 0.22 µM filter.
Magnesium sulphate ($MgSO_4$) 0.5 M	61.62 g $MgSO_4$ After weighing the salt was transferred to a 250 mL graduated flask and dissolved in 200 mL ddH_2O using a magnet stirrer. When fully dissolved the volume was

	adjusted to 250 mL. Sterilization was achieved by passing the buffer through a 0.22 µM filter.
Potassium phosphate monobasic (KH_2PO_4) 0.17 M Potassium phosphate dibasic (K_2HPO_4) 0.72 M	23.13 g KH_2PO_4 125.4 g K_2HPO_4 After weighing, the salt was transferred to a 1000 mL gradated flask before dissolving in 800 mL ddH_2O using a magnet stirrer. When fully dissolved the volume was adjusted to 1000 mL. Sterilization was achieved by passing the buffer through a 0.22 µM filter.

3.1.3 Buffers and solutions

Buffers made from stock solutions (**3.1.2**)

Buffers and solutions	**Contents**
Spheroplast buffer (100 mM Tris-HCl pH 8, 0.5M Sucrose, 5 mM EDTA pH 8, 0.1 mM PMSF)	100 mL 1M Tris-HCl pH 8 171 g Sucrose 1 mL 0.5 M EDTA pH 8 2 mL 50 mM PMSF Sucrose was weighed out and transferred to a 1000 mL graduated flask before adding the liquid stock solutions. ddH_2O was added to approximately ¾ of the total volume before dissolving using a magnet stirrer. When fully dissolved the volume was adjusted to 1000 mL. Sterilization was achieved by passing the buffer through a 0.22 µM filter.
Binding buffer (IMAC)	2.5 mL 2M Imidazole 20 mL 1M Tris-HCl pH 7.5

(5 mM Imidazole, 20 mM Tris-HCl pH 7.5, 200 mM Sodium Chloride)	40 mL 5M Sodium Chloride Imidazole was measured using a 1 mL pipette, NaCl and Tris-HCl were measured using a graduated cylinder. All components were transferred to a 1000 mL graduated flask before adjusting the volume to 1000 mL using ddH_2O. Sterilization was achieved by passing the buffer through a 0.22 µM filter.
Washing buffer (IMAC) (20 mM Imidazole, 20 mM Tris-HCl pH 7.5, 200 mM Sodium Chloride)	10 mL 2M Imidazole 20 mL 1M Tris-HCl pH 7.5 40 mL 5M NaCl Imidazole, NaCl and Tris-HCl stock solutions were measured using a graduated cylinder. All components were transferred to a 1000 mL graduated flask before adjusting the volume to 1000 mL using ddH_2O. Sterilization was achieved by passing the buffer through a 0.22 µM filter.
Elution buffer (IMAC) (500 mM Imidazole, 20 mM Tris-HCl pH 7.5, 200 mM Sodium Chloride)	250 mL (2 M) Imidazole 20 mL (1 M) Tris-HCl pH 7.5 40 mL (5 M) NaCl Imidazole, NaCl and Tris-HCl stock solutions were measured using a graduated cylinder. All components were transferred to a 1000 mL graduated flask before adjusting the volume to 1000 mL using ddH_2O. Sterilization was achieved by passing the buffer through a 0.22 µM filter.
Binding buffer (HIC) (50 mM Tris-HCl pH 8, 1M Ammonium sulphate)	50 mL (1M) Tris-HCl pH 8 132.14 g Ammonium sulphate (NH_4SO_4)

	After weighing, the salt was transferred to a 1000 mL graduated flask before adding 50 mL of the Tris-HCl stock solution. ddH_2O was added to approximately ¾ of the total volume before dissolving using a magnet stirrer, when fully dissolved the volume was adjusted to 1000 mL. Sterilization was achieved by passing the buffer through a 0.22 µM filter.
Elution buffer (HIC) (50 mM Tris-HCl pH 8)	50 mL (1M) Tris-HCl pH 8 Tris-HCl stock solution was measured using a graduated cylinder and transferred to a 1000 mL graduated flask before adjusting the volume to 1000 mL with ddH_2O. Sterilization was achieved by passing the buffer through a 0.22 µM filter.
Binding buffer (IEX) (50 mM Tris-HCl pH 8)	50 mL 1M Tris-HCl pH 8 Same procedure as Elution Buffer (HIC)
Elution buffer (IEX) (50 mM Tris-HCl pH 8, 500 mM Sodium Chloride)	50 mL (1M) Tris-HCl pH 8 100 mL (5M) Sodium Chloride (NaCl) Tris-HCl and NaCl stock solutions were measured using a graduated cylinder before transferring to a graduated cylinder before adjusting the volume to 1000 mL with ddH_2O. Sterilization was achieved by passing the buffer through a 0.22 µM filter.
SEC buffer (15 mM Tris-HCl pH 7.5, 150 mM Sodium Chloride)	30 mL (5M) Sodium Chloride (NaCl) 15 mL (1M) Tris-HCl pH 7.5 Same procedure as Elution buffer (IEX)

SDS-PAGE sample solution	5 mL NuPAGE® LDS buffer 4x 2 mL NuPAGE® Reducing agent 10X 3 mL ddH_2O The components were mixed in a 15 mL CellStar® tube for easy access during analysis.
Gel stain solution (10% Acetic acid, 25 % Isopropanol, 0.05% Coomassie Brilliant Blue R-250)	100 mL Glacial acetic acid (CH_3COOH) 250 mL Isopropanol 0.5 mL Coomassie Brilliant Blue R-250 The components are added to a 1 L blue cork bottle and the volume is adjusted to approximately 1 L with ddH_2O.
Gel de-stain solution (10% Acetic acid, 25% Isopropanol)	100 mL Glacial acetic acid 250 mL Isopropanol The components were added to a 1 L blue cork bottle and the volume is adjusted to approximately 1 L with ddH_2O.

3.2 Gel electrophoresis

3.2.1 DNA agarose gel electrophoresis

Agarose gel matrix creates pores for the negatively charged DNA to travel towards the cathode when an electric current is applied. The DNA charge to mass ratio is the same for all DNA fragments, enabling separation based on size alone. To visualize the DNA fragments, the gel is

laced with a fluorescent dye, in this case PeqGREEN which binds to DNA and is visualized using UV.

Materials:

- Agarose (Lonza)
- PeqGreen (PeqLab)
- TAE buffer 1x (Thermo Scientific)
- Erlenmeyer flask
- Microwave oven MD142 (Whirlpool)
- Mini-Sub GT cell (Bio-Rad)
- PowerPac™ Basic power supply (Bio-Rad)
- Gel Doc™ EZ imager (Bio-Rad)
- Ladder
    - Quick-Load® 1 Kbp (NEB)
    - Quick-Load® 100 bp (NEB)

Method:

For DNA gel electrophoresis, a 0.1% gel was prepared by dissolving 0.6 g of agarose in 60 mL TAE buffer in a 250 mL Erlenmeyer flask. Dissolving was performed by heating the mixtures in the microwave oven on maximum efficiency. Once the agarose was dissolved, the mixture was cooled to approximately 60°C under running tap water before adding 2.5 µL of PeqGREEN. The gel was cast in a transferrable mould, after solidifying, the gel was transferred to the Mini-Sub GT cell and covered with TAE buffer 1x. An appropriate ladder of either Quick-Load® 1kb or 100 bp was selected based on the expected DNA size. The ladder was applied on the gel together with the samples. Separation was achieved by applying 90 V of current for 45 minutes. After the gel electrophoresis, imaging was performed with the Gel Doc™ EZ imager to verify the DNA band size.

3.2.2 Sodium Dodecyl Sulphate PolyAcrylamide Gel Electrophoresis (SDS-PAGE)

SDS-PAGE is a general technique used to determine the size of the different proteins present and determine the purity of purified protein samples. The proteins were reduced with dithiothreitol (DTT) and denatured in a boiling water bath. The addition of the negatively charged SDS in the SDS-PAGE sample solution ensures a uniform charge of the protein. The electric current allows the negatively charge proteins to migrate in the poly acrylamide gel matrix separating molecules based on size.

Materials:

- TGS running buffer (1x) (Bio-Rad)
- Protein BenchMark™ Ladder (Invitrogen)
- SDS-PAGE sample solution
- mini-PROTEAN®TGX Stain Free gels (Bio-Rad)
- Mini-PROTEAN® Tetra cell (Bio-Rad)
- PowerPac™ 300 (Bio-Rad)
- Gel Doc™ EZ Imager (Bio-Rad)

Method:

Protein samples of either pure protein or protein extracts were treated equally during this method. Equal amounts of protein sample and SDS-PAGE sample solution were mixed for a total volume of 20 µL. The samples were incubated for 4 minutes in a boiling water bath to ensure protein denaturation. Precast mini-PROTEAN®TGX Stain Free gels were placed in mini-PROTEAN®Tetra cell gel chamber and filled with TGS running buffer. After placing the gel in the gel chamber, 3µL of the Protein BenchMark™ ladder was placed in the first well. Depending on either 15µL or 30µL well size, respectively 10-15µL of the sample was injected in the wells. The gel chamber was connected to the PowerPac™ 300 power supply and 275 V was applied for 17 minutes. After the completed gel electrophoresis, the gel was removed from the casing and transferred to the Gel Doc™ EZ Imager system and imaged using the high sensitivity option (5 minute imaging) in the Image Lab software.

3.2.3 Iso-electric focusing (IEF)

Iso-electric focusing is an electrophoretic method which separates protein samples based on their pKa values. The zwitter-ionic capabilities of proteins enable migration until the net-charge of the protein is zero. The pH when the protein is void of charge is referred to as the pI of the protein. IEF gels utilize a gel with a pH gradient allowing the proteins to migrate until the pI of the specific protein is reached (Bjellqvist et al., 1982). When the pH is above the protein pI, the protein is deprotonated and negatively charged. Migration of the negatively charged protein towards the cathode continues through the pH gradient ranging from high to low. IEF was performed as sample fractionation prior to LC-MS analysis and as a method to observe the presence of protein species based on pI separation.

Materials:

- Criterion™ precast IEF gels pH 3-10 (Bio-Rad)
- Anode buffer 1x (Bio-Rad)
- Cathode buffer 1x (Bio-Rad)
- Criterion™ cell (Bio-Rad)
- EPS 601 Power supply (GE Healthcare)
- IEF Standard 4.45-9.96 (Bio-Rad)
- 50 % Glycerol
- Coomassie stain solution
- De-stain solution

Method:

Protein samples were mixed 1:1 with the sample buffer (50 % glycerol) for a total volume of 20 µL before applying the full volume in the gel wells. In addition, 3 µL of the standard was applied. After application, the following electrophoretic running scheme was used.

- 100 V for one hour

- 250 V for one hour
- 500 V for 30 minutes

After completing the electrophoresis, the gel was removed from the casing and covered with Coomassie gel stain solution for one hour with low agitation on a shaking device. After staining, de-staining was performed by removing the gel from the staining solution and placing the gel in a 1:1 mixture of ddH_2O and de-stain solution on a shaking device with low agitation overnight. The following day the de-stain mixture was removed, and de-staining was continued with 100% de-staining solution until the gel was completely de-stained and the bands clearly visible. The gel was imaged using the Coomassie imaging tray and Gel Doc™ EZ Imager with the Image Lab Coomassie settings.

3.3 Determination of DNA concentrations using 260 nm spectrophotometry

During this study, DNA concentrations were determined spectrophotometrically at 260 nm. The concentration was determined by utilizing Beer-Lambert's law, stating that the Absorbance (A) is equal to the double stranded DNA extinction coefficient (ε) times the path length (l) times the concentration (c).

$$A = \varepsilon \times l \times c$$

The average double stranded DNA extinction coefficient is $(0.02\mu g/mL)^{-1}$ cm^{-1} and the path length was 1 mm. The spectrophotometer contains a 260 nm method created for the accompanying µCuvette® and outputs the DNA concentration in µg/mL.

Materials:

- DNA samples
- ddH_2O
- µCuvette® (Eppendorf)
- BioPhotometer® D30 (Eppendorf)
- Lens tissue paper

Method:

Before measuring the DNA concentration, the µCuvette® was cleaned with lens tissue paper. Following the cleaning step, the spectrometer was blanked by placing 2 µL of ddH_2O on the sample holder before inserting the µCuvette® in the spectrophotometer and measuring at 260 nm. The measurement of ddH_2O was saved as a blank sample. After establishing the blank measurement, the µCuvette® was cleaned with lens tissue paper before placing 2 µL of the DNA sample on the sample holder. The µCuvette® was again placed in the spectrophotometer and measured. The spectrophotometer has a dedicated µCuvette® program which outputs the DNA concentration in µg/mL.

3.4 Cloning of CbpD carrying a His-Tag in pGM931

The plasmid pGM931 was kindly provided by associate professor Federica Briani, University of Milan, Italy (Delvillani et al., 2014).

3.4.1 Insert amplification

In order to insert the *cbpD* gene into a Gram-negative shuttle vector, pGM931, the gene and its promotor was amplified using PCR amplification.

Materials:

- 5x Phusion buffer (NEB)
- dNTP mix (NEB)
- *P. aeruginosa* PA14 glycerol stock
- Phusion polymerase (NEB)
- $MgCl_2$ (NEB)
- CbpD-KpnI-His_FW primer
- CbpD-Sbf1-Rev primer
- Eppendorf PCR tube 0.2 mL
- µCuvette® (Eppendorf)

- BioPhotometer D30 (Eppendorf)
- Microwave oven MD142 (Whirlpool)

Method:

P. aeruginosa PA14 bacterial cells were obtained by streaking out the bacteria strain on a LB agar plate. Five colonies were picked and res-suspended in 200 µL ddH_2O in an Eppendorf tube. To extract genomic DNA, the cells were boiled in the microwave oven for 90 seconds at maximum efficiency. Following boiling, the sample was centrifuged at 5000 g for 3 minutes, before collecting the supernatant and transferring it to a clean Eppendorf tube. The cell pellet was discarded. The DNA concentration in the collected sample supernatant was measured using the µCuvette® spectrophotometer at 260 nm as described in section **3.3**.

Amplification of *cbpD* was performed using the primers CbpD-KpnI-His-FW and CbpD-Sbf1-His-Rev listed in **Table 4**. The amplification reaction was performed in 0.2 mL PCR tubes using the following conditions and PCR settings.

Table 6: PCR reaction components used to amplify the cbpD insert.

PCR reaction	**Final concentration**	**Volume**
ddH_2O	-	319.5 µL
5x Phusion Buffer	1x	45 µL
dNTP 10mM	0.2 mM	9 µL
$PA14_{CbpD}$ (150ng/µL)	6 ng/µL	18 µL
Phusion HF polymerase (2 units/µL)	0.02 U/µL	4.5 µL
$MgCl_2$ (50 mM)	1 mM	9 µL
KpnI-FW (20 µM)	1 µM	22.5 µL
Sbf1-Rev (20 µM)	1 µM	22.5 µL

Table 7: PCR conditions for insert amplification.

PCR conditions (Temperature/duration)	Cycles
98 °C (5 minutes)	1x
98 °C (10 seconds)	35x
58 °C (30 seconds)	
72 °C (120 seconds)	
72 °C (7 minutes)	1x

The PCR reaction was prepared as depicted in **Table 6** and performed as stated in **Table 7**. To ensure obtaining the correct amount of insert in a single attempt, the total volume of the PCR reaction was 400µL, that were divided in 8 PCR tubes each containing 50 µL.

3.4.2 Gel excision and purification

After the PCR cycle was finished the samples were loaded on an Agarose gel (0.1%) as described in section **3.2.1**.

Materials:

- Scalpel (Swann Moton)
- UV transilluminator (UVP)
- Eppendorf tubes 1.5 mL
- Nucleospin® PCR clean up Gel extraction Kit (Machery-Nagel)
- Gel Doc™ EZ imager (Bio-Rad)
- ddH_2O

Method:

The correct insert amplification was verified on agarose gel as described in section **3.2.1** and imaging the gel using Gel Doc™ EZ imager. The agarose gel was placed on a benchtop UV transilluminator and the bands were quickly excised in cubes with a clean scalpel. The gel pieces containing the correct DNA were collected in an Eppendorf tube. DNA purification was performed using Nucleospin® PCR clean up Gel extraction Kit. Protocol 5.2 "DNA extraction from agarose gel" was followed, however, the elution was performed using ddH_2O 37°C instead of the accompanying kit elution buffer.

3.4.3 Double digestion of pGM931

The purified plasmid was provided by my co-supervisor, purification of the pGM931 plasmid was therefore not performed.

Materials:

- pGM931 plasmid
- Cutsmart® buffer 10x (NEB)
- KpnI-HF restriction enzyme (NEB)
- Sbf1-HF restriction enzyme (NEB)
- Alkaline phosphatase CIAP (NEB)
- ThermoMixer™C (Eppendorf)

Method:

The primers used while amplifying the *cbpD* gene added restriction sites KpnI and SbfI to the insert, which will result in sticky ends that match with the linearized plasmid. Linearization of the plasmid was needed to incorporate the DNA insert into the plasmid. The following linearization reaction was performed.

Table 8: Double digestion of pGM931 reaction summary.

Reagents	End concentration	Volume
pGM931 (114 ng/mL)	1 µg	9 µL
Cutsmart® Buffer 10x	1x	5 µL

KpnI-HF	10 units	2.5 µL
Sbf1-HF	10 units	2.5 µL
ddH_2O	-	31 µL
Total		50 µL

The reaction was set in triplicates to ensure sufficient concentration of the linearized double digested plasmid after gel purification. The reaction was incubated in a thermomixer for 3 hours at 37°C with 600 rpm agitation. After 2 hours 45 minutes of reaction time, 1 µL of alkaline phosphatase was added to the reaction before continuing the incubation for 15 minutes to ensure that re-ligation did not happen. The samples were loaded on a 1% agarose gel for verification, extraction and purification of linearized product with a size of 5128bp, described in section **3.2.1**.

3.4.4 Ligation of insert

Ligation of the purified insert containing the *cbpD* gene into the linearized plasmid was performed in a ligation reaction using the In-Fusion® HD cloning kit. The In-Fusion kit allowed for a one step cloning method for inserting the insert in the linearized plasmid. An insert:plasmid ratio of 2:1 had been established as optimal for this plasmid.

Materials:

- Purified insert (96.12 ng/µL)
- Linearized plasmid (24.8 ng/µL)
- 5X in-Fusion HD Enzyme premix (Takara Bio)
- µCuvette® Eppendorf
- BioPhotometer® D30 (Eppendorf)
- Vortex MS3 basic (IKA)
- ThermoMixer™C (Eppendorf)
- ddH_2O

Method:

The calculation used for determining the appropriate amount of insert needed in the ligation reaction for insert amount was performed as follows:

$$\text{Plasmid amount (ng)} = \text{Insert amount (ng)} \,/\, \frac{\text{Plasmid length}}{\text{Insert length}} \,/\, \frac{\text{Insert}}{\text{Plasmid}}\ \text{Ratio}$$

$$\text{Plasmid amount (ng)} = 96.12\ \text{ng}/\mu\text{L} \,/\, \frac{6053}{1643} \,/\, \frac{2}{1}$$

Plasmid amount (ng) = 150 ng

The gel purified insert concentration was determined by measuring 260 nm as described in section **3.3**. The insert concentration was 96.12 ng/µL and linearized plasmid concertation was 24.8 ng/µL. Incorporation of the insert into the linearized plasmid was performed as described in **Table 9**.

Table 9: Infusion reaction of the CbpD insert with the linearized pGM931 plasmid

Reagents	**Volume**
Insert CbpD (96.12 ng)	1 µL
Plasmid pGM931 (24.8 ng)	6 µL
5X in-Fusion HD Enzyme premix	2 µL
ddH_2O	1 µL

Firstly, ddH_2O was placed in the bottom of the 1.5 mL Eppendorf tube before adding the digested insert solution and the linearized plasmid. Thereafter, the 5 x in-Fusion HD Enzyme premix was added to the bottom of the tube and mixed thoroughly using the lab bench vortex. The reaction was performed at 50°C in a thermomixer for 15 minutes before immediately placing on ice.

3.4.5 Transformation of *E. coli* Top10

ONE SHOT™ TOP 10 chemically competent *E. coli* cells (Invitrogen) were used for transformation. These cells were chosen for their ability of high efficiency cloning and plasmid propagation.

Materials:

- Plasmid obtained from ligation reaction (**3.4.4**)
- ONE SHOT™ TOP 10 chemical competent *E. coli* (Invitrogen)
- LB agar plates 100 µg/mL Ampicillin
- Culture tubes 13 mL (Sarstedt)
- S.O.C medium (Invitrogen)
- Ice
- Water bath 42°C (Jubalo)
- Incubator 37°C, Scientific Innova 44 (Eppendorf)
- Incubator 37°C (Termaks)

Method:

The ONE SHOT™ TOP 10 chemical competent *E. coli* cells were stored at -80°C and thawed on ice before continuing.

The thawed Top10 cells were transferred from the storage vials to cold 13 mL culture tubes which were pre-placed on ice. Following the transfer, 4.5 µL of the ligation product obtained as described in section **3.4.4** was transferred to the Top10 cell suspension and mixed gently by slowly pipetting up and down once. After mixing, the cell-plasmid mixture was incubated for 30 minutes on ice. Following the incubation period, the mixture was transferred to a water bath holding 42°C for exactly 60 seconds before quickly transferring the tube back to ice. After placing on ice, the mixture was incubated for 2 minutes. Finally, 200 µL of room temperature S.O.C medium was added and gently mixed prior to transferring the tubes to a 37°C incubator with 200 rpm agitation for 30 minutes.

After incubation the cells were plated on LB -ampicillin (100 µg/mL) plates. To ensure growth on the plates and the ability to select single colonies, 10, 50 and 100 µL volumes were plated to increase the chance of success. After plating the cells, the LB plates were transferred to a 37°C incubator overnight. The following day, five colonies were selected and performed colony PCR confirmation to ensure incorporation of the plasmid containing the insert, described in

section **3.6**. Colonies confirmed with colony PCR were plated on a fresh LB plate containing 100 µg/mL ampicillin before creating glycerol stocks for storage as described in section **3.7.1**.

3.4.6 Preparation of electrocompetent *P. aeruginosa* cells

Prior to incorporating the ligation product into *P. aeruginosa* PA14ΔCbpD cells, the cells were prepared to become electrocompetent. The transfer of plasmid DNA across cell membranes was performed by exerting a short electrical pulse through a cell-DNA mixture. The electric current briefly allows the cell wall to become permeable and take up the plasmid DNA (Neumann et al., 1982).

Materials:

- PA14ΔCbpD Glycerol stock
- LB medium
- 10% Sucrose (w/v)
- Ice
- Benchtop centrifuge 5418 R (Eppendorf)
- Incubator 37°C, Scientific Innova 44 (Eppendorf)
- Culture tubes, 13 mL (Sarstedt)
- Eppendorf tubes 1.5 mL

Method:

P. aeruginosa PA14 bacterial cells were obtained by streaking out the bacteria strain on a LB agar plate. One colony was picked with a sterile inoculation loop and used to inoculate 5 mL LB in 13 mL culture tubes before cultivating overnight at 37°C with 200 rpm agitation. The cell culture was aliquoted into 1 mL fractions placed in Eppendorf tubes. Using a tabletop centrifuge at 4°C the cells were harvested by centrifuging at 16 000 g for 2 minutes. The supernatant was discarded before washing the pellet with 1mL ice cold 10% sucrose by pipetting. This washing step was repeated several times with gradually decreasing volumes of (750 µL and 100 µL) before resuspending the pellet in 50 µL sucrose. After the final washing step, the cells were allowed to rest on ice for 1 hour before electroporation was performed.

3.4.7 Electroporation of CbpD-pGM931 into *P. aeruginosa.*

After transformation of the pGM931 plasmid containing the *cbpD* insert into TOP 10 *E. coli* cells, propagation and plasmid replication was performed by cultivating the *E. coli* cells in LB medium allowing the replication of the pGM931 plasmid containing the *cbpD* insert. After overnight cultivation, the plasmid DNA was extracted and purified before electroporation.

Materials:

- 1 mm electroporation cuvette (Bio-Rad)
- OneShot™Top10 *E. coli* Glycerol stock (**3.4.5**)
- LB medium
- Carbenicillin (200 mg/mL)
- GeneJET plasmid midi prep (Thermo Scientific)
- LB Agar plates (300 µg/mL carbenicillin)
- Gene pulser II (BioRad)
- Puls controller plus (BioRad)
- Incubator 37°C, Scientific Innova 44 (Eppendorf)
- Incubator 37°C (Termaks)
- CellStar® 50 mL tube
- Ice

Method:

A cell culture was created by inoculating 50 mL of LB medium as described in section **3.7.2** containing 100 µg/mL ampicillin with a OneShot™ Top10-pGM931 colony obtained from a LB agar plate and incubated overnight at 37°C with shaking at 200rpm. The cells were harvested and the plasmid was purified according to manufacturer protocol A in the GeneJET plasmid midi plasmid purification kit. Minor changes were performed by eluting the plasmid with ddH_2O. After elution the concentration was determined by measuring absorbance at 260

nm as described in section **3.3**. After determining the concentration, the samples were diluted to a final concentration of 10 ng/µL.

To ensure successful electroporation the experiment was performed with 10ng and 50ng of plasmid DNA. In addition, a negative control not containing DNA was added. The electrocompetent *P. aeruginosa* cells prepared as described in section **3.4.6** were added 0, 1 and 5 µL of 10 ng/µL of the purified plasmid DNA. The plasmid-cell mixture was incubated for 1 minute on ice. After incubation, the mixture was transferred to a 1 mm electroporation cuvette which was pre-cooled on ice. The cuvette was placed in the cuvette holder on the Gene pulser II (Bio Rad) and electroporation was performed with 1,5kV, 200Ω and 25µF settings. Following the electroporation, 1 mL of room temperature LB was mixed gently by slowly pipetting the LB down into the 1 mm cuvette and pipetting up the LB-cell mixture before transferring the mixture to 13 mL cultivation tubes. Finally, the sample was incubated at 37 °C with 200 rpm agitation for 3 hours.

After incubation, the cells containing the correct plasmid were selected using plates containing 300 µg/mL Carbecillin. For this process 10, 50 and 100 µL of the cells were plated, this allowed picking a single colony and preventing overgrowth. After plating the cells, the LB agar plates were transferred to a 37°C incubator overnight. The following day, five colonies were selected, and colony PCR confirmation was performed in order to confirm incorporation of the plasmid containing the insert, described in section **3.6**. Colonies confirmed with colony PCR were plated on a fresh LB agar plates containing 300 µg/mL carbenicillin before creating glycerol stocks of the confirmed colonies as described in section **3.7.1**.

3.5 Colony confirmation using DNA sequencing

After transforming the pGM931 plasmid containing the *cbpD* insert into OneShot™ TOP10 *E. coli* cells, colony PCR was performed as described in section **3.6**. However, to ensure the insert and plasmid were correct, DNA sequencing through Eurofins Genomics was performed.

Materials:

- Eppendorf tubes 1.5 mL

- AraC_FW_Confirmation primer
- CbpD-SbfI-His-Rev primer
- Eurofins Genomics barcodes (Eurofins)
- ddH_2O

Method:

Plasmid DNA was purified as described in section **3.4.7** and the concentration was measured spectrophotometrically as described in section **3.3**. Thereafter, the following samples were prepared according to manufacturer instructions:

Table 10 Sample components and concentrations for DNA sequencing.

Reagents	**Forward primer**	**Reverse primer**
AraC_FW_Confirmation primer	4.5 µM	-
CbpD-SbfI-His-Rev primer	-	4.5 µM
Plasmid DNA	40 ng/µL	40 ng/µL
ddH_2O	Up to 11 µL	Up to 11 µL
Total	11 µL	11 µL

The samples were prepared as stated in **Table 10** in 1.5 mL Eppendorf tubes before fitting the supplied barcodes. The samples were delivered to a GATC pickup point and sequencing was performed by Eurofins Genomics.

3.6 Colony confirmation using Polymerase Chain Reaction (PCR)

Colony PCR was performed to verify successful insert incorporation in the plasmid, primers listed in **Table 4** were designed by a co-supervisor.

Materials:

- RedTaq DNA polymerase master mix 2x (VWR)
- Forward primer
- Reverse primer
- DNA sample
- Thermal cycler, SimpliAmp (Thermo Scientific)
- Microwave oven MD142 (Whirlpool)
- PCR tubes 0.2 mL

Method:

After ligation and transformation of the pGM931 plasmid containing the *cbpD* insert into TOP 10 *E. coli,* colony confirmation verified correct ligation using the following primers.

- CbpD-Out-FW and CbpD-IntC-Rev
- AraC_FW_Confirmation and CbpD-IntC-Rev

However, after transformation of the pGM931 plasmid containing the *cbpD* insert into PA14ΔCbpD electrocompetent cells, confirmation of the correct plasmid and insert was performed using the following primers.

- AraC_FW_Confirmation and CbpD-IntC-Rev
- AraC_FW_Confirmation and CbpD-Sbf1-His_Rev
- CbpD-Out-FW and CbpD-IntC-Rev

Colonies selected using antibiotics, were picked with a sterile inoculation loop under laminar flow and transferred to a new plate containing the same antibiotics to minimize the chance of false positives. For the mentioned primer combinations, five colonies from each plate were picked and transferred to clean Eppendorf tubes containing 100 µL of ddH_2O. DNA extraction was achieved by boiling the samples in the microwave oven for 4 minutes at maximum efficiency. The colony PCR reaction was performed by mixing components listed in **Table 11** and performed as stated in **Table 12**.

Table 11: PCR reaction for colony PCR performed on both E. coli and P. aeruginosa.

Reagents	**Final concentration**	**Volume**
RedTaq 2x	1x	12.5µL
Forward primer	0.4 µM	0.5 µL
Reverse primer	0.4 µM	0.5 µL

Supernatant of the boiled cell mixture containing DNA		2 µL
ddH_2O		9.5 µL
Total volume		25 µL

The samples were mixed in PCR tubes before transferring to the PCR machine and applying the following PCR conditions.

Table 12: PCR conditions for colony PCR of CbpD-pGM931 in E. coli and P. aeruginosa.

PCR conditions (Temperature and duration)	**Cycles**
94°C (2 minutes)	1x
94°C (30 seconds)	35x
55°C (30 seconds)	
72°C (60 seconds)	
72°C (7 minutes)	1x

PCR reactions were confirmed on 1% Agarose gels described in section **3.2.1**. The colonies showing the correct product were picked. The purified plasmid DNA from the positive colonies was submitted for sequencing to confirm the verification.

3.7 Cultivation of bacteria

3.7.1 Preparation of glycerol stocks for long term storage of bacteria

Materials:

- Bacterial colonies
- LB medium
- Antibiotics (Carbenicillin, Ampicillin and Kanamycin)

- 13 mL cultivation tubes (Sarstedt)
- Incubator 37°C, Scientific Innova 44 (Eppendorf)
- Sterile 85% glycerol
- 2 mL cryogenic tubes (Sarstedt)

Method:

After transformation described in section (**3.4.5** and **3.4.7**), and PCR confirmation described in section (**3.2.1**) bacteria containing the correct plasmid were selected using the appropriate antibiotics stated in **Table 5** on LB agar plates. Preparation of glycerol stocks was performed by picking one colony with a sterile inoculation loop and inoculating 5 mL LB supplemented with the appropriate antibiotic in a 13 mL culture tube. After inoculation, the culture was transferred to a 37°C incubator with 200 rpm agitation for cultivation overnight. The following day, 830 µL of cell culture was transferred to a 2 mL cryogenic micro tubes containing 170 µL sterile 85% glycerol before transferring the 2 mL cryogenic tubes to the -80°C freezer.

3.7.2 Small scale cultivation of bacteria in Erlenmeyer flasks

Small scale cultivation in Erlenmeyer flasks was performed when creating inoculum cultures used in large scale protein production.

Materials:

- Erlenmeyer flask 100-500 mL
- LB medium
- Antibiotics (Carbenicillin or Kanamycin)
- Incubator 37°C, Scientific Innova 44 (Eppendorf)

Method:

Shaker flasks allowed cultivation of bacteria in incubators at fixed temperatures and agitation. The choice of flask was performed using a general rule stating that the media volume should represent approximately 25% of the total Erlenmeyer flask volume, allowing sufficient headspace. To ensure sufficient aeration, flasks with internal tabs increased the agitation of the culture (also referred to as baffled flasks). The media was always transferred to a sterile Erlenmeyer flask and closed using aluminium foil. Cell cultures were prepared by transferring cells from glycerol stocks using a sterile 1-10 µL pipette tip to LB medium containing the appropriate antibiotic. The Erlenmeyer flasks were secured on adhesive mats ensuring no spillage occurred.

3.7.3 Cultivation of *P. aeruginosa* for expression of CbpD

The rCbpD$_{PA}$ variants were expressed with the inducible pGM931 expression vector. The expression vector contains an araBAD operon consisting of the AraC protein and the pBAD promotor. Without arabinose present, the two subunits of the AraC protein bind together and loop the DNA. RNA polymerase is not able to bind the promotor region which is hidden in the DNA loop. During induction, arabinose was added which binds to both the AraC subunits, releasing the DNA loop which mediates the recruitment of RNA polymerase on the pBAD promotor (Schleif, 2010). Several methods were utilized to obtain an optimized cultivation strategy for *P. aeruginosa.*

3.7.3.1 Large scale cultivation in Erlenmeyer flasks

Materials:

- Glycerol stocks of rCbpD$_{PA}$
- LB medium
- Arabinose (100 mg/mL)
- Carbecillin (200 mg/mL)
- 2000 mL Nalgene Erlenmeyer shaker flasks.

- Antifoam 204 (Invitrogen)
- Incubator 37°C, Scientific Innova 44 (Eppendorf)
- Centrifuge, Avanti J-25s (Beckmann Coulter)

Method:

An overnight culture of a *P. aeruginosa* PA14 rCbpD$_{PA}$ variant was prepared for inoculation as described in section **3.7.2**. The following day 500 mL LB medium was transferred to a sterile 2000 mL Erlenmeyer flask and supplemented with 50 µL (100mg/mL) Arabinose and 750 µL (200 mg/mL) Carbenicillin for the final concentrations respectively 10 mg/L and 300 µg/mL. Inoculation was performed by adding 10 mL of overnight culture to the media before adding 150 µL of antifoam. After all additives were added the flask was transferred to the incubator holding 37°C with 200 rpm agitation for approximately 16-18 hours.

Harvesting the cell cultures was performed using 500 mL centrifugal flasks in the JA-10 rotor for 10 minutes at 8000 g in the Avanti J25 series centrifuge.

3.7.3.2 Cultivation of bacteria in the Lex-48 bioreactor.

Cultivation using the Lex-48 bioreactor system allows agitation and aeration by using an air flow dispersed through a porous sparger stone resulting in efficient cultivation of bacteria.

Materials:

- Glycerol stocks of rCbpD$_{PA}$ variant
- LB or BHI medium
- Carbecillin (200 mg/mL)
- Arabinose (100 mg/mL-250 mg/mL)
- Antifoam 204 (Invitrogen)
- Lex-48 bioreactor (Epiphyte3)
- Sparger threaded caps (Epiphyte3)
- Centrifuge, Avanti-J25s (Beckmann Coulter)

Method:

Cultivation in LB medium:

An overnight culture of a *P. aeruginosa* PA14 rCbpD$_{PA}$ variant was prepared for inoculation described in section **3.7.2**. The following day, 1 L of sterile LB medium was inoculated with 25-100 mL overnight culture supplemented with 1.5mL 200 mg/mL carbenicillin and 100 mg/mL arabinose for the final concentrations respectively 300 µg/mL and 10-1000 mg/L. The culture was divided into 1 L blue cork bottles with a total of 500 mL in each before adding 150 µL of antifoam. Sparger lids were placed on the bottles prior to transferring them from the laminar flow sterile bench to the Lex-48 bioreactor system. The culture was cultivated overnight (approximately 16-18 hours) at room temperature (22-25°C) before harvesting using the JA-10 rotor in the Avanti J25s at 8000 rpm for 15 minutes at 4°C.

Cultivation in BHI medium:

The use of BHI followed the same method as LB medium, however, optimizations of arabinose and inoculum volumes were not performed. Resulting in the use of 25 mL inoculum and 10 mg/L arabinose.

3.7.4 Cultivation of *E. coli* for expression of CbpD

The cultivation protocol for expression of rCbpD$_{EC}$ was previously established by laboratory manager Anne Cathrine Bunæs and adapted in this project. The *E. coli* expression vectors contain the *lac* operon which binds an allosteric repressor to inhibit RNA polymerase to bind the promoter. During induction, IPTG is added which binds the repressor and allosterically changes the repressor conformation, releasing the repressor (Parker, 2001).

Materials:

- LB medium
- TB 1.1 x medium
- Kanamycin (100 mg/mL)
- 0.17M K_2HPO_4 + 0.72 M KH_2PO_4 buffer
- IPTG 1 M (Sigma)

- Antifoam 204 (Invitrogen)
- ddH_2O
- Centrifuge, Avanti J25s (Beckmann Coulter)
- Incubator 37°C, Scientific Innova 44 (Eppendorf)
- Cell density meter, Ultrospec 10 (Biochrom)

Method:

An overnight culture of a rCbpD$_{EC}$ variant was prepared for inoculation as described in section **3.7.2**, in LB medium supplemented with 50 µg/mL Kanamycin. Inoculation was performed by adding the following to 0.9L of TB 1.1x.

- 25 mL overnight culture
- 25 mL 0.17M K_2HPO_4 + 0.72 M KH_2PO_4 buffer
- 100 mg/mL Kanamycin
- 50 mL ddH_2O

After inoculating, the culture was divided into 1 L blue cork bottles with a total of 500 mL in each before adding 150 µL of antifoam. The cultures were transferred to a 37°C incubator with 180 rpm agitation until the OD_{600} reached 0.6-0.8. After reaching the correct OD, the cultures were induced with 100 µL 1M IPTG to a final concentration of 0.2 mM. Subsequently, the cultures were transferred to the Lex-48 bioreactor system and grown at room temperature (22-25°C) overnight (approximately 16-18 hours) before harvesting the cells using the JA-10 rotor at 8000 rpm for 10 minutes at 4°C in the Avanti J25s centrifuge.

3.7.5 Monitoring growth curves in microtiter plates

Experiments which were dependent on investigating the growth curve prior to cultivation, were initially monitored using 96 well microtiter plates. The VarioSkan Lux (Thermo Scientific) allows the measurements of OD_{600} in microtiter plates with both temperature and agitation control. In addition, small scale experiments allow for high throughput analysis of bacterial growth under several different conditions. This system was used during this study to establish

optimal glucose concentrations in viability assays. Minimal media optimization required the investigation of several concentrations which was simplified by high throughput analysis in 96 well microtiter plates.

Materials:

- M9 minimal salts (2x) (Gibco)
- $MgSO_4$ (0.5 M)
- $CaCl_2$ (10 mM)
- Glucose (2%) w/v
- NUNC 96 well microtiter plates (Thermo Scientific)
- CellStar® tubes, 15 mL
- Culture tubes, 13 mL (Sarstedt)
- Petri dishes (Heger)
- Incubator 37°C, Innova 44 (Eppendorf)
- Incubator 37°C, (Termarks)
- Plate reader, VarioSkan Lux (Thermo Scientific)
- Centrifuge, Allegra X-30R (Beckmann Coulter)

Method:

Minimal media only containing the salts required to sustain growth was established, M9 1x (Gibco), 2 mM $MgSO_4$ and 0.1 mM $CaCl_2$ hereafter referred to as $M9_{Minimal}$.

The $M9_{Minimal}$ media contains no carbon source, therefore, growth curve analysis using different concentrations of glucose was performed. $M9_{Minimal}$ was supplemented with descending glucose concentrations for determination of the optimal glucose concentrations. The following concentrations were investigated with LB as a control **Table 13**.

Table 13: Concentrations of glucose used for establishing the ideal concentrations.

Samples	Glucose g/L	Dilution
1	2	1x
2	1	2x
3	0.5	4x
4	0.25	8x
5	0.125	16x

6	0.0625	32x
7	0.03125	64x
8	LB	

Inoculum of *P. aeruginosa* PA14 was prepared by plating a small loop of bacteria from the glycerol stock on BHI plates without any antibiotics and transferred to 37°C incubator. The following day, one colony was transferred to 5 mL LB in a 13 mL culture tube without antibiotics and incubated at 37°C with 200 rpm agitation for overnight growth. Subsequently, the bacteria were washed in PBS by centrifugation at 4 700 rpm for 10 minutes of the overnight culture before suspending the pellet in 10 mL PBS, thereafter the cells were centrifuged at 4700 rpm for 10 minutes before resuspending in $M9_{Minimal}$.

The different media were prepared in 15 mL CellStar® tubes containing $M9_{Minimal}$ supplemented with the glucose concentration specified in **Table 13**. After preparing the media, 3.42 mL of each media was transferred to petri dishes. Following the transfer, triplicates of 150 µL were transferred using a multi-channel pipette to a 96 well microtiter plate creating blanks for each media. After the transfer, 2.97 mL of media remained in the petri dishes. Thereafter, 30µL of the inoculum was mixed with the remaining media creating a 1:100 dilution of the bacteria. After thoroughly mixing, 150 µL triplicates of the inoculated media were transferred adjacent to the blank media samples. After pipetting, a clear plastic film covered the plate and small holes were made in the corner of the film to ensure oxygen entering the wells.

Growth was measured using the Varioskan Lux (Thermo Scientific) holding 37°C during the growth over 48 hours. OD_{600} was measured every 15 minutes with 200 rpm shaking for 15 seconds initiated 30 seconds before measurement to ensure homogeny in the wells before measuring.

3.8 Extraction of proteins

3.8.1 Extraction of periplasmic proteins

Protein variant containing the signal peptide were secreted to the periplasm. Proteins situated in the periplasm can be extracted by osmotic shock as described below, (gram-negative bacteria

contain a thin peptidoglycan resulting in vulnerability against osmotic pressure). In the osmotic shock procedure, the cells shrink in a high sucrose buffer prior to shifting the cells to ice cold ddH_2O, which ruptures the outer membrane and releases the periplasmic fraction (Neu & Heppel, 1965).

Materials:

- Spheroplast buffer
- Cell pellet (**3.7.3,3.7.4**)
- $MgCl_2$ (20 mM)
- cOmplete™ Protease Inhibitor Cocktail Tablet (Roche)
- phosStop (Roche)
- PMSF (50 mM)
- Ice cold ddH_2O
- Ice
- Stericup® 0.22 µM
- Centrifuge, Avanti J25s

Method:

A cell pellet obtained from either cultivation of *P. aeruginosa* or *E. coli* was first resuspended in 30 mL spheroplast buffer, followed by centrifugation at 8000 g for 10 minutes to pellet the cells again. After centrifugation, the supernatant was decanted, and the pellet was incubated at room temperature for 30 minutes. After incubation, the cells were resuspended in 30 mL ice cold ddH_2O supplemented with Complete™ Mini EDTA free protease inhibitors and PhosSTOP both with a final concentration of 1 tablet/ 10mL ddH_2O. After resuspension, the mixture was incubated on ice for 45 seconds before adding $MgCl_2$ (20 mM) to the final concentration of 1 mM. Following the incubation, the cell mixture was transferred to 30 mL centrifugal tubes. Using the JA25.50 rotor and centrifuged at 22 000 rpm for 15 minutes, the supernatant was decanted and passed through 0.22µm filter. After filtration, PMSF was added

to the periplasmatic extract to the final concentration of 1 mM and the extract was stored at 4 °C prior to purification.

3.8.2 Extraction of cytosolic proteins

Truncated variants of rCbpD$_{EC}$ without a signal peptide were extracted from the cytosolic protein fraction. These proteins were expressed in the *E. coli* production system.

Materials:

- Cell pellet (3.7.3,3.7.4)
- Binding buffer (IMAC)
- PhosSTOP (Roche)
- cOmplete™Mini EDTA free protease inhibitor cocktail tablet (Roche)
- Lysozyme (Sigma)
- DNase 1 (NEB)

Method:

The harvested cell pellet was resuspended in 30 mL ice cold binding buffer (IMAC) supplemented with Complete™ Mini EDTA free protease inhibitors and PhosSTOP both with a final concentration of 1 tablet/10mL buffer. After resuspending the pellet, 3µL of DNase 1 and 300 µL 10mg/mL lysozyme was added before incubating on ice for 30 minutes while shaking the mixture every 10 minutes. Extraction of proteins from the cytosol was performed using one of the following methods.

3.8.2.1 Cell lysis achieved by sonication

Sonication utilizes a high frequency vibration to disrupt cell membranes and retrieve proteins from the cytosol.

Materials:

- 70% ethanol v/v
- ddH_2O
- Centrifuge, Avanti J25s
- Vibra Cell (Sonics)
- CellStar® tubes, 50 mL
- Ice
- Stericup® 0.22 µM (Merck)

Method:

After incubation on ice as described in section **3.8.2**, the cell suspension was aliquoted into 30 mL fractions placed in 50 mL CellStar tubes, the sonication probe was washed with 70% ethanol before submerging approximately 1 cm into the mixture. Sonication was performed for 10 minutes at 30 % amplitude 5 seconds on and 5 seconds off. The cell lysate was centrifuged using the JA-25.50 rotor at 22 000 rpm for 15 minutes at 4°C before decanting and filtering the supernatant through a 0.22 µm filter.

Equipment failure in the laboratory resulted in establishing the microfluidizer method.

3.8.2.2 Cell lysis achieved by microfluidizer

The microfluidizer utilizes an abrupt change in pressure to rupture the cells. For *E. coli* the manufacturer instructions specify 15 000 psi as optimal.

Materials:

- 70% ethanol v/v
- ddH_2O
- Microfluidizer LM20 (Siemens)
- Centrifuge, Avanti J25s
- Stericup® 0.22 µM (Merck)

Method:

The microfluidizer sample application cylinder was stored in 70% ethanol, which was washed out with 2 x 300 mL ddH_2O before sample application. The sample was applicated in the sample reservoir and passed through the microfluidizer at 15 000 psi rupturing the cells. The cell lysate was centrifuged using the JA-25.50 rotor at 22000 rpm for 15 minutes at 4°C before decanting the supernatant and filtering through a 0.22µm filter.

After the cell lysate was collected, the microfluidizer tubing was washed with ddH_2O and 70 % ethanol the sample application cylinder was stored in 70% ethanol.

3.9 Purification methods

3.9.1 Immobilized metal affinity chromatography (IMAC)

IMAC purification was performed for protein variants containing a His-Tag fusion tag.

Materials:

- Binding buffer (IMAC)
- Weak/strong wash buffer (IMAC)
- Elution buffer (IMAC)
- Protein extract
- HisTrap HP 5 mL column (GE Healthcare)
- 20% Ethanol v/v
- ddH_2O
- Äkta Start (GE Healthcare)

Method:

Purification was performed using Äkta Start combined with the HisTrap HP 5 mL column. IMAC purification was performed manually at the constant flowrate of 2 mL/min. The system tubing and HisTrap HP 5 mL column were stored in 20% ethanol. Prior to purification, the storage ethanol was flushed with 5 column volumes ddH_2O prior to buffer equilibration to prevent buffer interactions with ethanol. The choice of Wash buffer (IMAC) was decided based on the downstream application of the protein. If further purification using SEC was planned, the weak wash buffer (IMAC) was used, resulting in a higher yield with more contaminants. If the sample was not to be purified further, the strong wash buffer was used, resulting in a purer protein sample with a lower yield. However, the following general protocol was constant for all IMAC purifications performed.

Before applying the sample, the column was equilibrated by running 5 column volumes (CVs) of binding buffer (IMAC) through the column before autozeroing the UV detector. Following the autozeroing, the sample was loaded using the sample applicator pump (maximum 75 mL). After sample application, the binding buffer (IMAC) was passed through the column, removing unspecific binding until the UV signal stabilized. After the UV had stabilized, the strong/weak wash buffer (IMAC) was applied while simultaneously collecting the wash fraction, the washing step continued until the UV signal stabilized again. Finally, the protein was eluted with the elution buffer (IMAC) and 2 mL fractions were collected. After being used, the system tubing and column were washed with ddH_2O prior to storing the tubing and column in 20% ethanol.

After purification the system tubing and column was flushed with ddH_2O before storing the system tubing and column in 20% ethanol. Protein samples from the protein extract, column flow through during sample application, wash fraction and elution fractions were analysed using SDS-PAGE gel analysis as described in section **3.2.2**. If further purification was planned, all elution fractions were collected for protein concentration. However, if further purification was not planned, only the purest elution samples (>90%) were concentrated as described in section **3.10**. Following the protein concentrating step, the protein concentration was determined by Bradford protein concentration determination assay described in section **3.11.1**.

3.9.2 Hydrophobic interaction chromatography (HIC)

Materials:

- Ammonium sulphate (NH_4SO_4)
- Binding buffer (HIC)
- Elution buffer (HIC)
- HiTrap Phenyl FF HS 5 mL column (GE Healthcare)
- 20 % Ethanol v/v
- ddH_2O
- 50 mL CellStar® tube
- Eppendorf tubes, 2 mL
- Äkta start (GE Healthcare)

Method:

The protein sample was prepared for HIC purification by adjusting the sample to approximately 1 M ammonium sulphate (NH_4SO_4). The salt was added slowly into the protein sample while simultaneously stirring with a magnet stirrer. Once the protein sample was adjusted, the sample was stored at 4°C until the HIC purification was initiated.

The HiTrap Phenyl FF HS 5 mL column on the Äkta start were used for HIC purification. The purification was performed automatically at the constant flowrate of 2 mL/min. The system tubing and HisTrap HP 5 mL column were stored in 20% ethanol. Prior to purification, the storage ethanol was flushed with 5 column volumes of ddH_2O before buffer equilibration, to prevent buffer interactions with the storage ethanol. The buffer A tubing was placed elution buffer (HIC) while buffer B tubing was placed in the binding buffer (HIC). Before starting, the sample application tubing was equilibrated with binding buffer (HIC) prior to placing the tubing in the sample. An automatic HIC protocol was created, and purification was performed as follows.

Firstly, the column was equilibrated with 10 column volumes (CVs) of binding buffer (HIC). Following the column equilibration, the sample was applied through the sample application pump while simultaneously collecting the flow through in 50 mL CellStar® tubes. After the sample was loaded on the column, 8 CVs were passed through the column as a washing step and removing un-specific binding. After the washing step was completed, a gradient was employed by increasing the concentration of the binding buffer (HIC) over 20 CV while simultaneously collecting 2 mL fractions. Following the elution gradient, 25 mL of ddH_2O was

applied washing out all remaining bound protein. After being used, the system tubing and column were washed with ddH_2O prior to storing the tubing and column in 20% ethanol.

After HIC purification, peak fractions from the elution gradient, flow through, protein extract and ddH_2O elution peaks were analysed using SDS-PAGE described in section **3.2.2**. HIC purified protein required SEC purification, therefore, the fractions containing the protein of interest were pooled and concentrated to the final volume of 1 mL as described in section **3.10**. The concentrated protein sample was subsequently purified further with SEC purification as described in section **3.9.4**.

3.9.3 Ion exchange chromatography (IEX)

Theoretical pI was established using the CbpD sequence without signal peptide with the Protparam tool on ExPASy to select the correct column.

Materials:

- Binding buffer (IEX)
- Elution buffer (IEX)
- HiTrap Q FF 5 mL Anion exchange column (GE Healthcare)
- 20 % Ethanol (v/v)
- ddH_2O
- NaCl 1M
- CellStar® tube, 50 mL
- Eppendorf tube, 2 mL
- Äkta start (GE Healthcare)

Method:

IEX purification was performed with the HiTrap Q FF 5 mL column on the Äkta start. The purification was performed with an automatic method with a constant flowrate of 2 mL/min. The system tubing and HiTrap Q FF 5 mL column were stored in 20% ethanol. Prior to purification, the storage ethanol was flushed with 5 column volumes of ddH_2O before buffer equilibration, to prevent buffer interactions with the storage ethanol. The Buffer tube A was placed in the binding buffer (IEX), buffer tube B was placed in the elution buffer (IEX). The sample application tube was flushed with binding buffer (IEX) prior to placing the sample application tube in the protein sample.

Firstly, the column was equilibrated with 5 column volumes (CVs) of binding buffer (IEX). Following the equilibration, the protein sample was applied while simultaneously collecting the flow through in 50 mL CellStar® tubes. After sample application, the column was washed with 10 CVs binding buffer (IEX) removing un-specific protein binding. Following the washing step, a gradient elution was performed by increasing the elution buffer (IEX) concentration from 0-100% over 20 CVs while simultaneously collecting 2 mL fractions. Finally, 1 M sodium chloride (NaCl) was applied to elute all bound protein. After being used, the system tubing and column were washed with ddH_2O prior to storing the tubing and column in 20% ethanol.

Fractions from the protein extract, flow through and peaks during gradient elution were analysed further on SDS-PAGE as described in section **3.2.2**. The protein fractions of interest identified with SDS-PAGE were collected, for either further purification or protein concentrating as described in section **3.10** and determining the protein concentration as described in section **3.11.1**.

3.9.4 Size exclusion chromatography (SEC)

Materials:

- SEC buffer
- SEC column storage buffer
- ddH_2O
- 20% Ethanol (v/v)
- HiLoad 16/600 column (GE Healthcare)
- 10 mL syringe
- 1 mL syringe

- 0.7 mm injection needle (GE Healthcare)
- Eppendorf tubes, 2 mL
- Äkta purifier system (GE healthcare)

Method:

Further purification of protein samples was achieved by SEC purification. The following protocol was based on the pre-analysis of the CbpD elution pattern. The purification was performed using the HiLoad 16/600 column on the Äkta purifier system. Prior to buffer equilibration, both the column and Äkta purifier system tubing was flushed with ddH_2O to remove the storage solutions, respectively (20% ethanol + 0.2 M Sodium acetate ($NaCH_3COO$) and 20% ethanol). Following the washing step, the column was equilibrated with the SEC buffer, and equilibration was achieved once the conductivity signal had increased and stabilized. After column equilibration, the flowrate was reduced to 0.2 mL/min. Prior to applying the sample, 10 mL SEC buffer was flushed through the sample tubing using a 10 mL syringe. After washing the sample tube, the protein sample was transferred to a 1 mL syringe and injected into the sample tubing. Once the sample was loaded the flowrate was increased from 0.2-1 mL/min over a 10 minute time span.

Fractionation was initiated at 40 minutes after sample application and 3 mL fractions were collected. At the 60 minute mark the fractionation volume was set at 1.5 mL and collected in 2 mL Eppendorf tubes. The proteins of interest eluted at approximately 65-70 minutes. The purity of the fractions was determined with SDS-PAGE as descried in section **3.2.2**. Pure protein fractions were concentrated as described in section **3.10** before measuring the concertation as described in section **3.11.2**.

3.9.5 Chitin bead affinity chromatography

Chitin bead affinity chromatography utilizes a chitin resin to retain proteins with chitin affinity. This method was attempted during $rCbpD_{PA}$ Native purification. Studies reported in literature show that CbpD retains affinity towards chitin (Jindra Folders, 2000). Initial screening was performed with several elution buffers to evaluate the viability of chitin bead affinity chromatography for this study.

Materials:

- Chitin resin (NEB)
- 100 mM EDTA pH 8
- 0.2 M acetic acid (CH_3COOH) pH 3
- 1 M N-acetylglucosamine
- 0.05 M hydrochloric acid (HCl)
- Protein extract from the periplasm of $rCbpD_{PA}$ Native
- CellStar® tubes, 15 mL
- β-Chitin 0.85mm particle size (Squid pen, France Chitin)
- Multi RS-60 rotator (Biosan)
- ThermoMixer™C (Eppendorf)
- Centrifuge, Allegra X-30R (Beckmann Coulter)
- Centrifuge, 5418R (Eppendorf)
- ddH_2O

Method:

The chitin resin was washed by adding 1 mL of chitin resin a 15 mL CellStar® tube and centrifuged in the Allegra X-30R centrifuge at 4700 rpm for 15 minutes before decanting the supernatant. The chitin bead pellet was resuspended in 10 mL ddH_2O before centrifuging again. The washing step was performed three times. Following the washing steps, 10 mL of the periplasmic protein extract was transferred to the washed chitin resin pellet. The resin-protein mixture was agitated in a multi RS-60 rotator at low speed for 60 minutes at room temperature. After incubating, the chitin-protein mixture was washed twice with 10 mL PBS by centrifuging at 4700 rpm to remove un-specific protein binding. After washing the pellet with PBS, elution was performed by adding 500 µL of the elution solution to the chitin pellet with enzyme bound. The chitin resin and elution solution were transferred to 2 mL Eppendorf tubes and incubated at room temperature with 600 rpm agitation for 15 minutes in a Thermomixer™ C. After incubation, the tubes were centrifuged for 10 minutes at 16 700 rpm before retrieving the supernatant and analysing the elution fractions using SDS-PAGE as described in section **3.2.2**.

3.10 Protein concentrating and buffer exchange

After purification the protein was situated in an elution buffer. In addition, the protein sample was eluted in several fractions resulting in a larger volume of diluted protein. Before using the protein in assays and analysis, the protein was concentrated while simultaneously exchanging the buffer for suitable downstream analysis. Full length rCbpD$_{EC/PA}$ is 39 kDa in size, allowing the use of Vivaspin Polyether sulfone (PES) with a 10 000 molecular weight cut off (MWCO). However, for the truncated variants rCbpD$_{EC}$ M2+M3 and rCbpD$_{EC}$ M1 respectively 23 and 16 kDa, the Vivaspin PES with a 3 500 MWCO was used.

Materials:

- Vivaspin 20 centrifugal concentrators 3 500-10 000 MWCO (Sartorius)
- Protein samples
- Protein sample buffer
- Centrifuge, Allegra X-30R

Method:

The protein fractions were loaded in the reservoir compartment of the centrifugal concentrator before adjusting the volume to 20 mL with the exchange buffer. Centrifugation was performed at 4700 rpm at 4°C until the volume had reduced to 1 mL. This was repeated a total of 3 times resulting in an 8000x dilution of the elution buffer. The 1-2 mL protein sample was transferred to a new container before measuring the concentration of the protein described in section **3.11**.

3.11 Protein concentration determination

3.11.1 Bradford protein assay

Bradford protein assay is a quick method for quantification of protein which involves binding of Coomassie brilliant blue G-250 to protein. The binding mechanism shifts the absorption maximum of the dye from 465 nm to 595 nm (Bradford, 1976). The measurement was

performed using a spectrophotometer which was calibrated with BSA standards from 0-1.25 mg/mL. The calibration was prepared and conducted by the laboratory manager.

Materials:

- Bio Rad protein assay (Bio-Rad)
- Protein sample
- Protein sample buffer
- BioPhotometer D30 (Eppendorf)
- Micro cuvettes (Eppendorf)
- Eppendorf tubes, 1.5 mL
- Vortex, MS3 basic (IKA)

Method:

To eliminate the contribution of buffer components to the absorbance, both the blank and protein samples were diluted using the exact same buffer as the protein was dissolved in. The following reaction scheme was performed.

Table 14: Bradford protein quantification assay reaction scheme.

Contents	**Blank**	**Sample**
Buffer	800 µL	795 µL
Bio Rad protein assay	200 µL	200 µL
Protein	-	5 µL

Firstly, buffer and protein were combined before adding protein dye. Samples were vortexed to ensure homogeny and incubated on the laboratory bench for 5 minutes before measuring, as per manufacturer instructions. The spectrophotometer was first blanked before measuring the triplicates at 595 nm. After measuring, the triplicates were averaged and corrected for the dilution factor using the following calculations.

$$\frac{5\ \mu L\ \text{protein}}{800\ \mu L\ \text{Buffer} + 5\ \mu\text{L protein}} = 0.00625\ \text{dilution factor}$$

$$\frac{\text{Measured concentration } \mu g/mL}{\text{Dilution factor}} = \text{protein concentration } \mu g/mL$$

3.11.2 Absorbance at 280 nm (A_{280})

Determining the protein concertation using absorbance of 280 nm (A_{280}) was used to determine the protein concentration of pure protein with the theoretical extinction coefficient of all rCbpD variants. Using the Protparam tool supplied by ExPASy the extinction coefficient was determined using the amino acid sequence without the signal peptide. Absorptivity at 280 nm is specific to each protein and dependant on the aromatic rings in tryptophan and tyrosine and disulphide bonded cysteine residues (Simonian, 2002).

Materials:

- Protein sample
- Protein sample buffer
- D30 BioPhotometer (Eppendorf)
- µCuvette® (Eppendorf)
- Lens tissue paper
- ddH_2O

Method:

The Eppendorf µCuvette® was cleaned using ddH_2O and lens cleaning paper. After cleaning, 2 µL of buffer was placed within the sample holder before closing the µCuvette® creating an optical pathlength of 1 mm. After blanking the instrument with buffer, the µCuvette® was cleaned using lens paper before applying the samples. The A_{280} absorbance values were noted and the concentration was calculated.

$$\text{Concentration mg/mL} = \frac{Absorbance}{Extinction\ coefficeint\ \times path\ length} \times Molecular\ weight$$

3.11.3 Absorbance at 205 nm (A_{205})

During proteomic analysis proteins were digested, resulting in the possibility for peptide chains not containing tyrosine and tryptophan. In addition, the sample volumes of proteomic samples are low. These limitations excluded the use of Bradford (**3.11.1**) and A_{280} (**3.11.2**) methods. The peptide bond in proteins absorb 205 nm UV light, allowing the determination of peptide concentration. However, the method uses the assumption that 1 mg/mL is equal to an absorbance value of 31 (Simonian, 2002).

Materials:

- Peptide sample
- NanoDrop One (Eppendorf)
- Peptide solvent (2% ACN, 0.1% TFA)
- ddH_2O
- Lens tissue paper

Method:

Using the Nanodrop One (Eppendorf), the pedestal was first clean using ddH_2O before blanking the system by placing 2 µL of peptide solvent on the pedestal and closing the sample carrier arm to create the optical pathway. Thereafter, the samples were analysed, and the concentration was calculated using the assumption of 1 mg/mL is equal to the absorbance value 31. The Nanodrop One software performed the calculations, and the path length (0.03-1.0 mm) was auto ranging depending on the surface tension of the sample.

$$\text{Concentration (mg/mL)} = \frac{\text{Absorbance}}{31 \times \text{Path length}}$$

3.12 Enzyme activity assay

Enzyme assays were performed to ensure that the protein was active and that the correct protein had been isolated and purified. In addition, activity assays were performed during characterization of rCbpD. Mutants were screened by observing differences in chitin oligomer product profiles and product production followed over time.

Materials:

- β-Chitin (France Chitin)
- Tris-HCl pH 7 (1M)
- $CuSO_4$ (5 mM)
- Ascorbic acid (250 mM)
- ddH_2O
- rCbpD variants
- 2 mL Eppendorf tubes
- Thermomixer™ C (Eppendorf)
- Centrifuge, 5418 R (Eppendorf)
- Vortex, MS 3 basic (IKA)

Method:

The activity assays were performed with and without ascorbic acid as a reductant for control measures. In addition, enzyme assays planned to only investigate the general presence of activity were added exogenous copper sulphate ($CuSO_4$).

Table 15: Chitin activity assay experiment conditions.

Reagents	**End concentration**	**Volume**
β-Chitin (20 g/L)	10 g/L	100 µL
Tris-HCl pH 7 (1M)	20 mM	4 µL
$CuSO_4$ (5mM)	30 µM	1,2 µL
ddH_2O		Up to 200 µL
Ascorbic acid (250 mM)	1 mM	0,8 µL
rCbpD variant (1µM)	1 µM	
Total volume	-	200 µL

Firstly β-Chitin, Tris-HCl pH 7 and CbpD were combined and incubated at room temperature for 5 minutes. After incubation, the rest of the reagents were added and mixed well by vortex

before briefly centrifuging to settle the mixture. Thereafter, the Eppendorf tubes were transferred to a Thermomixer™ C (Eppendorf) and incubated for 2 hours at 37°C, with 600 rpm agitation. After incubation the samples were centrifuged at 16 700 rpm for 5 minutes in a Centrifuge 5418 R (Eppendorf), the supernatant was analysed further by either HILIC or MALDI-TOF MS.

3.12.1 MALDI-TOF MS analysis of oxidized chitin oligomers

Materials:

- UltraFlextreme MALDI-TOF-MS (Bruker)
- MTP 384 ground steel BC MALDI-TOF target plate (Bruker)
- MTP Target Fame III (Bruker)
- 2,5 Dihydroxybenzoic acid (DHB) (Bruker)
- Chitooligomer samples

Method:

MALDI-TOF MS analysis of oxidized chitin oligomers was performed on the supernatant of enzyme assays designed to assess the presence of activity in rCbpD variants as described in section **3.12**.

After the samples were centrifuged to settle the chitin particles, 1 µL of the supernatant was retrieved with a pipette and mixed with 1 µL of DHB matrix in the cap of a PCR tube. The sample-matrix mixture was mixed by pipetting up and down. After mixing, 0.5 µL was transferred to the MTP 384 ground steel BC MALDI-TOF target plate and the spots were dried in room temperature. Following the drying of the spots, the target plate was fitted on the MTP Target Fame III and placed in the MALDI-TOF MS.

The laser method utilized, fired 1000 shots without laser wandering with an intensity of 40-60%. One spectrum was comprised of a 1000 shot run, during analysis the sum of 5-6 spectra created the result spectrum for the sample. After saving the spectra for each sample, the spectra were opened in the analysis software, peak masses were automatically annotated by the

software. However, the oxidized chitin oligomers were manually annotated the spectra after analysis.

3.12.2 Analytical HILIC analysis of oxidized chitin oligomers

Analytical hydrophilic interaction liquid chromatography (HILIC) analysis was performed to relatively quantify oxidized products produced during an enzyme assay. The assay was performed as described in section **3.12**.

Materials:

- Buffer A Tris-HCl pH 8, (15 mM)
- Buffer B Acetonitrile (100%)
- Supernatant from enzyme assay
- In-house produced oxidized standards of $[GlcNac]_2$-$[GlcNac]_6$ supplied by Sophanit Mekasha PhD
- HPLC Vials and caps
- ddH_2O
- HPLC, Agilent 1290 (Agilent technologies)
- 150 mm BEH amide 1.7 µM column (Acquity)

Method:

HILIC was performed using the 150 mm BEH amide 1.7 µM column in the Agilent 1290 HPLC system. Sample preparation was performed by transferring 13 µL of the supernatant obtained from the chitin activity assay as described in section **3.12** into HPLC vials containing 37 µL acetonitrile. In addition to the oxidized product samples, one ddH_2O sample with 13 µL ddH_2O and 37 µL acetonitrile was also prepared. The HPLC vials were capped with HPLC caps and placed in the sample tray. The ratio of 13 µL of sample to 37 µL of acetonitrile equates to the initial buffer system ratio of 74% acetonitrile.

HILIC analysis was performed with the Chromeloen 7 software. The Agilent 1290 HPLC system tubing and column were stored in 26% ddH_2O and 74% acetonitrile, before initiating sample application, the column was equilibrated with 26% Tris-HCl pH 8 and 74% acetonitrile by ramping the flowrate from 0-0.4 mL/min over a 2 hour period. Following the column equilibration, a sample queue was prepared in the software. The first three samples were 10 µL injections of the ddH_2O sample ensuring the gradient profile did not show any obvious errors. After the ddH_2O samples were applied, 10 µL injections of the chitin oligomers samples were applied.

Chitin oligomers were detected using two UV signals, both 205 nm and 195 nm were recorded. For analysis of the chitin oligomers, a 12 minute gradient was executed at 0.400 mL/min with initial concentrations A: 26% 15 mM Tris-HCl pH and B: 74% Acetonitrile. Column equilibration was performed with 5 minutes of the initial A and B concentrations. Thereafter, a 2 minute gradient decreasing the B concentration from 74-62% before holding 62% B for an additional 2 minutes. The B concentration was subsequently increased from 62-74% over a 2 minute gradient before holding 74% B for an additional 2 minutes, concluding the 12 minute analysis run. After the sequence of samples was terminated, the chromatograms were analysed in Chromeleon 7 where blank subtraction and peak integration was completed.

3.13 Analysis of bacterial viability and growth

Experiments to verify bacterial viability in chitin supplemented media was initiated and several methods were employed.

3.13.1 Viability determined by OD_{600} and Colony Forming Units (CFU)

Materials:

- M9 minimal salts 2x (Gibco)
- Magnesium Sulphate ($MgSO_4$) 0.5M
- Calcium Chloride ($CaCl_2$) 1M

- Casamino acids (Gibco)
- β-Chitin 20g/L (France Chitin)
- Nunc™ 96 well polystyrene round bottom plates (Thermo Scientific)
- Culture tubes, 13 mL
- Glucose 20% (w/v)
- ddH_2O
- LB medium
- Glycerol stocks *P. aeruginosa* PA14
- BHI plates
- Erlenmeyer flasks 100 mL
- Eppendorf UVette®
- Incubator 37°C, Scientific Innova 44 (Eppendorf)
- Incubator 37°C (Termaks)
- Cell density meter, Ultrospec 10 (Biochrom)
- Sonication waterbath (Grant)

Method:

Inoculum of *P. aeruginosa* PA14 strain was prepared by plating a small loop of bacteria from the glycerol stock on BHI plates without any antibiotics before transferring the plates to a 37°C incubator. The following day, one colony from each was transferred to 5mL LB medium in 13 mL culture tubes without antibiotics and incubated at 37°C with 200 rpm agitation.

The following stock solutions were prepared:

Table 16: Stock solutions prepared for initial investigation of P. aeruginosa growth on chitin

Stock solutions (Final concentration)	**M9 + Glucose + Chitin**	**M9 -Glucose + Chitin**	**M9-Glucose - Chitin**
M9 minimal salts (1x)	30 mL	30 mL	30 mL
$MgSO_4$ (2mM)	240 µL	240 µL	240 µL
$CaCl_2$ (0.1mM)	6 µL	6 µL	6 µL
Casamino acids (0.5%)	1.5 mL	1.5 mL	1.5 mL

β-Chitin (0.5%)	15 mL	15 mL	-
Glucose (0.2%)	1.5 mL	-	-
ddH_2O	11.7 mL	13.2 mL	28.2 mL

A total of 15 mL of the different media was transferred to sterile 100 mL Erlenmeyer flasks. Inoculation was performed with 150 µL of *P. aeruginosa* PA14 inoculum, diluting the LB 100 fold.

Samples were taken at 0h, 2h, 4h, 6h, 24h and 48h. At the given time points, the Erlenmeyer flasks were agitated rigorously and immediately after agitation, 150 µL of cell culture was extracted before directly measuring OD_{600} in Eppendorf UVette. After measuring, a new agitated sample of 150 µL was extracted and transferred to a clean Eppendorf tube. The Eppendorf tubes were sonicated in an ultrasonic cleaner of 90 seconds to dissociate bacteria bound to the chitin particles. The freshly sonicated Eppendorf tube was immediately placed under the laminar flow until the chitin particles had settled. A 96 round bottom microtiter plate was prepared with triplicates of 180µL of PBS in the first 8 wells. Thereafter, 20 µL of chitin free cell culture was added to the first wells mixing thoroughly. After mixing the first wells, a serial dilution was performed by transferring 20 µL with a multi-channel pipette from the first well to the next and step wise moving 20 µL of the diluted culture through all wells. After mixing in the last well, 20 µL was discarded to ensure a consistent volume throughout all wells. The wells contained dilutions from $1x10^{-1}$ to $1x10^{-8}$. Following the serial dilution, a multi-channel pipette retrieved 10 µL from $1x10^{-3}$ – $1x10^{-8}$ dilutions. The dilutions were deposited on the BHI plate by slowly pipetting down while simultaneously moving the multi-channel pipette over the plate in a straight line. Once the dilution was deposited in a straight line, the plate was tilted backwards and forwards to spread out the six dilutions on a single plate. The BHI plates were incubated at 37°C overnight and counted the following day.

The colony formation unit was determined by counting the BHI plates containing colonies in the range of 30-300. Thereafter, the total amount of bacteria present was calculated as follows.

$$\mathrm{CFU/mL} = \frac{\text{Colonies} \times \text{Dilution factor}}{\text{Plated volume (mL)}}$$

3.13.2 Monitoring bacterial respiration by GC-MS

Monitoring the respiration of *P. aeruginosa* PA14 was performed by GC-MS to remediate issues encountered with in-soluble chitin supplemented media. The oxygen consumption and carbon dioxide production were measured with equipment built by the Nitrogen group (NMBU). Prof. Lars Bakken and PhD student Lars Molstad have created the system and established the data analysis software for the system. A detailed description of the system is supplied in the initial publication (Molstad et al., 2007). The system was initially created to monitor denitrifying cultures; however, oxygen and carbon dioxide may also be analysed. During this section the term "air" refers to the atmospheric composition of air (78% N_2, 21% O_2 and 1% other gasses) whilst oxygen refers to 100% oxygen.

Materials:

- 120 mL serum flasks
- 20 mm Butyl rubber stopper (Supleco)
- Serum flask crimp seal (Lab Teknik)
- High standard 10 000 ppm CO_2 (AGA)
- Low standard 780 000 ppm N_2, 210 000 ppm O_2 (AGA)
- Oxygen (AGA)
- Helium (AGA)
- LB medium
- Glycerol stock *P. aeruginosa* PA14
- Culture tubes, 13 mL
- Incubator 37°C, Scientific Innova 44 (Eppendorf)
- Incubator 37°C (Termaks)
- Gas chromatograph, CP-4900 (Varian)

Method:

Inoculum of *P. aeruginosa* PA14, was prepared by plating a small loop of bacteria from the glycerol stock on BHI plates without any antibiotics and transferred to a 37°C incubator. The following day, one colony was transferred to 5mL LB in a 13 mL culture tube without antibiotics and incubated at 37°C with 200 rpm agitation for overnight growth.

To ensure a sterile system, 120 mL serum flasks with magnets were autoclaved at 121°C for 20 minutes and all sample preparation was performed under a sterile laminar flow work bench. Thereafter, 50 mL of each media listed in **Table 16** was transferred to the serum flasks and inoculated with 500 µL of inoculum diluting the LB medium 100 fold. The flasks were sealed with a 20 mm butyl septum before crimping the seal, ensuring a closed system. If the experiment required the removal of air, the flasks were transferred to the (self-made) evacuation system described in (Molstad et al., 2007). A vacuum pump removes the air and flushes the samples with Helium in four cycles removing the gasses before adding controlled amounts of oxygen back into the system with gas syringes. If the experiment was initiated with the same oxygen concentrations as found in the atmosphere (i.e. 21% oxygen), the helium washing was skipped. Since the nitrogen concentrations were not of interest, the initial atmospheric concentrations of nitrogen (i.e. 78% Nitrogen) does not affect the experiment. Furthermore, the initial carbon dioxide concentrations of (0.04%) was low enough to also not affect the experiment.

After preparation and sealing the flasks, they were transferred to a water bath holding 37°C on a 600 rpm magnet stirring plate. Potential over-pressure was removed by puncturing the seal with an ethanol (70%) filled water lock, this step was performed before initiating analysis and after injecting oxygen during the experiment. The analysis was initiated using a python script written by Lars Molstad instructing the auto sampler to retrieve a gas sample every hour. The robot system sampled each vial every hour and applied the sample on the Varian CP4900 microGC equipped with both a 10 and 20 m poraPLOT U 5 Å Molsieve column. The carbon dioxide and oxygen concentrations were monitored, and the cultures oxygen was injected when the concentration reached 2.5 % oxygen, ensuring oxidic conditions. Initial oxygen concentration, media composition and inoculum were altered depending on the research question. However, the general method for utilizing the robot system was similar.

To enable analysis of the data, two standards were prepared by evacuating sealed 120 mL serum flasks with a vacuum pump, the vacuum in the vials was replaced with one High and one Low standard, comprised respectively of 10 000 ppm carbon dioxide and air (i.e. 780 000 ppm N, 210 000 ppm O_2). The standards were used to calibrate the results for analysis.

This method described the workflow of the system, several different media were attempted in the system and are described in the results.

3.14 Proteomic sample preparation

3.14.1 In solution protein digestion

When working with a single pure protein, in-solution digestion was performed as a preparation for analysis by Orbitap ESI-MS. The protein was thoroughly purified to ensure minimal contamination. Before starting the proteomics workflow, buffer exchange was performed as described in section **3.10** to 20 mM Tris-HCl pH 8, ensuring correct pH for the digestion reaction.

Materials:

- 20 mM Tris-HCl pH 8
- 1 M Dithiothreitol (DTT)
- 500 mM Iodoacetamide (IAA)
- 500 ng/µL Digestion enzyme (Trypsin or Chymotrypsin)
- 10% (v/v) Trifluoracetic acid (TFA) solution
- ddH_2O
- ThermoMixer™ C (Eppendorf)
- Protein LoBind 2 mL (Eppendorf)

Method:

The protein samples were reduced by adding Dithiothreitol (DTT) to a final concentration of 10 mM and incubating the sample for 30 minutes in a Thermomixer, 56°C with 600 rpm agitation. Following sample reduction, the cysteine residues were alkylated by adding Iodoacetamide (IAA) to a final concentration of 15 mM and incubating the sample for 30 minutes in a thermomixer at room-temperature with 600 rpm agitation, in the dark. After the alkylation step, the digestion enzyme (Trypsin or Chymotrypsin) was added at an enzyme-to-protein concentration ratio of (1:40) before incubating the sample overnight at 37 °C in a thermomixer with 600 rpm agitation.

The digestion reaction was terminated by adding 10 % Trifluoric acid (TFA) by lowering the pH. The final TFA concentration was below 1%. The sample volume was reduced by vacuum evaporation at 30°C prior to peptide cleaning and desalting.

3.14.2 In-gel protein digestion

In-gel protein digestion was performed on protein samples which were separated by Iso-electric focusing. The separation of protein samples created protein fractions for detailed analysis.

Materials:

- Proteomics grade Acetonitrile (ACN)
- 1M Ammonium bicarbonate (AmBic)
- 500 mM Iodoacetamide (IAA)
- 1M Dithiothreitol (DTT)
- 500 ng/µL Digestion enzyme (Trypsin)
- 10% Trifluoracetic acid (TFA solution)
- ddH_2O
- Liquid aspiration system, Vacusafe Comfort (Integra Biosciences)
- ThermoMixer™ C (Eppendorf)
- Vacufuge
- Scalpel (Swann Morton)
- Protein LoBind tubes, 2 mL (Eppendorf)
- Sonication water bath (Grant)

Method:

Protein samples were separated with IEF gel electrophoresis and visualized with Coomassie staining as described in section **3.2.3**. Prior to analysis, the protein bands were excised from the gel in 1x1 mm cubes before transferring the cubes to protein LoBind Eppendorf tubes.

Decolouring and cleaning of the gel pieces:

The protein gel cubes contain Coomassie stain which was removed by first adding 200 µL ddH_2O and incubating the tubes in a thermomixer for 15 minutes at room temperature with 600 rpm agitation swelling the cubes. After incubation, the liquid was aspirated before adding 200 µL of a de-staining mixture containing 50% ACN with 25mM Ammonium Bicarbonate (AmBic) before incubating the tubes at room temperature in a thermomixer for 15 minutes and 600 rpm agitation. This step was repeated once before continuing. Following the de-staining, the liquid was aspirated, and the gel cubes were dehydrated by adding 100 µL of 100% ACN and incubating the tubes for 5 minutes in a thermomixer at room temperature with 600 rpm agitation. After incubation, the liquid was aspirated, and the gel cubes were air dried under a fume hood. The gel pieces were white and shrunken at the final stage of this protocol.

Reduction and alkylation of the protein:

At the final stage of the aforementioned protocol the gel cubes were shrunken to allow the reduction solution to penetrate the gel cubes and access the protein. Reduction was performed by adding 50 µL of a solution containing 55 mM Dithiothreitol (DTT) with 100 mM Ammonium Bicarbonate (AmBic) and incubated for 30 minutes at 56 °C in a thermomixer with 600 rpm agitation. After the incubation, the tubes were cooled down in room temperature before removing the liquid by aspiration. Following the reduction, the cysteine residues were alkylated by adding 50 µL of an Iodoacetamide (IAA) solution containing 55 mM IAA + 100mM Ammonium Bicarbonate (AmBic). The tubes were incubated for 30 minutes in a thermomixer at room temperature with 600 rpm agitation. After alkylation, the liquid was aspirated, and the cubes were dehydrated. The dehydration was performed by adding 200 µL of 100% ACN before incubation for 5 minutes in a thermomixer at room temperature with 600 rpm agitation. The gel pieces were white and shrunken at the final stage of this protocol.

Digestion reaction:

At the final stage of the aforementioned protocol the gel cubes were shrunken to allow the digestion solution to penetrate the cubes and access the proteins within. The gel cubes were covered with 50 µL of a 10 ng/µL Trypsin solution before placing the tubes on ice for 30 minutes. During the incubation period, the cubes swelled and increased in size. After incubation, all tubes were examined to ensure the cubes were completely covered by liquid, additional trypsin solution was added if needed. After ensuring all cubes were covered by trypsin solution, the tubes were transferred to a thermomixer and incubated at 37 °C overnight with 600 rpm agitation. The following day, 40 µL of 10% TFA was added to each tube terminating the digestion reaction. After termination, the tubes were transferred to a sonication water bath for 15 minutes to aid the release of digested peptides from the gel cubes. Following the sonication, the liquid was recovered and transferred to a new low bind Eppendorf tube and vacuum evaporated until dryness before peptide desalting and cleaning.

3.14.3 Peptide desalting and cleaning

After digestion, detergents which may cause issues with MS analysis were removed by washing.

Materials:

- Proteomics grade Acetonitrile 100% (ACN)
- Proteomics grade Methanol 100% (MeOH)
- 10% Trifluoric acids (TFA)
- ZipTip (Merck)
- Digested peptides
- HPLC vials and caps
- Vacufuge plus (Eppendorf)
- Sonication water bath (Grant)

Method:

Solid phase extraction using C_{18} membrane was used for cleaning and desalting the digested peptides. ZipTip (Merck) were used for this process. Prior to initiating peptide cleaning and

desalting, the ZipTip were conditioned by pipetting and discarding the following solutions in the stated order:

- 10µL 100% MeOH
- 10 µL 70% ACN/0,1% TFA
- 10 µL 0.1% TFA

After conditioning and equilibration of the C_{18} membrane material the samples were pipetted up and down four times to ensure binding of the peptides to the membrane. Thereafter, washing the membrane with 10µL 0.1% TFA before eluting the peptides in 10 µL 70% ACN/0.1% TFA solution. The samples were vacuum evaporated until dryness before dissolving the clean peptides in 2%ACN /0.1%TFA. To ensure resuspension of the peptides, the samples were placed in a sonication water bath for 5 minutes. The suspended peptides were transferred to HPLC vials and applied on the LC-MS.

3.15 Proteomic analysis of peptides using MALDI-TOF MS

MALDI-TOF analysis on peptides was performed to investigate the rCbpD variants with peptide mass fingerprinting.

Materials:

- UltraFlextreme MALDI-TOF-MS (Bruker)
- α-Cyano-4-hydroxycinnamic acid (HCCA)
- Peptide calibration standard (Bruker)
- MTP 384 ground steel BC MALDI-TOF target plate (Bruker)
- MTP target frame III (Bruker)
- MALDI-TOF Ultraflex (Bruker)

Method:

Peptides digested by either in-solution or in-gel digestion and cleaned as described in section **3.14.3** were used for MALDI-TOF-MS analysis. The peptides were stored in 2%ACN /0.1%TFA after the peptide cleaning and desalting protocol and required no further sample handling prior to MALDI-TOF analysis.

To ensure high accuracy mass lists, the MALDI-TOF was calibrated using the Peptide Calibration Standard (Bruker). To ensure the calibration was the same for all samples, the following plating setup was employed.

A 3x3 spot grid was allocated for sample application, 1 µL of the standard was mixed with 1 µL of α-Cyano-4-hydroxycinnamic acid (HCCA) matrix solution in a PCR cap before transferring 0.5 µL to the centre of the 3x3 grid. Thereafter, the peptide-matrix solution was prepared by mixing 1µL of peptide solution with 1µL of α-Cyano-4-hydroxycinnamic acid (HCCA) matrix solution in a PCR tube cap. After mixing, 0.5 µL of the mixture was plated on the locations surrounding the standard. The plating setup ensured the same distance from the standard to each sample, resulting in reproducible conditions during sample analysis. After all samples were plated the target plate was air dried in room temperature.

The MALDI-TOF was calibrated in the flexControl 3.4 software (Bruker) as per the description of the manufacturer. The analysis method utilized a 40% laser intensity firing 1000 shots without laser wandering. The masses were observed in the 600-3500 Da range which corresponds with the calibration window. Each 1000 shot run created a mass spectrum, 5-6 of the spectra were overlapped and summed to create the sample result spectrum which was stored for further analysis. After all samples were analysed, the flexAnalysis 3.4 software (Bruker) was launched and the sample spectra were filtered with a contaminant mass list by the software. The filtered mass lists were used for searches in Mascot.

3.16 Proteomic analysis of peptides using LC-MS/MS

The peptides were situated in HPLC vials containing 2%ACN/0.1%TFA after cleaning and desalting as described in section **3.14.3**. The vials were transferred to the sample holders of the UltiMate™ 3000 RSLC nano liquid chromatography system. Separation of the peptides was performed using the Acclaim™PepMap™ 100 C18 column utilizing a gradient of solvent A:

0.1% Formic acid, and solvent B: 80% Acetonitrile, 0.1% Formic acid. Since only one protein was analysed and the sample complexity was low, a 50 minute gradient was utilized at 300 nL/min flowrate as follows:

- 0-2 minutes, 3.2-10% B
- 2-30 minutes, 10-40% B
- 30-30.1 minutes, 40-80% B
- 30.1-35 minutes, 80% B
- 35-35.1 minutes, 80-3.2% B
- 35.1-50 minutes, 3.2% B

The LC-MS analysis was run in positive mode on the Q-Exactive hybrid quadrupole Orbitrap MS (Thermo Scientific) described in section **1.8.7.1.**

3.17 PEAKS studio database search

After the LC-MS/MS analysis, both full scan and tandem MS files were concatenated in ms.raw files which were uploaded directly into the PEAKS software. The files were loaded into individual samples and the protease used for digestion was specified for each sample. To decrease the search time, the PA14 proteome (Proteome ID: UP000000653) was uploaded as the database and the default contaminant database utilized. Semi-specific digestion was allowed with a maximum of 3 missed cleavages. The search was initiated with carbamidomethylating of cysteines as a fixed modification. Methionine oxidization and deamidation of glutamate and asparagine were set as variable modifications. In addition, the built in PTM list were searched as variable modifications. Search error tolerance parameters for parent ion and fragments was set at respectively 10 ppm and 0.2 Da. After the search was completed, the peptides were filtered with an FDR of 0.1% and modifications were deemed confident with an Ascore > 20 (Pvalue=0.01).

3.18 Protein crystallization

3.18.1 Manual crystallization

Manual crystallization was performed using predetermined buffer kits, which contain salts, precipitants and buffered solutions to aid in crystallization of the protein. The manual crystallization process was based on the hanging drop method. Protein and buffer are mixed in equal amounts on a glass slide, the same buffer is placed in the well reservoir. Since protein and buffer are mixed 1:1 the concentration of buffer in the drop is halved relative to the concentration in the buffer reservoir. When placing the glass slide over the reservoir a seal of grease creates an airtight seal and a closed system. In the closed system vapour diffusion from the drop to the reservoir occurs, resulting in increased concentration of protein which aids in crystallization.

Materials:

- rCbpD$_{EC}$ M1 (18.9 and 43 mg/mL)
- Crystallization screens (**2.3**)
- 18 mm siliconized glass slides (Hampton Research)
- 24 well crystallization plates (Hampton Research)
- Stereoscope, Mz6 (Leica)

Method:

The protein sample was thoroughly purified to a high purity by only selecting the centre peak during SEC elution. The protein sample was concentrated to a high concentration of 18.9 and 43 mg/mL as described in section **3.10**. Crystallization screens were performed in 24 well crystallization plates with 18 mm siliconized glass cover slides. 1 µL of protein was placed on the glass slide, thereafter, 1µL of buffer was mixed with the protein before placing the glass slide with the drop hanging upside down over the buffer reservoir. This was performed for all the buffers in the crystallization screens.

The plates were stored at room temperature in the dark and routinely examined for crystal growth using a 0.63-5x stereoscope.

3.18.2 Robotic crystallization

Robotic crystallization is a high throughput system for testing several crystallization conditions quickly. Using the Mosquito® crystal nanoLitre protein crystallization robot allowed for micro reactions which saves both protein and buffer with pipetting volumes of 250 nL. The sitting drop method uses a 384 well plate containing 96 buffer reservoirs allowing a total of three protein concentrations for each buffer. Each compartment is comprised of one buffer reservoir with three raised levels situated around the reservoir. The robot mixes buffer and protein and places the drop on the raised level. After pipetting is finished, the plate is sealed using a clear film which creates a closed system for each of the compartments. This allows vapour diffusion which aids in protein crystallization. The use of robots is a preliminary screen which should be repeated manually after positive crystallization conditions have been observed.

Materials:

- rCbpD$_{EC}$ protein variant
- Crystallization screens
- iQ 384 well plate (SPT Labtech)
- Mosquito® crystal nanoLitre protein crystallization robot (SPTlabtech)
- 96 well liquidator™ (Rainin)
- Rock Imager (Formulatrix)
- Crystal clear sealing tape (Hampton Research)

Method:

The protein sample carrier on the crystallization robot contains four rows with six protein sample reservoirs. The six protein reservoirs correspond to the vertical A-H positions on the iQ 384 plate. The rCbpD$_{EC}$ protein sample was prepared in three 25 µL dilutions, respectively (1, ½ and ¼) of the initial protein concentration. The protein dilutions were transferred to the protein sample carrier, each dilution required one row of six protein reservoirs each containing 3 µL protein sample.

The iQ 384 plates were prepared using the Rainin 96 well liquidator™. The plate preparation entailed transferring 100 µL of the 96 buffers from the pre-prepared crystallization screen block to the buffer reservoirs in the iQ 384 well plates. After the iQ 384 plate was filled, the plate was transferred to the allocated location on the crystallization robot sample carrier. Once both the protein sample and buffer plates were placed on the crystallization robot sample carrier, the buffer-protein mixing was initiated. Using capillaries, 250 nL of buffer was mixed with 250 nL

of protein before being placed on the elevated position in the sample compartment. Each dilution was independently placed on the raised sample position. After the three dilutions were plated, the plate was removed and crystal clear 96 well tape was placed over the plate before sealing each compartment thoroughly. The plates were placed in a crystallization hotel holding 25°C for 21 days. The hotel imaged the plate every third day using a camera and with UV once a week. The pictures were analysed after the imaging period was over.

3.19 Microscale Thermophoresis (MST) for protein-ligand interactions

MST analysis was performed according to manufacturer instructions with the Monolith N.115 accompanied with the Monolith His-Tag labelling Kit RED-tris-NTA. Only the initial binding screening was performed during this study.

Materials:

- rCbpD$_{PA}$ protein variant
- Protein sample buffer
- Monolith N.115 (Nano Temper Technologies)
- Monolith His-Tag labelling Kit RED-tris-NTA (Nano temper technologies)
- Standard coated capillaries (Nano temper technologies)
- PCR tubes 0.2 mL

Method:

Purified rCbpD$_{PA}$ was situated in 150 mM NaCl + 15 mM Tris-HCl at pH 7.5 as the recommended buffer for MST analysis. Preparation according to manufacturer instructions were performed as follows.

The supplied 5x PBS-T vials were diluted with 8 mL ddH_2O to the final concentration of 1x PBS-T. After dilution the PBS-T buffer, the supplied protein dye vials were dissolved with 50 µL 1xPBS-T to a final concentration of 5 µM. A working concentration of protein dye was created by mixing 2 µL of the 5 µM dye solution with 98 µL of PBS-T to a final concentration

of 200 nM. The rCbpD$_{PA}$ protein was diluted to a final concentration of 200 nM. Following the preparation of dye and protein solution, 100 µL of both the dye and protein solution were mixed by pipetting and incubated at room temperature for 30 minutes in the dark. While waiting, the ligand was dissolved in same buffer as the protein sample to a final concentration of 1 mM.

The Monolith NT.115 system temperature was set at 25°C to ensure a stable temperature baseline. Prior to initiating the binding experiments, a capillary scan of the protein solution and ligand solution was performed to ensure that the capillary did not present affinity towards the solutions. Following the determination of appropriate capillary, 10 µL of dyed protein solution and ligand solution were mixed and loaded in the capillary. Binding affinity measurements were performed with 60% UV power and 20, 40 and 60% MST power.

3.20 Protein melting point analysis

Protein melting point analysis was performed to investigate the melting temperature (Tm) for different rCbpD protein variants. This was performed by thermal shift analysis.

Materials:

- rCbpD protein variants
- SYPRO orange dye (8x) (Thermo Scientific)
- Tris-HCl pH 7.5 15 mM
- Copper sulphate 5 mM ($CuSO_4$)
- qPCR StepOnePlus™ (Applied Biosystems)
- Plate centrifuge, Plate spin II (Kubota)
- MicroAmp™ optical 96-well reaction plate (Applied Biosystems)
- MicroAmp™ Adhesive optical covers (Applied Biosystems)
- ddH_2O

Method:

Protein melting point was determined using the Step One Plus system (Applied biosystems) with optical 96 well plates. All protein and no protein samples were performed using 4 replicates as per the recommendation from the manufacturer. The dye was always covered with aluminium foil to limit light pollution and degradation of the protein dye. The 96 well plate was placed on ice while preparing the samples. The following reaction was performed.

Table 17: Protein thermal shift reaction overview

Reagent	**Protein sample**	**No protein sample**
SYPRO orange dye	12.5 µL	12.5 µL
Protein sample	10 µL	-
Tris-HCl pH 7.5 15mM	25 µL	25 µL
$CuSO_4$ 5mM	3 x molar mass of the protein	3 x molar mass of the protein
ddH_2O	Up till 100 µL	Up till 100 µL

The samples were thoroughly mixed before extracting 20 µL for each well in four replicates. The 96 well plate was sealed with optical adhesive film before centrifugation using a plate centrifuge at 1000 g for 1 minute. Subsequently, the plate was moved to the qPCR instrument. Following the manufacturer recommendations, the plate was incubated at 25°C for two minutes before ramping the temperature from 25°C to 97°C over 50 minutes before holding at 97°C for two minutes. Measurements were conducted continuously throughout the ramping procedure.

4 Results

4.1 Enzyme properties

Chitin binding protein D hereafter known as CbpD is a 389 amino acid protein secreted by *P. aeruginosa* as a 364 amino acid protein after the signal peptide is cleaved during secretion. Misunderstandings surrounding CbpD still linger in literature and is annotated as 23 kDa protein called LasD (Park & Galloway, 1995). Clarification was achieved when CbpD was identified as a chitin binding protein (Jindra Folders, 2000). Because of mischaracterizations in the literature, theoretical protein characterization was performed.

The Protparam software on the ExPASy server was used to determine the different physiochemical properties that are calculated based on the amino acid sequence.

Table 18: Theoretical values determined with the amino acid sequence using Protparam on the ExPASy server. *The full length enzyme is a 389 aa protein which contains a signal peptide (SP) predicted by the SignalP server. All of the enzymes except for rCbpD$_{PA}$ Native contains a His-Tag which explains the increased aa sequence length. Molecular weight (MW) both with and without SP, pI and extinction coefficient (ε) are calculated with the His-Tag, except for rCbpD$_{PA}$ Native. The extinction coefficient (ε) and pI are theoretical values and are calculated without the signal peptide, since it is not present in-vivo.*

Enzyme	**aa**	**aa w/o SP**	**MW$^+$ kDa**	**MW w/o SP$^+$ kDa**	**pI**	**ε**
rCbpD$_{PA}$ -His	396	371	42.8	40.1	6.42	82 320
rCbpD$_{PA}$ Native	389	364	41.9	39.2	5.98	82 320
rCbpD$_{EC}$ -His	396	371	42.8	40.1	6.42	82 320
rCbpD$_{EC}$ M1 -His	214	189	22.3	19.6	6.46	35 785
rCbpD$_{EC}$ M2+M3 -His	186	186	19.3	-	5.28	46 535

The SignalP website (http://www.cbs.dtu.dk/services/SignalP/) was used to predict a possible signal peptide.

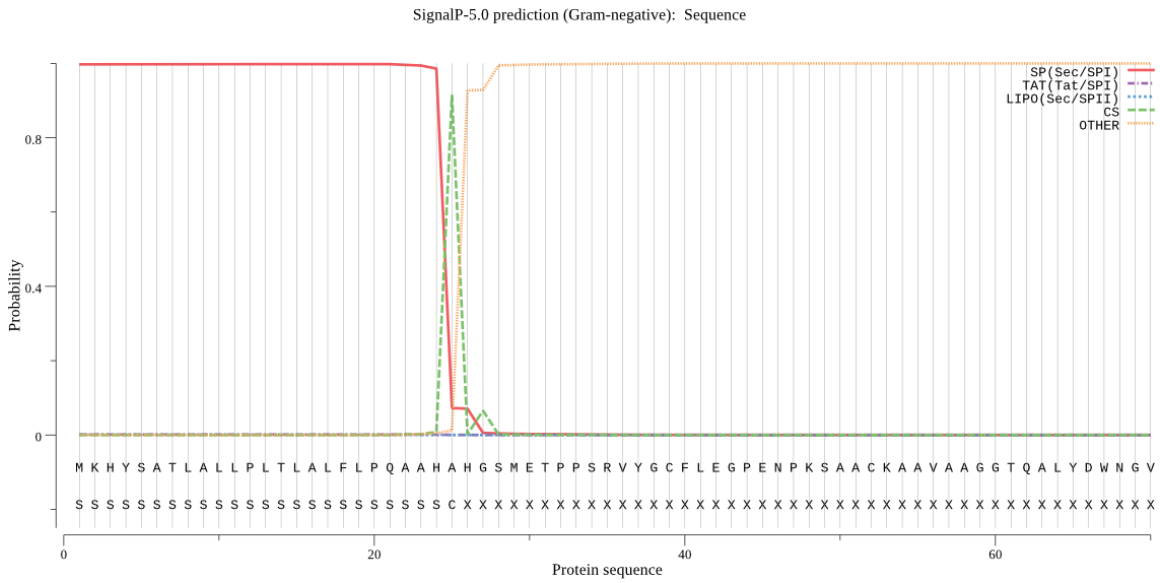

Figure 4-1: Signal peptide prediction by SignalP-5.0. *This graph shows the predicted signal peptide placement on CbpD the SignalP-5.0 website (http://www.cbs.dtu.dk/services/SignalP/). The SignalP website identifies signal peptides secreted by either Sec or Tat translocon (Sec/Tat) and if they are cleaved by Signal peptidase I or II (SPI/SPII). In addition to Lipoprotein signal peptides (LIPO). The cleavage site (CS) is predicted in green whilst the rest of the sequence is indicated as OTHER in yellow. The cleavage site is predicted to be between amino acids A and H (i.e. AHA\|HGS)*

The prediction software identified a signal peptide sequence from residue 1-25 as seen in **Figure 4-1** which coincides with previous observations (Jindra Folders, 2000). Further research shows that CbpD is annotated in the manually curated carbohydrate active enzymes database (CAZy) with an AA10 LPMO domain and a carbohydrate binding module 73 (CBM73). Further analysis of the amino sequence was performed using Pfam, which allowed classification of protein families (https://pfam.xfam.org). The sequence without signal peptide was uploaded to the Pfam database. The search presented significant sequence identity of the 26-207 aa sequence with the LMPO 10 protein domain. In addition, the 217 to 315 aa sequence showed significant sequence identity with the second domain of N-acetylglucosamine binding protein A (GbpA). Combining these results, suggest a modular structure as described in **Figure 4-2**.

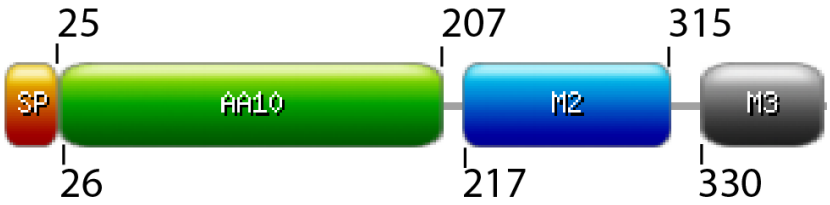

Figure 4-2 In-silico determination of CbpD module structure. *The image illustrates the predicted CbpD domain structure. The aa positions under the structure indicate the start of the module, whilst the aa position above indicates the end of the module. There are four predicted modules, signal peptide (SP) 1-25, AA10 LPMO module 26-207, Module 2 (M2) 217-315 and Module 3 (M3) 330-389. The module positions are based on in-silico analysis of the sequence.*

A large multiple sequence alignment was attempted on LPMOs from selected pathogenic gram-negative bacteria. The genetic diversity was large creating difficulties in establishing a sequence alignment. However, the alignment showed the conserved histidine brace, the outer shell of either glutamate or glutamine and the aromatic phenylalanine which is already well established (Results not shown).

4.2 Cloning of the rCbpD$_{PA}$-His recombinant gene

In order to amplify the *cbpD* gene, PCR was performed on the *P. aeruginosa* PA14 genomic DNA using the CbpD-KpNI-His-FW and CbpD-SbfI-His-Rev primers. The resulting PCR product showed a size of approximately 1600 bp (**Figure 4-3**, panel A), which corresponds to the expected size of the insert (1643 bp). Some additional bands of smaller size than the insert can be observed, these most likely represent unspecific amplification products or primer-dimers. For ligation of the insert into the *P. aeruginosa* expression vector pGM931, the vector was linearized by double digestion using the KpnI-HF and SbfI-HF restriction enzymes. The size of the linearized vector was approximately 6000 bp (**Figure 4-3**, panel B), which corresponds to the expected theoretical size (6053 bp). A band with a larger size was also observed in the gel, which represents the un-linearized/un-digested pGM931 vector. After insertion into TOP10 cells, colony PCR was performed using primer mixtures AraC-FW/IntC-Rev (expected size 1320 bp) and OutC-FW/IntC-Rev (expected size 563 bp). This primary selection was performed in order to select colonies that contained the pGM931 plasmid. Out of five examined colonies, colony two and three provided correct PCR products with the expected size (**Figure 4-4**; panel A and B). Colony two and three were cultivated and the plasmid was purified and confirmed with DNA sequencing. After confirmation, the vector was transformed into *P. aeruginosa* PA14ΔCbpD before spreading the transformed bacteria on LB plates (300 µg/mL Carbenicillin) and incubated overnight. Successful transformation of the plasmid was verified using primer mixtures (AraC-FW/Sbf1-Rev, AraC-FW/IntC-Rev and OutC-FW/IntC-Rev; with expected PCR product sizes (2151, 1320 and 563 bp). Out of five screened colonies from colony two and three, colonies 2.4 and 2.5 contained the expected colony PCR products (**Figure 4-5**)

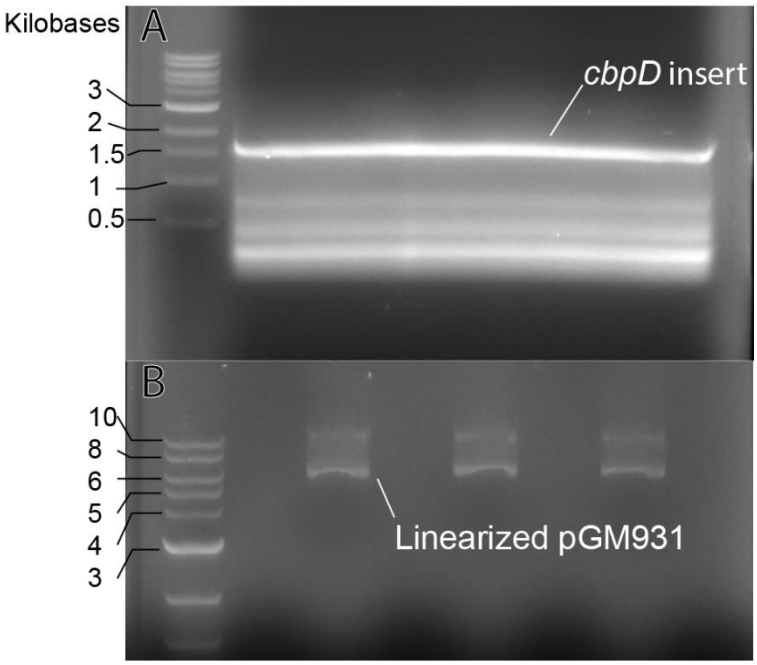

Figure 4-3: Agarose gel analysis of PCR products from cbpD amplification and linearization of pGM931*. (A): PCR amplification of cbpD (1650 bp) from P. aeruginosa PA14. Lane 1: QuickLoad® 1kb ladder, lane 2-8 are merged wells that contain 200µL of the PCR reaction. (B): Linearization of the plasmid using KpnI-HF and SbfI-HF (theoretical size of linearized plasmid is 6053 bps).*

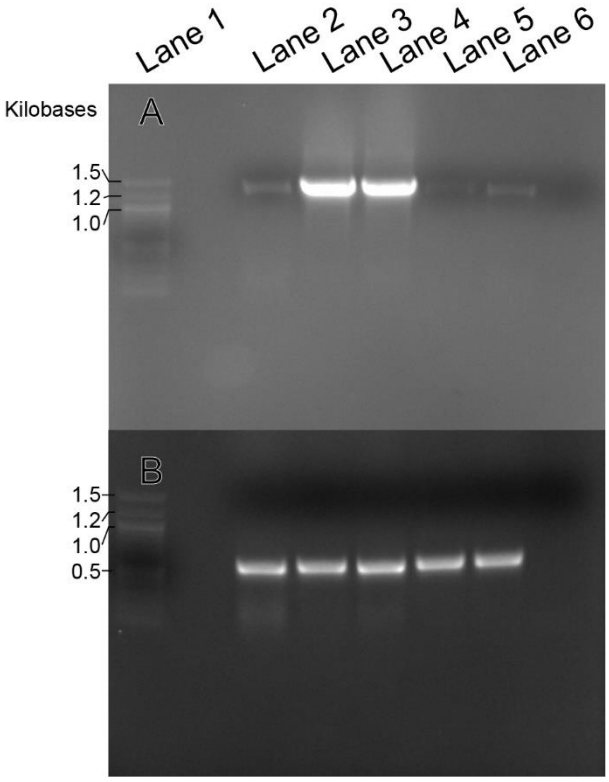

Figure 4-4. Colony PCR performed on OneShot™Top10 E. coli cells cbpD-pGM931*. The gel image shows the colony PCR results of OneShot™ Top10 E. coli cells (A): AraC-FW-IntC-Rev (Expected size: 1320bps), lane 1 contains the ladder (Quickload® 1kb) and (B): OutC-FW-IntC-Rev (Expected size: 563 bps), lane 1 contains the ladder (QuickLoad® 100 bp). Lane 2-6 contains five randomly selected colonies.*

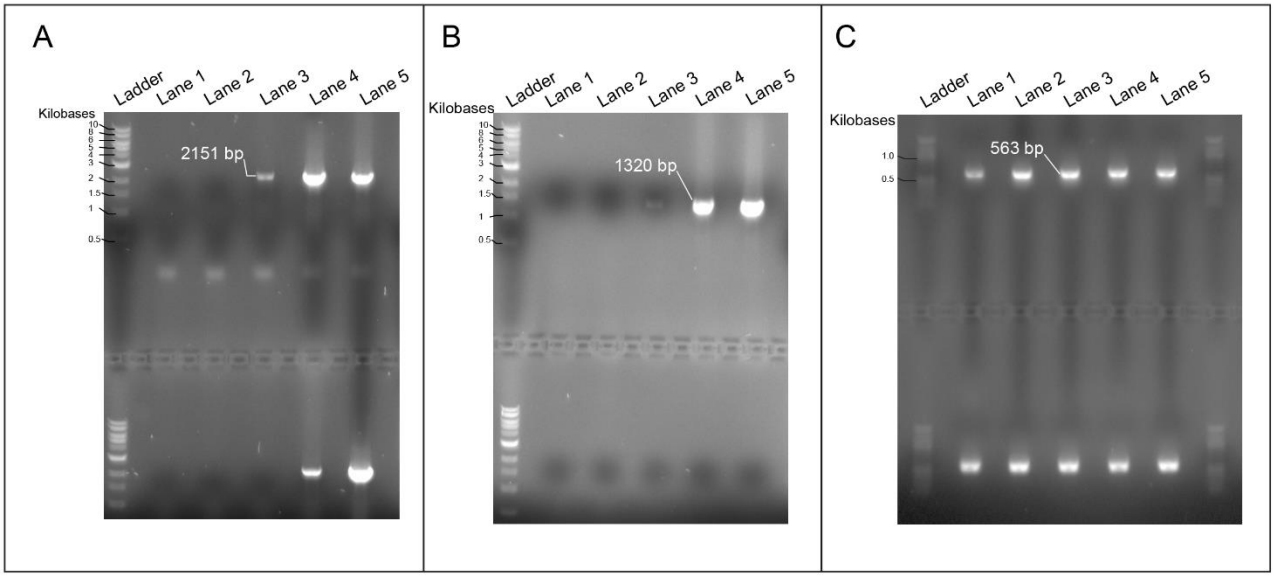

Figure 4-5. Colony PCR performed on P. aeruginosa cells cbpD-pGM931. *The gel image shows colony PCR results of PA14ΔCbpD with containing the recombinant CbpD gene. (A): AraC-FW-SbfI-Rev (Expected product size:2151 bps), (B): AraC-FW-IntC-Rev (Expected size: 1320 bps) and (C): OutC-FW-IntC-Rev (Expected size: 563 bps). The ladder (A and B; Quickload® 1kb) and (C; Quickload® 100 bp) are placed in the outermost lane to the left in all gels. The upperpart of the gel contains five colonies from (**Figure 4-4**; lane 3) and the lower part of the gel contains five colonies from (**Figure 4-4**; Lane 4).*

4.3 Enzyme production and purification

4.3.1 Optimization of P. aeruginosa cultivation

Cultivation optimization of the *P. aeruginosa* was optimized by identifying the optimum cultivation temperature, inoculation volumes and induction concentrations.

Initial screening of cultivation methods included cultivation until OD 1.2, overnight in baffled flasks at 37°C with 200 rpm agitation and the Lex-48 bioreactor overnight at room temperature. Observations on pellet size and firmness resulted in further optimization of the Lex-48 bioreactor system and ruling out other initial screening methods. Cultivation in the Lex-48 bioreactor system at room temperature (22-25°C). The more nutrient rich BHI cultivation was not viable when comparing protein yield. Therefore, the optimizations were performed in the LB medium.

4.3.2 Enzyme production and purification

A total of six enzymes were purified during this study, the utilization of general chromatography methods allowed successful purification of all enzymes, these methods are summarized in **Table 19**.

Table 19: Overview summarizing the purifications step needed for enzyme purification of the different protein variants.

Protein variant	**IMAC**	**HIC**	**IEX**	**SEC**
$rCbpD_{PA}$	x			x
$rCbpD_{PA}$Lys	x			x
$rCbpD_{PA}$ Native		x	x	x
$rCbpD_{EC}$	x			x
$rCbpD_{EC}$ M2+M3	x	x		x
$rCbpD_{EC}$ M1	x			x

Full length enzymes:

Full length enzymes containing a C-terminal His-Tag were all purified in the same manner as stated in section **3.9.1** with similar results. IMAC elution centre peak fractions were collected and analysed with SDS-PAGE to establish purity. IMAC purification resulted in approximately 85-95% purity determined by SDS-PAGE analysis, as seen in representative SDS-PAGE gels (**Figure 4-6**; Gel images on the left in panel A and B).

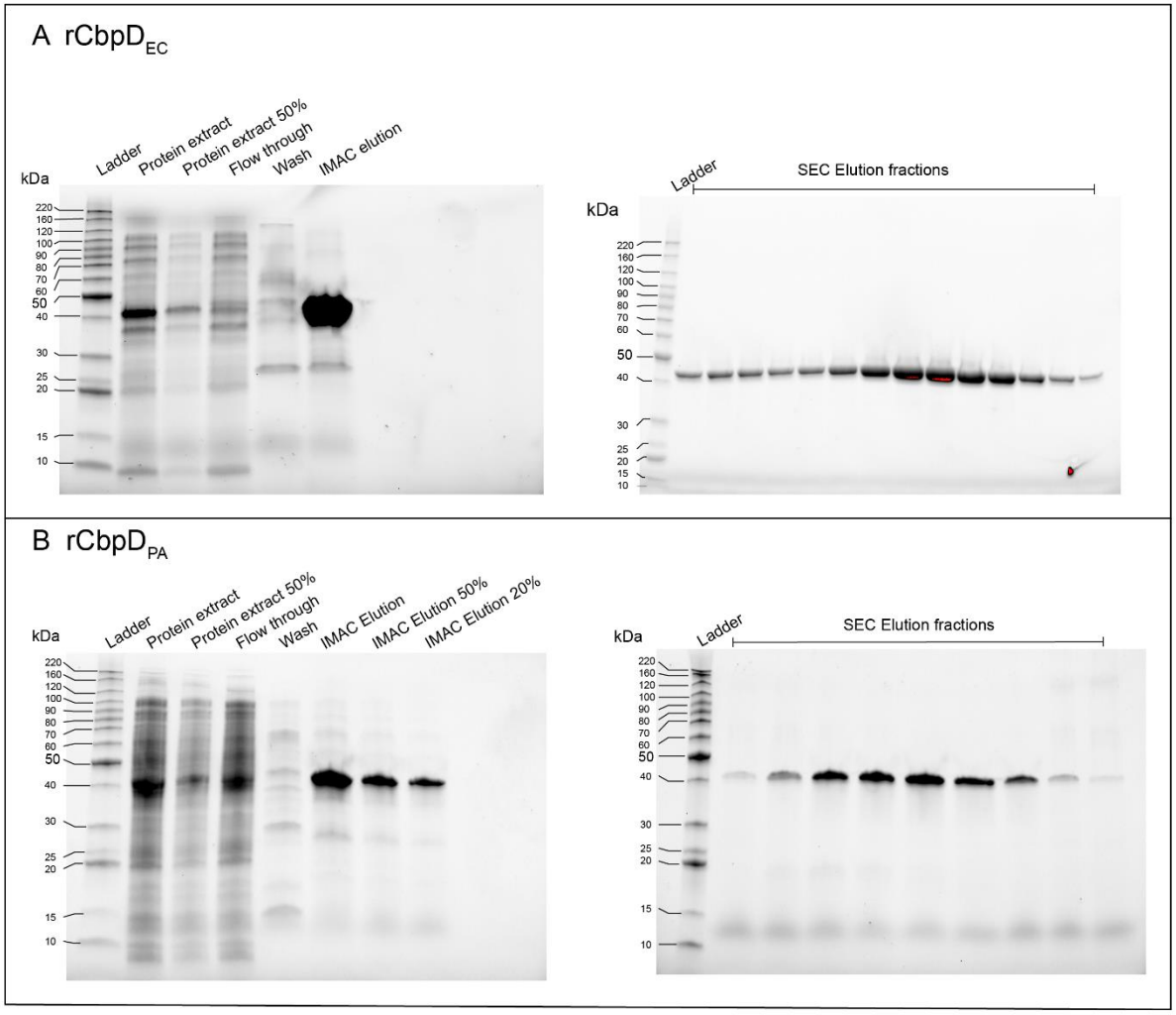

Figure 4-6. SDS-PAGE analysis of CbpD full length variants and their purification. *Images of SDS-PAGE gels show analysis of (A): rCbpD$_{EC}$ and (B): rCbpD$_{PA}$. The sources of the samples are indicated above each well. The protein molecular weight ladder (Protein BenchMark™) is present in all gels in the outer left lane with masses indicated in kDa. Sample volumes were 20 µL of the undiluted sample solution.*

The entirety of the SEC elution peak was collected. The degree of purity needed determined which SEC fractions to pool for concentrating. The full-length rCbpD$_{PA}$ Lys variant is covered in a separate section.

Truncated variants:

Production of the rCbpD$_{EC}$ M1 and rCbpD$_{EC}$ M2+M3 variants were both cultivated in *E. coli*. However, protein extraction was respectively performed from the periplasm and cytosol descried in section **3.8**. The protein extracts were both initially purified using IMAC as

described in section **3.9.1**. rCbpD$_{EC}$ M1 was purified to a high purity with IMAC and SEC purification (**Figure 4-7**; Panel B). However, purification of the rCbpD$_{EC}$ M2+M3 variant required additional purification steps, a cleavage occurred either before or during IMAC purification resulting in two proteins with 10 kDa in difference (**Figure 4-7**; panel A, gel image on the left). Since both proteins elute during high imidazole concentrations, both proteins are theorized to contain a His-Tag. HIC purification utilized the different physiochemical properties of the M2 and M3 domain resulting in the removal of the cleaved M2 domain as observed in (**Figure 4-7**; panel A, image to the right, flow through sample). The ionic strength in the HIC elution buffer, containing 50 mM Tris-HCl pH 7.5 was sufficient to retain rCbpD$_{EC}$ M2+M3 on the column. Elution of rCbpD$_{EC}$M2+M3 was achieved with ddH_2O which decreased the ionic strength and pH of elution solution (**Figure 4-7**; Panel A, image to the right).

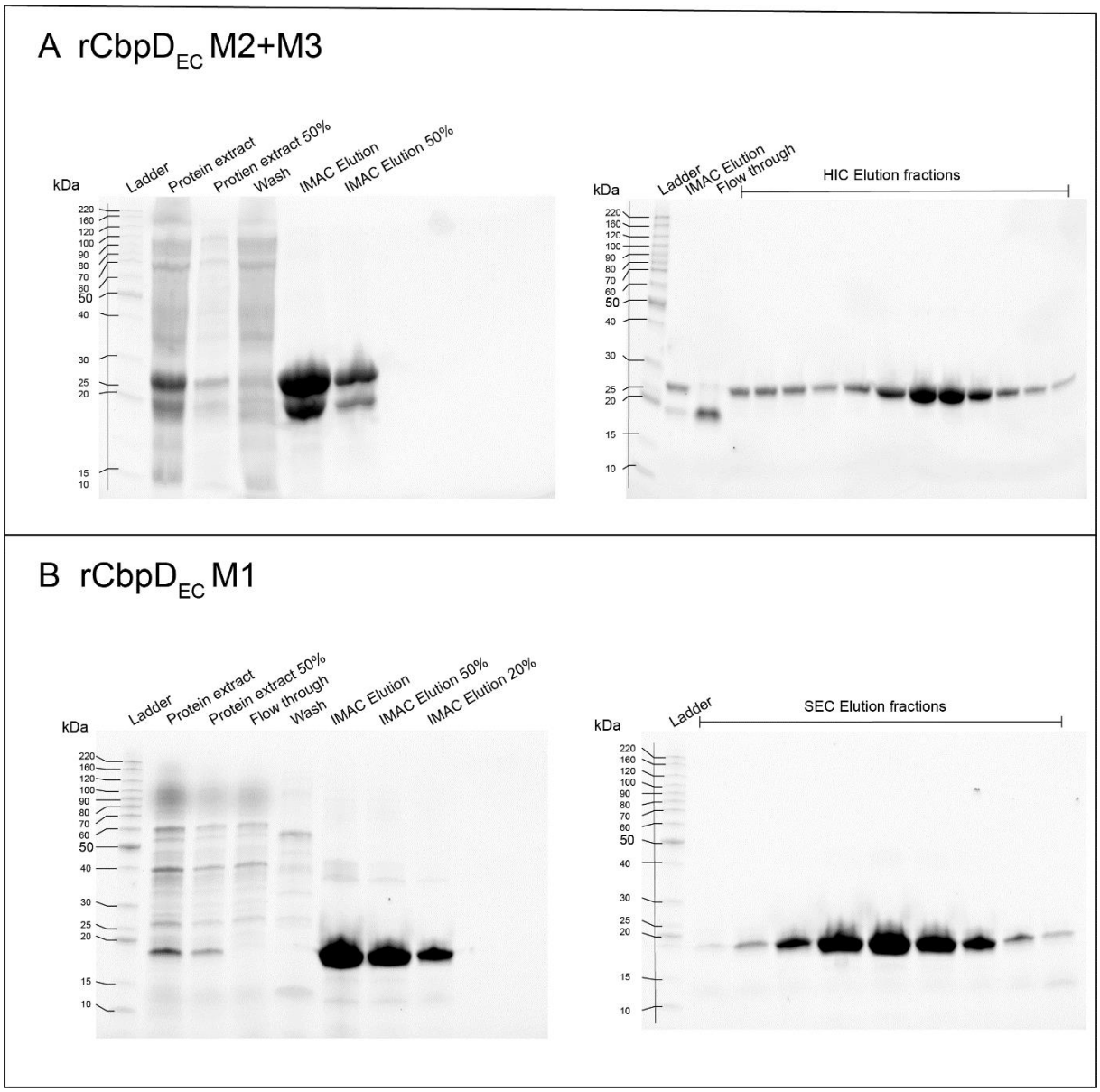

Figure 4-7: ***SDS-PAGE analysis of CbpD truncated variants and their purification.*** *Images of SDS-PAGE analysis (A): rCbpD$_{EC}$ M2+M3 and (B): rCbpD$_{EC}$ M1. The sources of the samples are indicated above each lane. The protein molecular weight ladder (Protein BenchMark™) is present in all gels in the outer left lane with masses indicated in kDa. Sample volumes were 20 µL of the undiluted sample solution.*

Native enzyme:

The purification of rCbpD$_{PA}$ Native attempted several methods. Firstly, chitin affinity chromatography was attempted with different eluents.

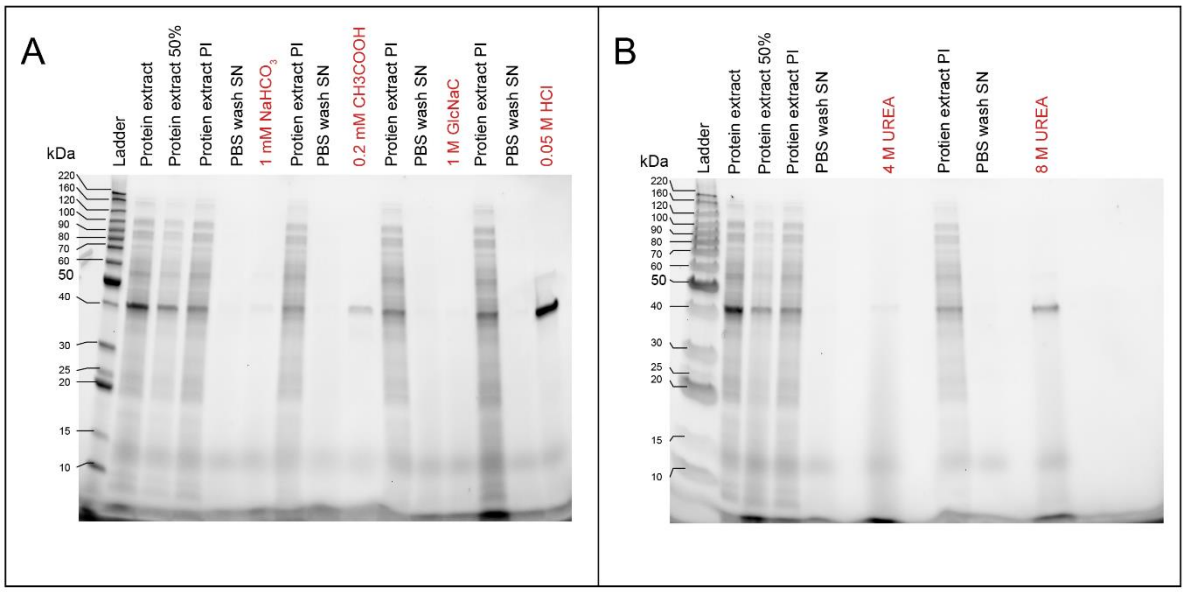

Figure 4-8: Visualization of rCbpD$_{PA}$ Native affinity towards β-Chitin. *SDS-PAGE images showing attempts to elute rCbpD$_{PA}$ native from β-chitin. The ladder (Protein BenchMark™) is placed in the outermost lane on the left for both gels. rCbpD$_{PA}$ Native protein extract incubated with 15mg β-Chitin for 60 minutes eluted by different solutions. The source of each sample is stated above each well with abbreviations for post incubation (PI) and supernatant (SN). The elution solutions are stated in red. (A): Chitin samples treated with 0.1 $NaHCO_3$, 0.2 mM CH_3COOH, 1 M GlcNac and 0.05 M HCl. (B): Chitin samples treated with 4 and 8 M UREA. The sample volumes were 20 µL of undiluted samples.*

When comparing the protein extract with the protein extract post incubation (PI) samples, the protein band at approximately 40 kDa shows lower intensity after incubation with chitin. (**Figure 4-8**; panel A and B). Washing with PBS was performed to remove unspecific biding; however, no protein was eluted from the chitin particles using PBS (**Figure 4-8**; panel A and B). Elution was most successful with 0.05 M HCl (**Figure 4-8**; panel A); however, there are faint bands of low intensity for all elution solutions. Chitin affinity chromatography was not successful as a purification method for rCbpD$_{PA}$ Native.

The final purification protocol required investigating the correct order and combination of purification techniques enabling a reproducible result. IEX was the first round of purification followed by HIC and lastly SEC purification.

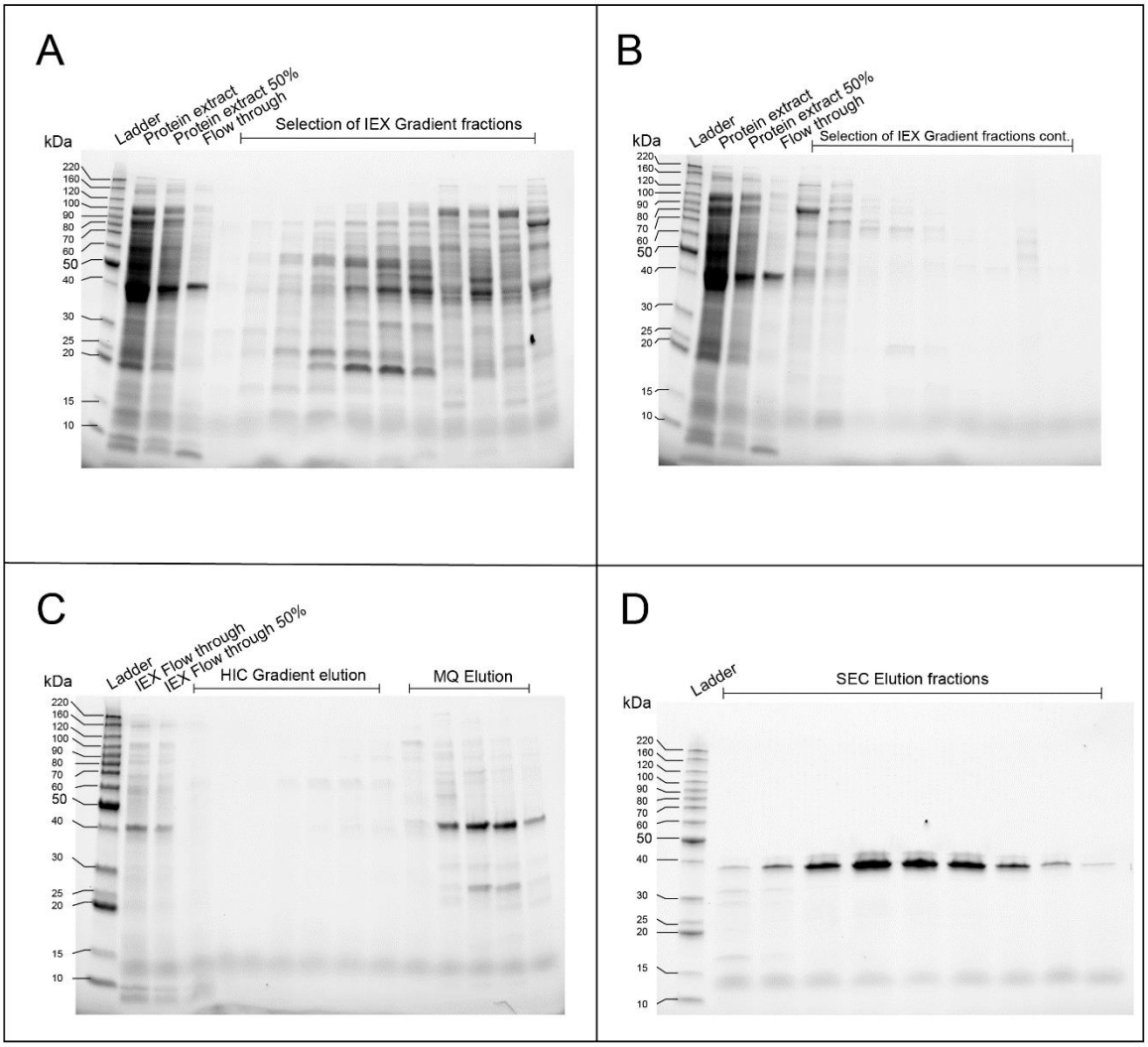

Figure 4-9. SDS-PAGE analysis of rCbpD$_{PA}$ Native purification steps. *Images of SDS-PAGE analysis. (A): IEX purification of the protein extract from rCbpD$_{PA}$ Native (B): Continued IEX gradient fractions (C): HIC purification of the IEX flow through (D): SEC elution fractions from the ddH_2O elution. The sources of the samples are indicated above each lane. The protein molecular weight ladder (Protein BenchMark™) is present in all gels in the outer left lane with masses indicated in kDa. Sample volumes were 20 µL of the undiluted sample solution.*

The IEX flow through shows a band in approximately the correct size of 40 kDa (**Figure 4-9**; Panel A, flow through sample). Further purification of the IEX flow through was performed with HIC purification. The elution was performed with ddH_2O after the HIC elution gradient (**Figure 4-9**; panel C, ddH_2O elution samples). Lastly SEC purification was performed, there are faint bands slightly higher than the CbpD band showing some contaminants remain (**Figure 4-9**; panel D). Verification of correctly purified protein was performed with an enzyme assay.

4.4 Enzyme melting point determined by thermal shift analysis

Protein thermal shift analysis was performed to investigate the melting temperature (Tm) of rCbpD$_{PA}$ and truncated variants rCbpD$_{EC}$ M1 and rCbpD$_{EC}$ M2+M3. The melting temperature data was visualized by showing the differentialized fluorescence data. The steepest incline on the fluorescence data indicates the temperature when the protein denatures the fastest. This point is visualised as the lowest point in the differentialized fluorescence data.

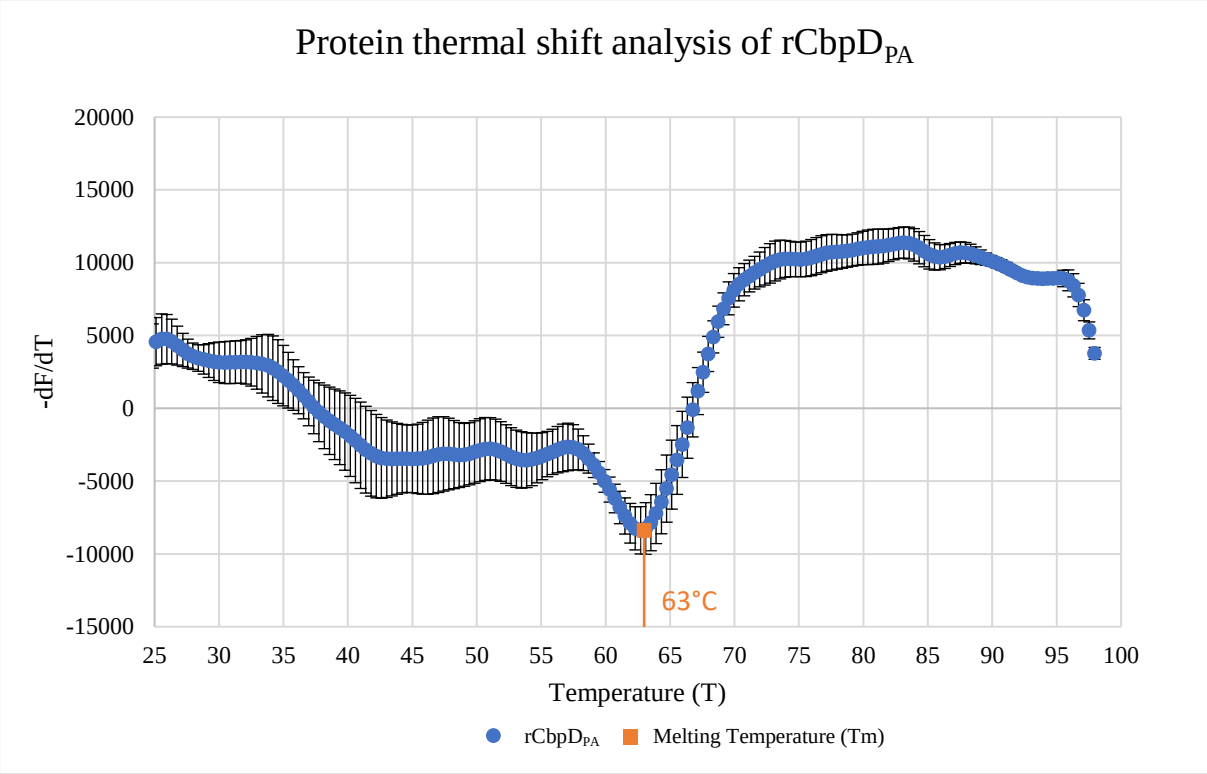

Figure 4-10: Melting point analysis of rCbpD$_{PA}$. *Melting point determined by thermal shift analysis. The Y axis shows the derivative of the fluorescence measurements (F) with respect to temperature (T) while the x-axis shows the temperature (°C). The blue line represents the average of four replicates, the error bars represent the standard deviation of the measurements. The melting temperature in orange is defined as the lowest point of the first derivative which is the steepest part of the fluorescence measurements of rCbpD$_{PA}$.*

Melting temperature of the full-length enzyme presented as the differentialized fluorescence data showed the denaturing curve is uneven suggesting that the protein denatures unevenly as a subtle downward curve. As seen in (**Figure 4-10),** the lowest point indicating the steepest incline on the fluorescence measurements is 63°C. To further investigate the melting

temperature of rCbpD, the truncated variants were also considered to gain insight of how the different domains contribute to the melting temperature.

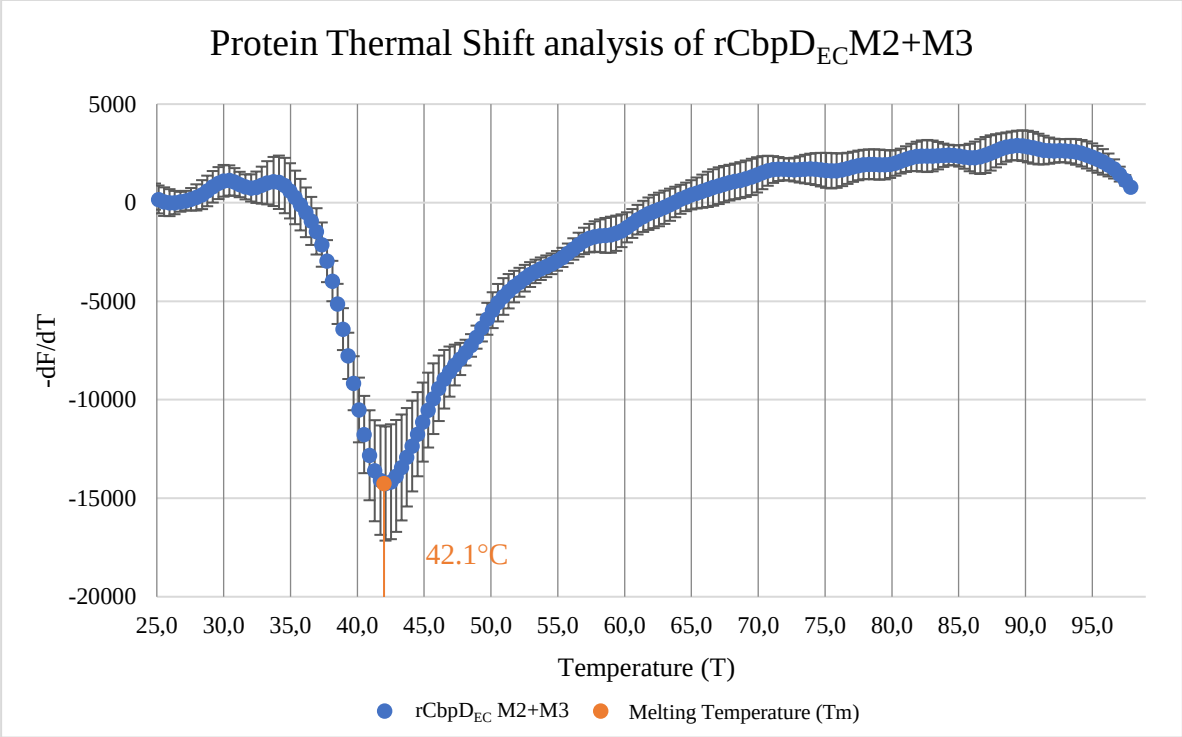

Figure 4-11. ***Melting point analysis of rCbpDEC M2+M3****. Melting point determined by thermal shift analysis. The Y axis shows the derivative of the fluorescence measurements (F) with respect to temperature (T) while the x-axis shows the temperature (°C). The blue line represents the average of four replicates, the error bars represent the standard deviation of the measurements. The melting temperature in orange is defined as the lowest point of the first derivative which is the steepest part of the fluorescence measurements of rCbpDEC M2+M3.*

.

The truncated variant rCbpD$_{EC}$ M2+M3 without the LPMO domain, shows a significant shift in melting temperature compared to the full-length protein. The melting temperature for rCbpD$_{EC}$ M2+M3 is determined at 42.1°C (**Figure 4-11**). The melting temperature of the truncated variant has decreased by 20.9°C. To further investigate the melting temperature of rCbpD, the truncated rCbpD$_{EC}$ M1 variant (AA10 module) was analysed.

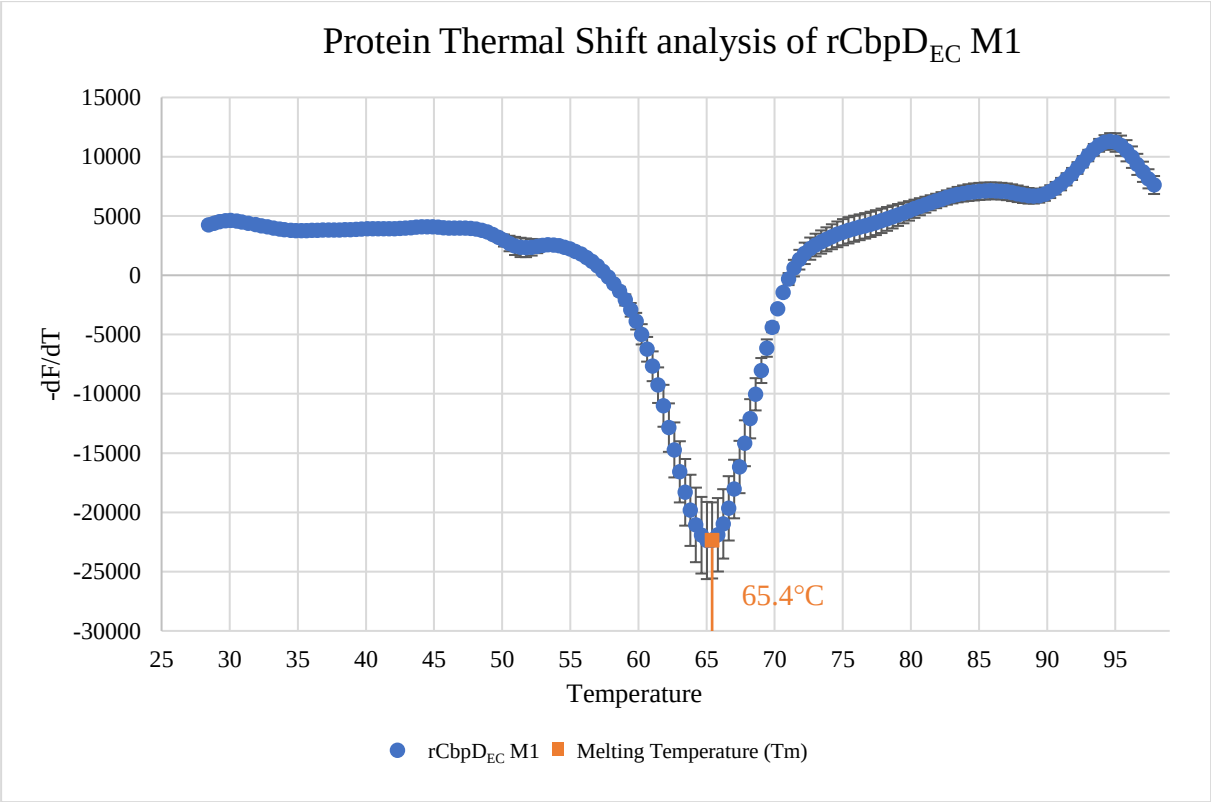

*Figure 4-12: **Melting point analysis of rCbpD$_{EC}$ M1**. Melting point determined by thermal shift analysis. The Y axis shows the derivative of the fluorescence measurements (F) with respect to temperature (T) while the x-axis shows the temperature (°C). The blue line represents the average of four replicates, the error bars represent the standard deviation of the measurements. The melting temperature in orange is defined as the lowest point of the first derivative which is the steepest part of the fluorescence measurements of rCbpD$_{EC}$ M1.*

Protein thermal shift analysis of the truncated variant rCbpD$_{EC}$ M1 shows that the melting temperature is 65.4 °C which is comparable with the full length enzyme. When comparing the full length enzyme (**Figure 4-10**), rCbpD$_{EC}$ M2+M3 (**Figure 4-11**) and rCbpD$_{EC}$ M1 (**Figure 4-12**) the uneven denaturing curve suggests the denaturing of the M2 and M3 domain first, prior to the denaturing of the M1 domain.

4.5 Post-translational modification of CbpD

4.5.1 Analysis of CbpD by SEC and IEF

While purifying rCbpD$_{PA}$ and rCbpD$_{EC}$, SEC purification revealed different elution patterns for the enzyme produced in *P. aeruginosa* and *E. coli*. To investigate the differences, iso-electric focusing was performed for the two protein variants.

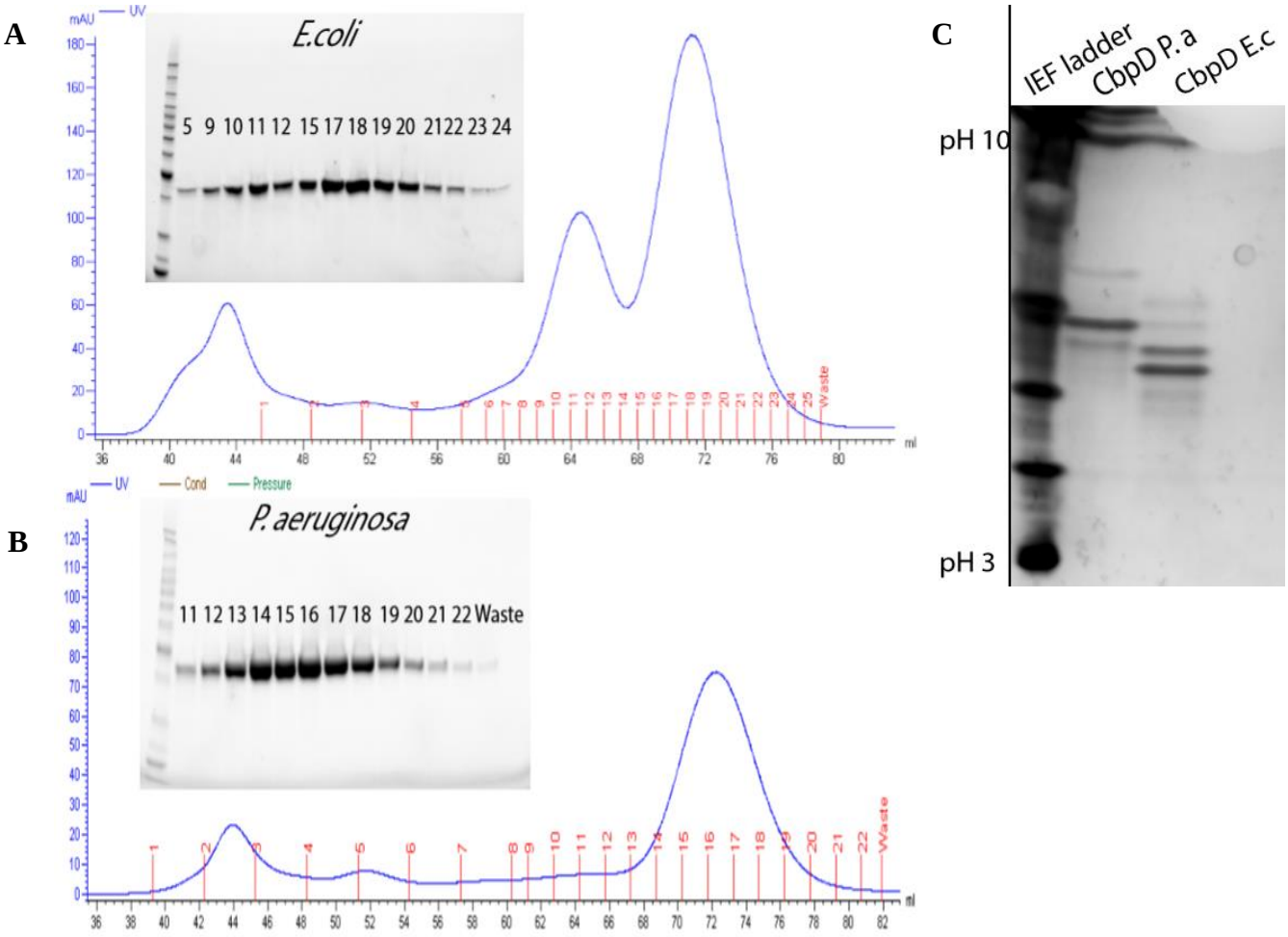

Figure 4-13 Analysis of CbpD with size exclusion chromatography and iso electric focusing. *(A): Size exclusion chromatography analysis of rCbpD$_{EC}$ with the resulting SDS-PAGE analysis. (B): Size exclusion chromatography analysis of rCbpD$_{PA}$. (C): Iso-electric focusing (IEF) gel image of rCbpD$_{PA}$ and rCbpD$_{EC}$. In SDS-PAGE gel (A and B) the ladder (Protein BenchMark™) is placed in the outermost lane on the left. In the IEF gel (C) the ladder (IEF standards; BioRad) is placed in the outer most lane. The SEC fractions (A and B) correspond to the SDS-PAGE analysis and are stated above the lane. For SDS-PAGE (A and B) 10 µL of undiluted sample solution was placed in each lane. For IEF (C), 20 µL of sample solution with a final protein concentration of 0.5 mg/mL was placed in each lane.*

Interestingly, differences in SEC elution pattern was observed for rCbpD$_{EC}$ and rCbpD$_{PA}$. While purifying rCbpD$_{EC}$, the SEC elution chromatogram shows two distinct peaks, however, the SDS-PAGE analysis shows the same size product (**Figure 4-13**; Panel A). The latter phenotype was not observed during purification of rCbpD$_{PA}$ (**Figure 4-13**; Panel B) In an attempt to investigate a possible explanation for the difference in phenotype, and Iso-electric focusing was performed on the purified proteins. Iso-electric focusing showed differences in band intensity and migration pattern (**Figure 4-13**; Panel C) To ensure that the separation caused by pI observed for CbpD is not shared with other selected LPMOs, the AA10 LPMO Cels2 and CBP21 from respectively, *Streptomyces coelicolor* and *Serratia marcescens*, were applied on a separate IEF gel and run under the same conditions. Only CbpD presented several bands while Cels2 and CBP21 did not show any separation on pI alone (**Figure 8-1**). Further

characterization of CbpD and the presentation of a heterogenous protein group was further investigated by mass spectrometry.

4.5.2 Analysis of CbpD PTMs by MALDI-TOF-MS

Digestion of the protein samples allowed a mass spectrometry approach to attempt identification of possible PTMs. Firstly, the use of MALDI-TOF and mass fingerprinting was performed to identify modifications. Peptide masses expected by digestion using trypsin were established by the PeptideMass tool on the ExPASy platform. (https://web.expasy.org/peptide_mass/) By allowing one missed cleavage, peptide masses were calculated and searched against MALDI-TOF mass spectrometry generated mass lists. Lysine residues previously identified as modified described in section **1.6** were in focus.

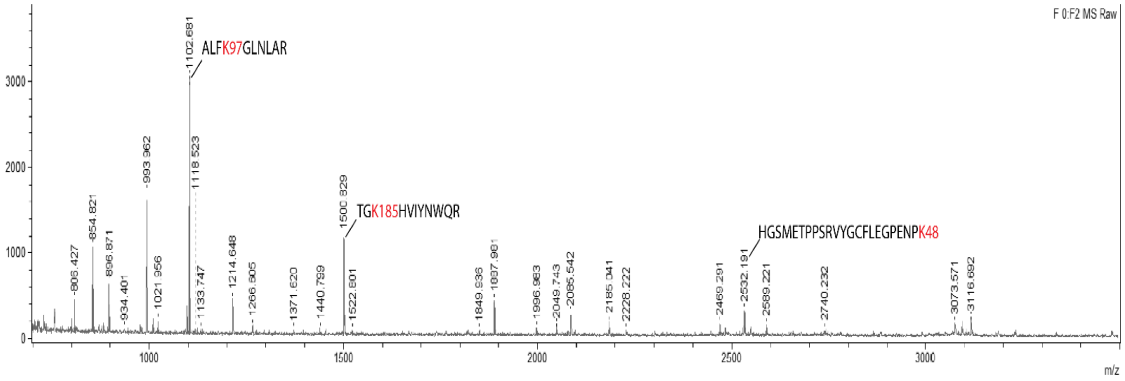

Figure 4-14: MALDI-TOF spectra generated from trypsin digested rCbpD$_{PA}$. *This mass spectrum shows the mass fingerprint of rCbpD$_{PA}$. The x-axis is the mass over charge (m/z) which is compiled as a mass list, while the y-axis is the intensity measured in absorbance units (a.u). The lysine residues of interest (red) and sequence are annotated above their respective masses. The generated mass lists were filtered for known contaminants and searched against the Mascot database.*

High intensity peaks for K97 and K185 were observed in the mass fingerprint containing missed cleavages. In addition, K48 was observed as correctly cleaved (**Figure 4-14**; Lysine residues marked in red). K166 and K262 were not observed in the MALDI-TOF mass spectrum. MASCOT searches of the generated mass lists did not observe any PTMs on the lysine residues. In addition, K262 peptides was outside the detection range (600-3500 Da). Therefore, LC-MS was performed allowing more detailed analysis of peptides and peptide fragments.

4.5.3 Analysis of CbpD PTMs by LC-MS

Firstly, pure protein samples of rCbpD$_{PA}$ and rCbpD$_{EC}$ were digested with trypsin described in **3.14.1** prior to cleaning and desalting the peptides described in section **3.14.3**. The peptides were analysed with nano spray ESI LC-MS running a 50 minute HPLC reverse-phase C18 gradient stated in section **3.16**. The peptide mass list for both MS and Tandem MS were searched using PEAKS software detailed in section **3.17**. Initial testing of LC-MS analysis presented several missed cleavages which reduced the sample coverage, in addition to artefacts from sample preparation caused by cOmplete inhibitor cocktail tablets (Results not shown).

rCbpD$_{EC}$ and rCbpD$_{PA}$ were purified without cOmplete inhibitor cocktail tablets and parallel samples were digested with respectfully trypsin and chymotrypsin. Data analysis was performed as described in section **3.17**. Sequence coverage from trypsin and chymotrypsin samples were combined resulting in rCbpD$_{EC}$ coverage of 99% (**Figure 4-15**; panel A) and rCbpD$_{PA}$ achieved a sample coverage of 91% (**Figure 4-15**; panel B)

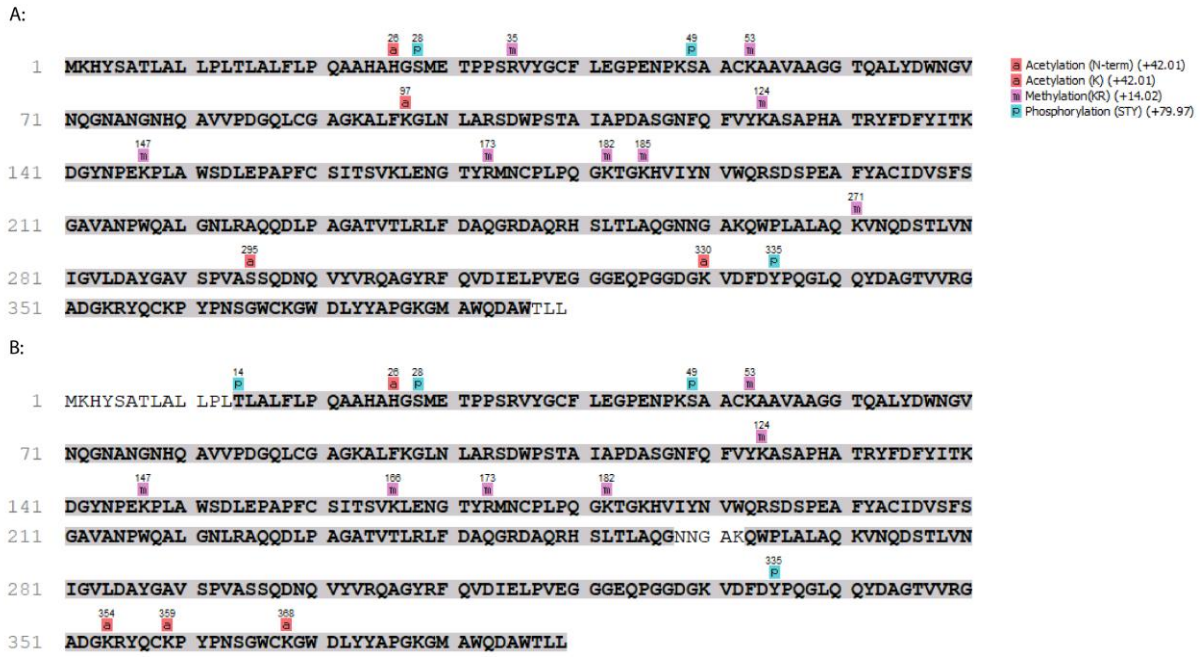

Figure 4-15: Sequence coverage map with observed PTMs*. This image shows sequence coverage of rCbpD from E. coli and P. aeruginosa with annotated PTMs above the sequence. The sequence coverage is comprised of parallels from two samples, one digested with chymotrypsin and the other with trypsin for respectively (A): rCbpD$_{EC}$ with 99% sequence coverage and (B): rCbpD$_{PA}$ with 91% sequence coverage. Sequence coverage is indicated with the grey shading over the sequence. For both A and B, FDR of 0.1% and Ascore > 20 were utilized during data analysis.*

The high sequence coverage was achieved by merging the trypsin and chymotrypsin digested samples during data analysis. A variety of post-translational modifications on proteins from

both *E. coli* and *P. aeruginosa* are observed. The modifications observed are situated on lysine residues, arginine residues and S/T/Y phosphorylation's.

4.5.4 LC-MS analysis of CbpD species separated by IEF

Further analysis of the pI separated protein species was performed in attempts to characterize if variable PTMs account for the shift observed in (**Figure 4-13**; panel C). In addition, the rCbpD$_{PA}$ Lys variant with mutated lysine residues to arginine was added to investigate if lysine modification contributed to the pI.

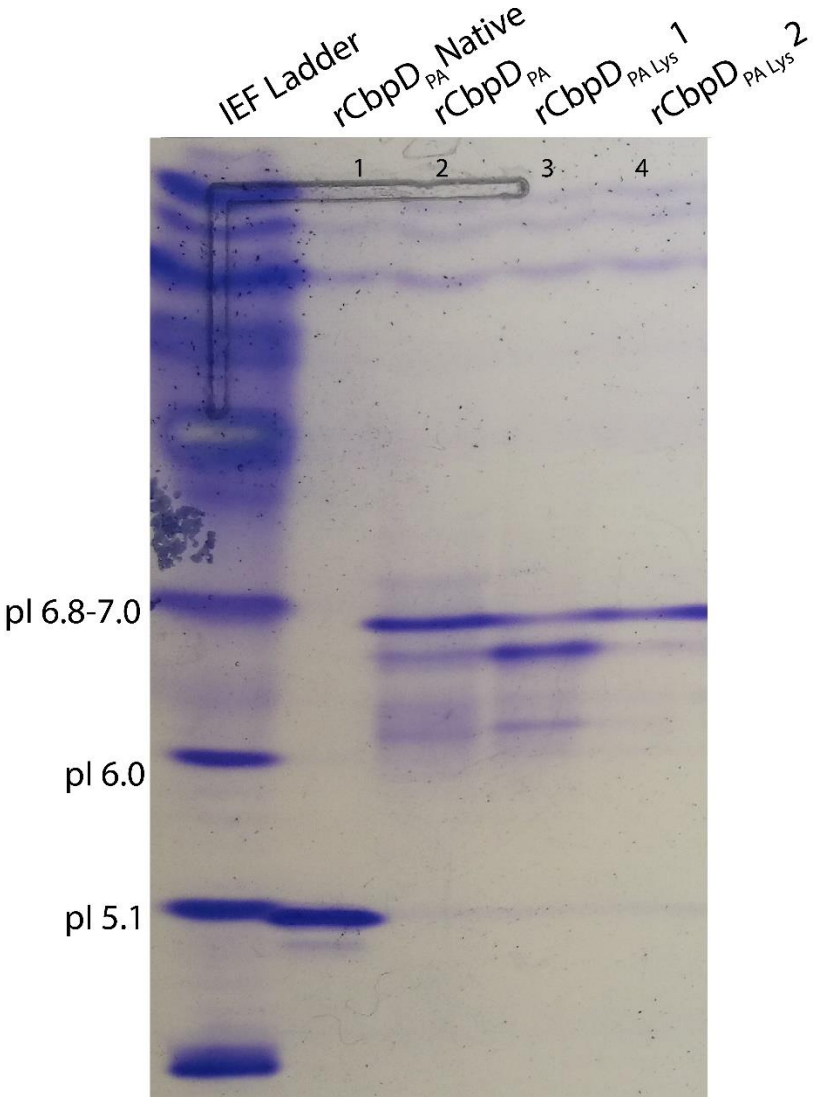

Figure 4-16: Separation of rCbpD variant protein species by iso-electric focusing. *This IEF gel image shows the distribution of protein species based on pI. The ladder (IEF standards; BioRad) is placed in the outermost lane on the left. The protein variants are numbered, and names are stated above their respective lane. The sample volume of 20 µL with a final protein concentration of 0.5 mg/mL is applied for each sample. The gel is coloured with Coomassie stain solution and de-stained before imaging.*

Protein samples purified to 95% purity were separated into several bands by iso-electric focusing. The contribution of the His-tag is clearly visible as rCbpD$_{PA}$ Native has a pI ≈ 5.1 (**Figure 4-16**; Lane 1) and rCbpD$_{PA}$ ≈ 6.8 (**Figure 4-16**; Lane 2). In addition, there are visible differences of protein band distribution for different batches of rCbpD$_{PA}$ Lys (**Figure 4-16**; lane 3 and 4). The rCbpD$_{PA}$ Native variant does not present the same degree of separation as the other variants. For further analysis, LC-MS was performed on selected bands.

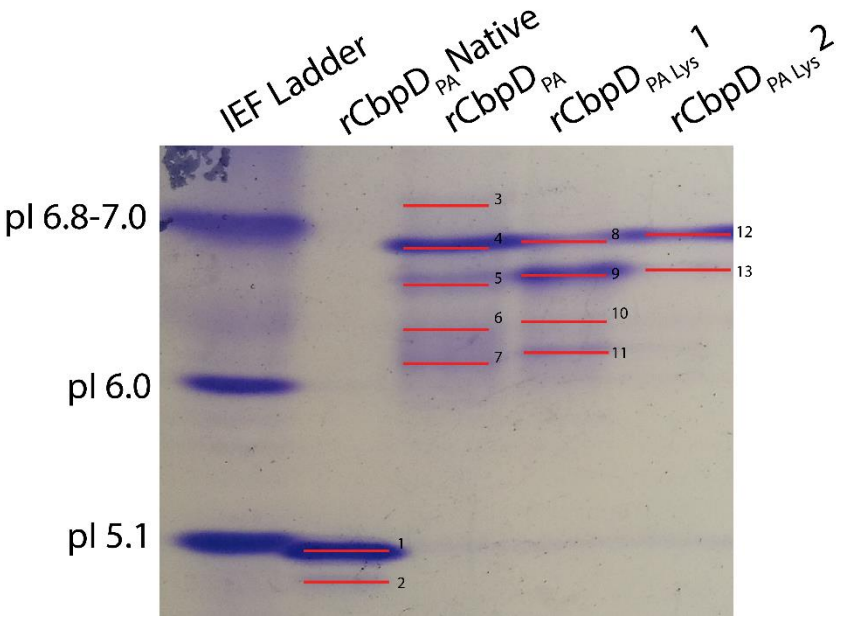

Figure 4-17: Iso electric focusing gel image of rCbpD variants visualizing sample excision*. This gel image shows the distribution of samples excised from the IEF gel (**Figure 4-16**). The excised samples are indicated with red lines and are numbered on the righthand side.*

Excised bands indicated with red lines (**Figure 4-17**) were analysed with LC-MS, the results were searched with stringent search criteria as described in section 3.17. The 13 samples were identified as CbpD with a sequence coverage average of 74% (**Figure 4-18**).

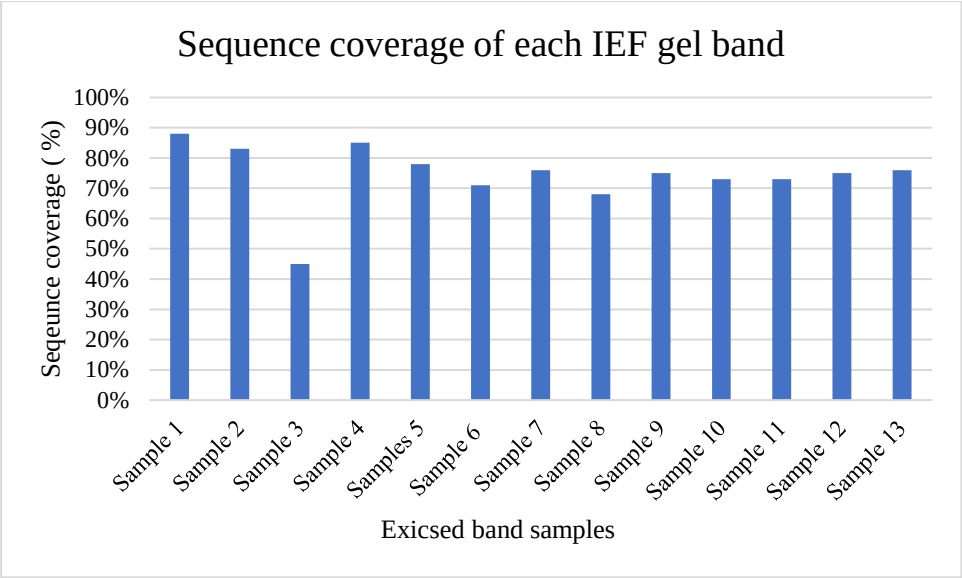

Figure 4-18: Sequence coverage of excised IEF gel samples. *The bar graph shows the sequence coverage of each sample excised from the IEF gel. The x-axis shows the samples excised as annotated in* ***Figure 4-17****, while the y-axis is the percentage of coverage obtained.*

All bands were identified as CbpD, however sample 3 was identified with a sequence coverage of 45 % compared to the other samples with a sequence coverage between 68 – 88 %. When concatenating all the sequences to create an overview, 90% of the sequence is covered. However, by removing the signal peptide from the calculations, the sequence coverage is 97.5% (**Figure 4-19**).

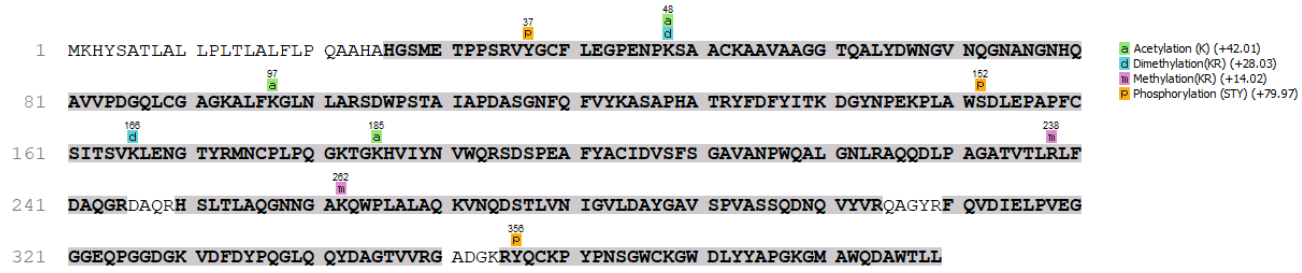

Figure 4-19: PTM analysis of the combined IEF samples showing PTM presence. *This image shows the combined data from samples excised from the IEF gel. The sequence coverage is indicated as the grey shading over the sequence. PTMs observed are annotated above the sequence.*

The concatenated sample overview shows several modifications in rCbpD. However, the determination of why rCbpD presents as several pI bands cannot be deduced by PTM analysis at this point. Therefore, the data was not analysed further.

4.6 Microscale thermophoresis of protein-substrate interaction

Attempts to investigate substrate affinity was performed on soluble chitooligomers. With micro scale thermophoresis (MST), the potential binding affinity towards soluble chitin hexose ($GlcNac_6$) was investigated. MST indicates binding by measuring the rate of diffusion in the protein sample. Capillary screening showed that the protein and ligand showed no affinity towards the standards capillaries prior to protein-ligand analysis. Initial screening with a high concentration of $GlcNac_6$ revealed no differences between the protein control and the protein-ligand sample. Therefore, a serial dilution assay was not performed.

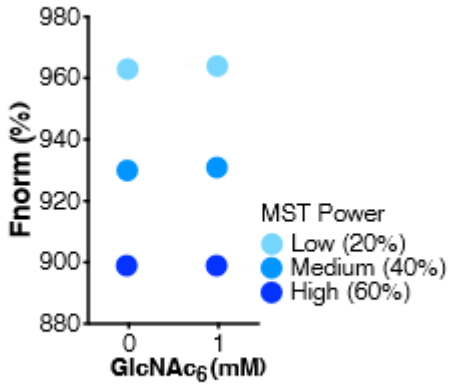

Figure 4-20. Binding affinity determined by MST analysis of rCbpD$_{PA}$. *The graph shows the binding affinity of rCbpD$_{PA}$ towards [GlcNac]$_6$. The x-axis presents the [GlcNac]$_6$ concentrations (0 and 1 mM) while the y-axis is the normalized fluorescence (F_{norm}). F_{norm} is determined by measuring fluoresce before and after IR laser heating (MST power). MST power for 20, 40 and 60% was used for quality control ensuring confident binding data. Figure supplied by Fatemeh Askarian PhD.*

The MST data shown in **Figure 4-20** indicate that CbpD is not able to bind soluble chitin oligomers since there is no observable difference in F_{norm} for samples with and without $GlcNac_6$ present. The substrate affinity is important in understanding the biological function of CbpD.

4.7 Enzyme activity

CbpD has previously shown LPMO activity towards chitin in an unpublished experiment (Askarian, pers.comm.). Enzyme assays were performed to determine the activity of the protein

variants. The LPMO reaction requires an external reductant, which in this case was ascorbic acid, therefore, a negative control without ascorbic acid was added to eliminate artefacts. The rCbpD$_{PA}$ variant shows enzyme activity with ascorbic acid present (**Figure 4-21**; panel A) however, does not present any activity without the reductant (**Figure 4-21**; panel B) coinciding with LPMO literature.

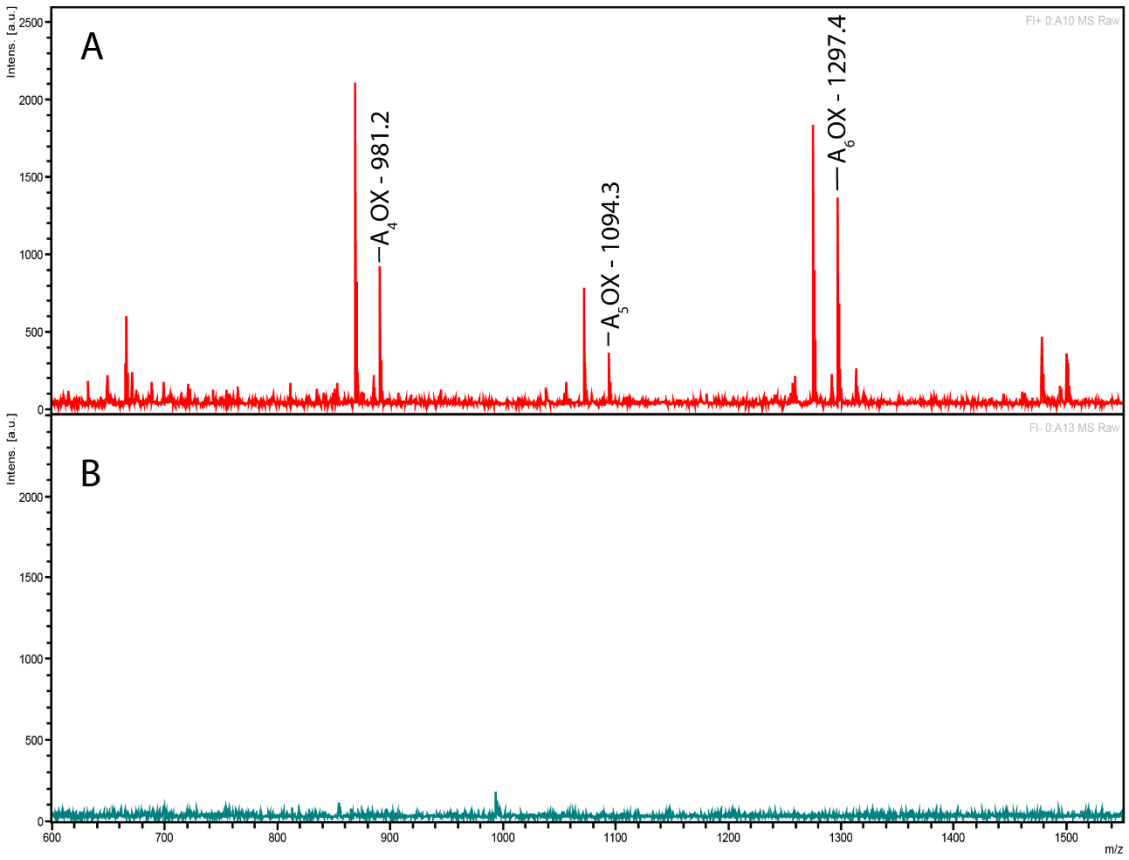

Figure 4-21: MALDI-TOF analysis of enzyme activity towards β-chitin for rCbpD$_{PA}$. *The MALDI-TOF spectrum shows enzyme assays of rCbpD$_{PA}$ both with and without an exogenous reductant. The y-axis represents the intensity in absorbance units (a.u) while the x-axis represents the mass over charge (m/z). (A): rCbpD$_{PA}$ enzyme assay with ascorbic acid present as an external reductant. (B): rCbpD$_{PA}$ enzyme assay performed without ascorbic acid as an external reductant.*

Enzyme activity assays were performed for all full length enzymes presenting activity towards β-chitin. These activity assays show that the proteins were handled correctly, and the enzymes still retain enzyme activity. Enzymes purified from both *P. aeruginosa* (**Figure 4-22**; panel A and C) and *E. coli* (**Figure 4-22**; Panel B) show activity towards β-chitin. The rCbpD$_{PA}$ Lys variant is covered in section 4.9. The enzyme assays are not intended to be comparable and the varying intensities do not imply differences in enzyme activity.

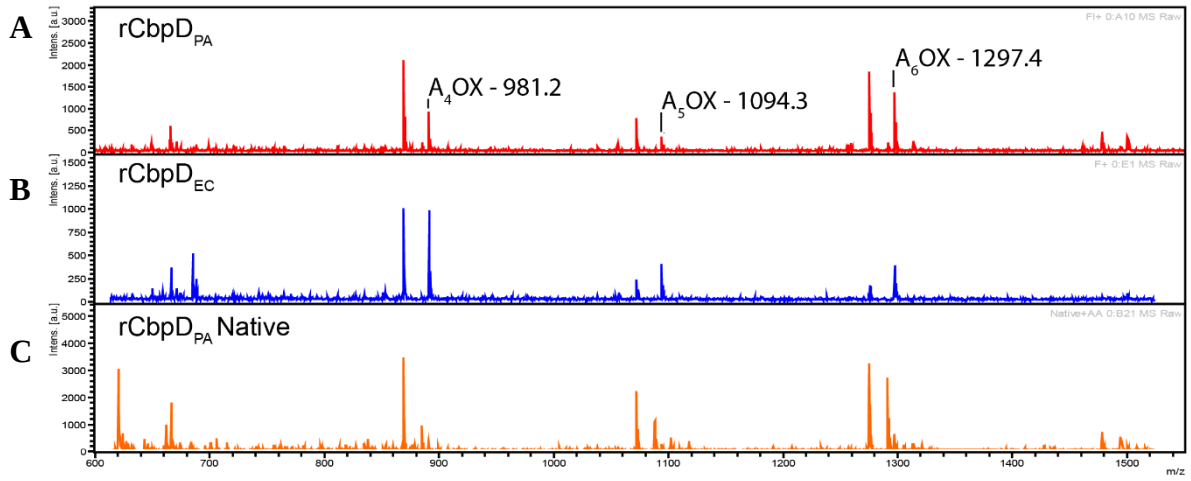

Figure 4-22: MALDI-TOF analysis of enzyme activity towards β-chitin for full length enzymes. *The MALDI-TOF spectra show activity assays for full length enzymes performed by incubating 20 mg/mL β-chitin with 1 µM protein and 1 mM ascorbic acid. The y-axis represents the intensity while the x-axis represents the mass over charge (m/z). (A): rCbpD$_{PA}$, (B): rCbpD$_{EC}$ and (C): rCbpD$_{PA}$ Native.*

In (**Figure 4-22**; A and C) there are faint peaks of A_7OX chitooligomers, however, they were not annotated in **Figure 4-22**.

4.8 The ability of *P. aeruginosa* to utilize chitin as a carbon and/or nitrogen source

The presence of a chitinase and a chitin active LPMO in the *P. aeruginosa* genome, prompted us to investigate whether *P. aeruginosa* could utilize chitin as a carbon and/or nitrogen source. Firstly, this ability was investigated by culturing the bacteria in media containing chitin and exploring growth using OD_{600} and CFU counting as described in section **3.13.1**. Initial minimal media comprised of M9 minimal salts 1x, 2 mM $MgSO_4$, 0.1 mM $CaCl_2$ and 5 g/L casamino acids hereafter referred to as $M9_{PA}$ was firstly attempted.

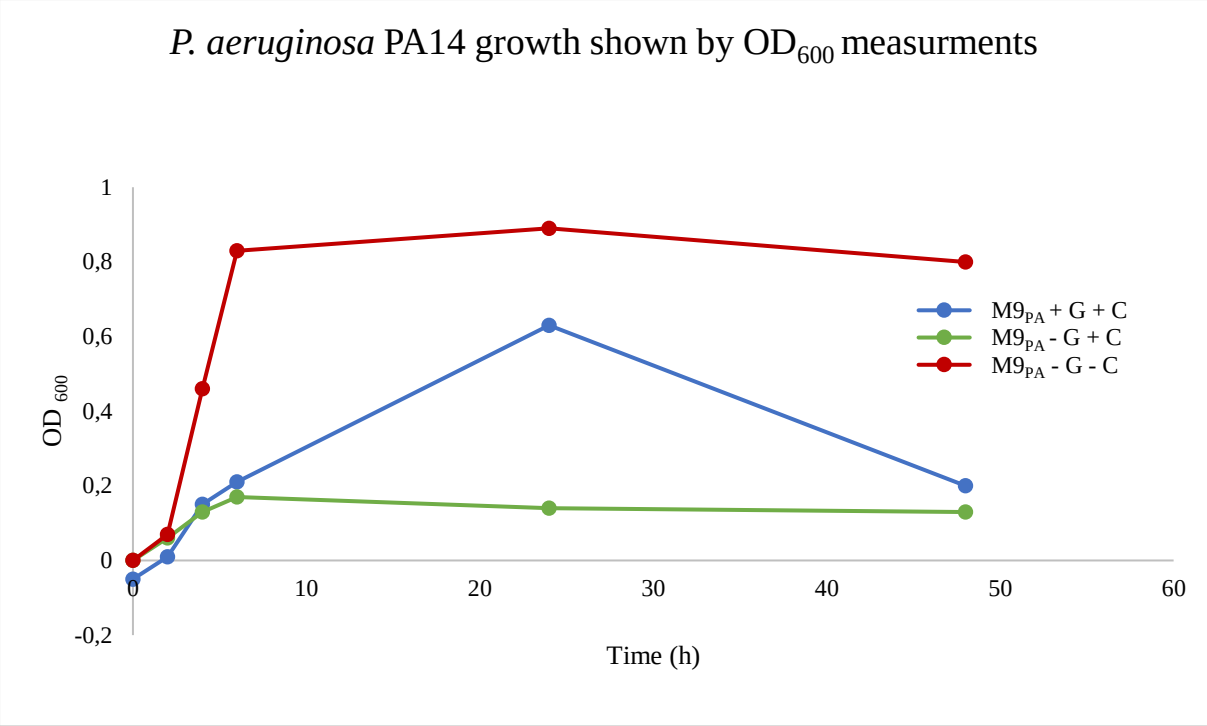

Figure 4-23: Investigating the utilization of chitin by monitoring OD_{600} measurements. *This graph presents the growth rates of PA14 cultivated in $M9_{PA}$ supplemented with either chitin (C), glucose (G), both or none. Supplemented medium components are indicated as present (+) or absent (-). Measurements were conducted at 0h, 2h, 4h, 6h, 24h, and 48h which are indicated by the line indicators. The x-axis indicates the time in hours (h) while the y-axis indicates the OD_{600} measurements.*

When measuring OD_{600} the culture was continuously agitated during sample retrieval ensuring a representative sample, in addition the sample was transferred to the cuvette and immediately measured to ensure ensuring the chitin particle remained suspended. A serial dilution was performed for every timepoint and counted the following day. However, at the 24 hour measurement the cultures showed clumps in the chitin supplemented media. The visible clumps created issues during sample retrieval. In addition, the retrieved samples were not representative for the cultures. These observations were complemented at the 48 hour mark (results not shown). However, the OD measurements showed a decrease in cell density. These observations led to the conclusion that OD is not suitable for this research question and (**Figure 4-23**) cannot be trusted. The CFU counting measurement (data not shown) were not useable as after 8 hours the triplicates showed large variations and the clumping of bacteria created bias during sample retrieval. Therefore, analysis of chitin utilization was attempted by monitoring metabolism by analysis of gas phase O_2 and CO_2.

4.8.1 Growth analysis by robotized GC-MS

The same medium and conditions as tested in **3.13.1** which resulted in OD_{600} measurements in **Figure 4-23** were applied in the robotized incubation sampling system.

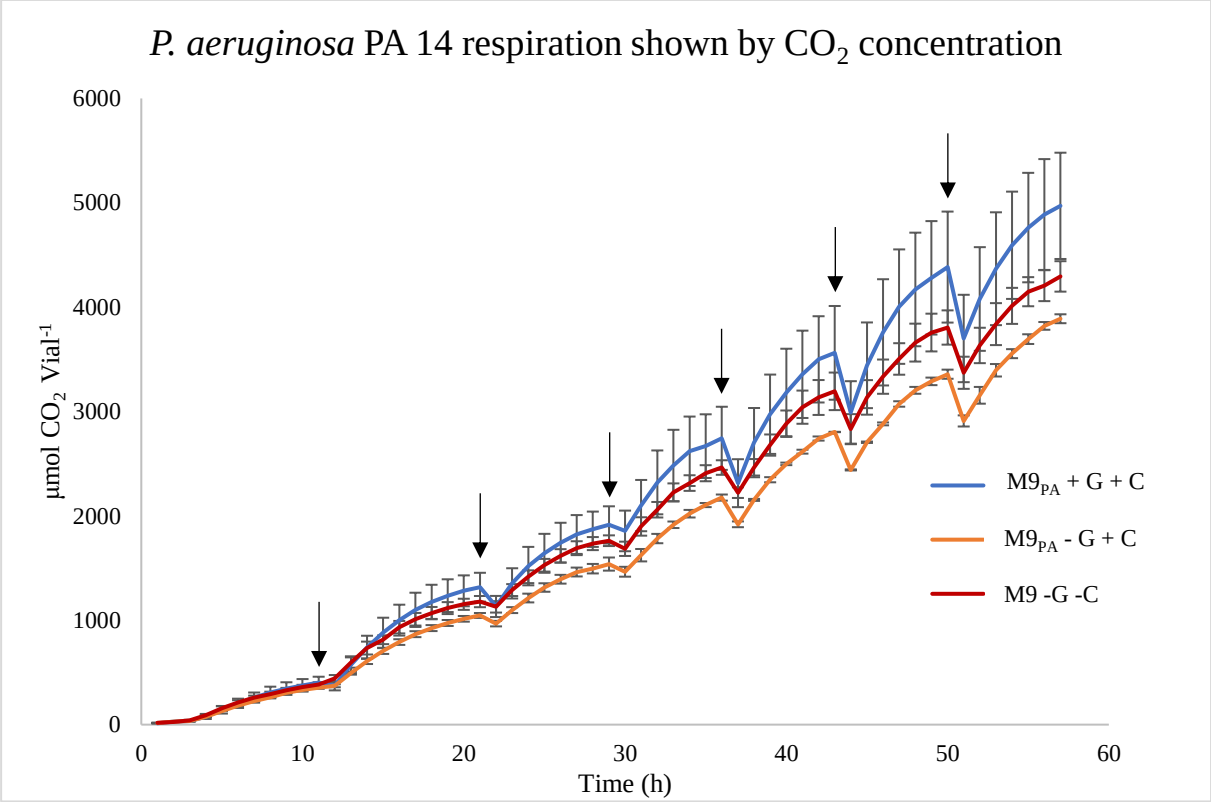

Figure 4-24: Investigating the utilization of chitin by monitoring gas metabolism. *This graph presents the growth rates of PA14 cultivated in $M9_{PA}$ supplemented with either chitin (C), glucose (G), both or none. Supplemented medium components are indicated as present (+) or absent (-). The growth is monitored by measuring CO2 production gas chromatography coupled with an automatic gas sampling robot. The growth curves are the average of triplicates and the error bars indicate the standard deviation for the triplicates. The x-axis presents the time in hours (h) while the y-axis presents the CO_2 measurements in µmol per vial (µmol CO_2 Vial $^{-1}$) The arrows signify the addition of oxygen, the following data point after addition is voided.*

The use of closed systems coupled with gas chromatography allowed monitoring the concentrations of oxygen and carbon dioxide gas present in the vials. This method eliminated the need for representative sample retrieval. In (**Figure 4-24**) the first attempt for measuring the growth showed that the background nutrients in the $M9_{PA}$ media masked the potential contribution of β-chitin and glucose. Casamino acids in $M9_{PA}$ was utilized as the carbon source, therefore casamino acids were removed and glucose used as the only carbon source.

Table 20: List of the optimized media created after initial establishment of the robotic gas sampling system altering the glucose concentration and removing casamino acids.

Media	M9 + G + C	M9 + G	M9 + C	M9
$M9_{Minimal}$	+	+	+	+
0.5 g/L Glucose	+	+		
2 g/L β-Chitin	+		+	

Optimizations of $M9_{PA}$ medium was performed by removing casamino acids. The optimized minimal medium was comprised of M9 minimal salts (1x), 2 mM $MgSO_4$ and 0.1 mM $CaCl_2$ hereafter referred to as $M9_{Minimal}$. $M9_{Minimal}$ supplemented with 0.5 g/L glucose concentrations as established by small scale media optimization described in section **3.7.5**. The optimized minimal medium allowed the investigation of each medium component. **Table 20** shows an overview of the different media.

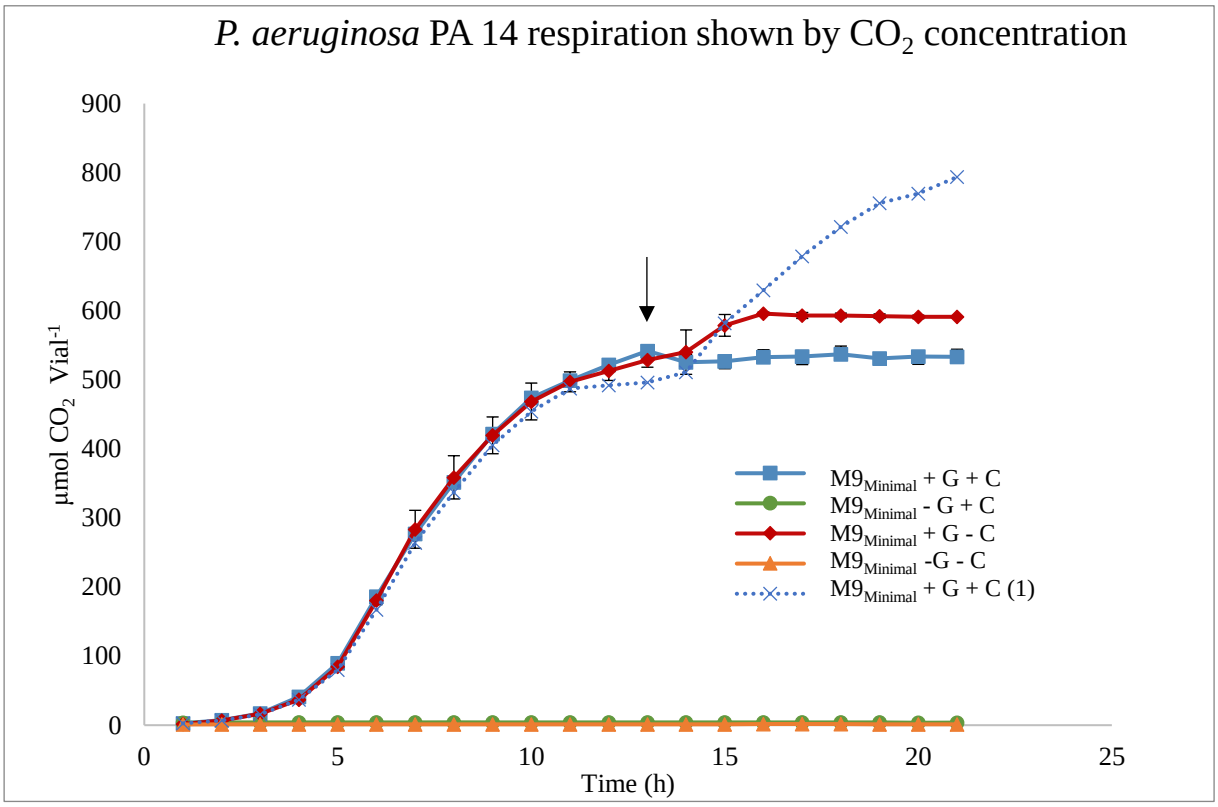

Figure 4-25: Investigating the utilization of chitin by monitoring gas metabolism in optimized minimal media. *This graph presents the growth rates of PA14 cultivated in $M9_{Minimal}$ supplemented with either chitin (C), glucose (G), both or none. Supplemented medium components are indicated as present (+) or absent (-). The growth is monitored by measuring CO2 production with gas chromatography coupled with an automatic gas sampling robot. The growth curves are the average of triplicates and the error bars indicate the standard deviation for the triplicates. The x-axis presents the time in hours (h) while the y-axis presents the CO_2 measurements in µmol per vial (µmol CO_2 Vial $^{-1}$). Oxygen was added at the 13 hour mark (arrow), voiding the 14 hour results.*

For control measures, both $M9_{Minimal}$ media alone and $M9_{Minimal}$ supplemented with chitin were added to investigate background nutrients. During the analysis, no CO_2 was observed in the control samples (**Figure 4-25**). This suggests that there are no background nutrients in the $M9_{Minimal}$ medium alone or the M9 medium supplemented with chitin. These results show that *P. aeruginosa* is not able to grow on chitin alone and suggest that the chitin used is not laced with other carbon sources. However, $M9_{Minimal}$ supplemented with glucose and $M9_{Minimal}$ supplemented with glucose and chitin both show similar growth curves. At the 13 hour mark,

5 mL of oxygen was added to ensure oxidic conditions and voiding the 14 hour data points. Interestingly, after adding oxygen one replicate in $M9_{Minimal}$ medium supplemented with chitin and glucose increased the carbon dioxide production as the rest of the triplicates and $M9_{Minimal}$ supplemented with glucose samples stagnated. Since the phenotype was only observed in one, the possibility of error from either contamination or sample preparation was further investigated.

Since *P. aeruginosa* utilizes quorum sensing which is mediated by cell density, glucose concentrations were further analysed to investigate the theory that the one replicate in **Figure 4-25** had surpassed a putative cell density threshold and engaged in chitin utilization. This was performed by measuring carbon dioxide production in $M9_{minimal}$ supplemented with glucose concentrations both lower and higher than the initial experiment. Therefore, $M9_{minimal}$ was supplemented with 0.4, 0.5 and 0.6 g/L glucose. $M9_{Minimal}$ and $M9_{minimal}$ supplemented with chitin were excluded, since triplicates has previously shown no growth with these conditions.

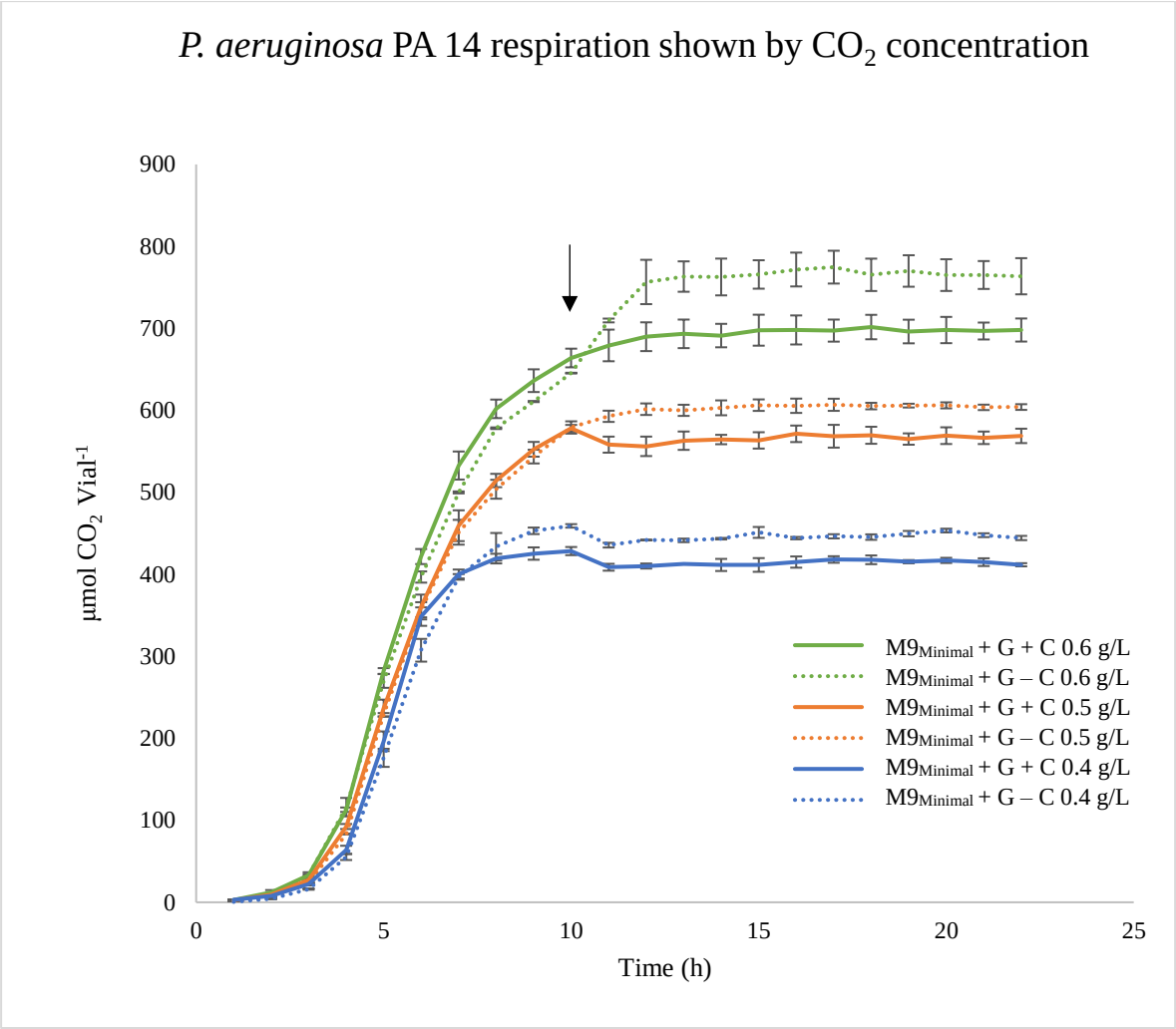

Figure 4-26: Investigating possible growth contribution of chitin in different glucose concentrations by monitoring gas metabolism. *This graph presents the growth rates of PA14 cultivated in $M9_{minimal}$ supplemented with either chitin (C), variable glucose concentrations (G) or both (G+C). Supplemented medium components are indicated as present (+) or absent (-). Samples are colour coded and stated in figure legend. The growth is monitored by measuring CO2 production with gas chromatography coupled with an automatic gas sampling robot. The growth curves are the average of triplicates and the error bars indicate the standard deviation for the triplicates. The x-axis presents the time in hours (h) while the y-axis presents the CO_2 measurements in µmol per vial (µmol CO_2 Vial $^{-1}$). Oxygen was added at the 10 hour mark (arrow), voiding the 11 hour results.*

The initial glucose concertation was studied closer in (**Figure 4-26**)**.** At the 10 hour mark 5 mL of oxygen was added to ensure oxidic conditions throughout the experiment (**Figure 4-26**; Black arrow). Both increasing and decreasing the glucose concentration from the initial 0.5 g/L concentration illustrates how glucose contributes to the growth. Media supplemented with both chitin and glucose and only glucose show the same growth tendencies and follow the same trajectory. When increasing the concentration of glucose, the trajectory stays constant, however the curve stagnates at a higher concentration of carbon dioxide suggesting a higher amount of growth. These results suggest that chitin does not contribute to the growth since the samples absence of chitin presents the same growth curve as media containing chitin. Glucose

concentrations do not explain the replicate observed in **Figure 4-25**. Therefore, environmental stress factors such as hypoxia and nutrient limitations were investigated to observe if stressing cells could trigger regulatory mechanisms allowing *P. aeruginosa* to utilize chitin. $M9_{minimal}$ supplemented with 0.5 g/L glucose + 2 g/L chitin and $M9_{minimal}$ supplemented with 0.5 g/L glucose were prepared in parallels of triplicates. One parallel was kept oxidic the entire experiment, whilst the other entered anoxic conditions.

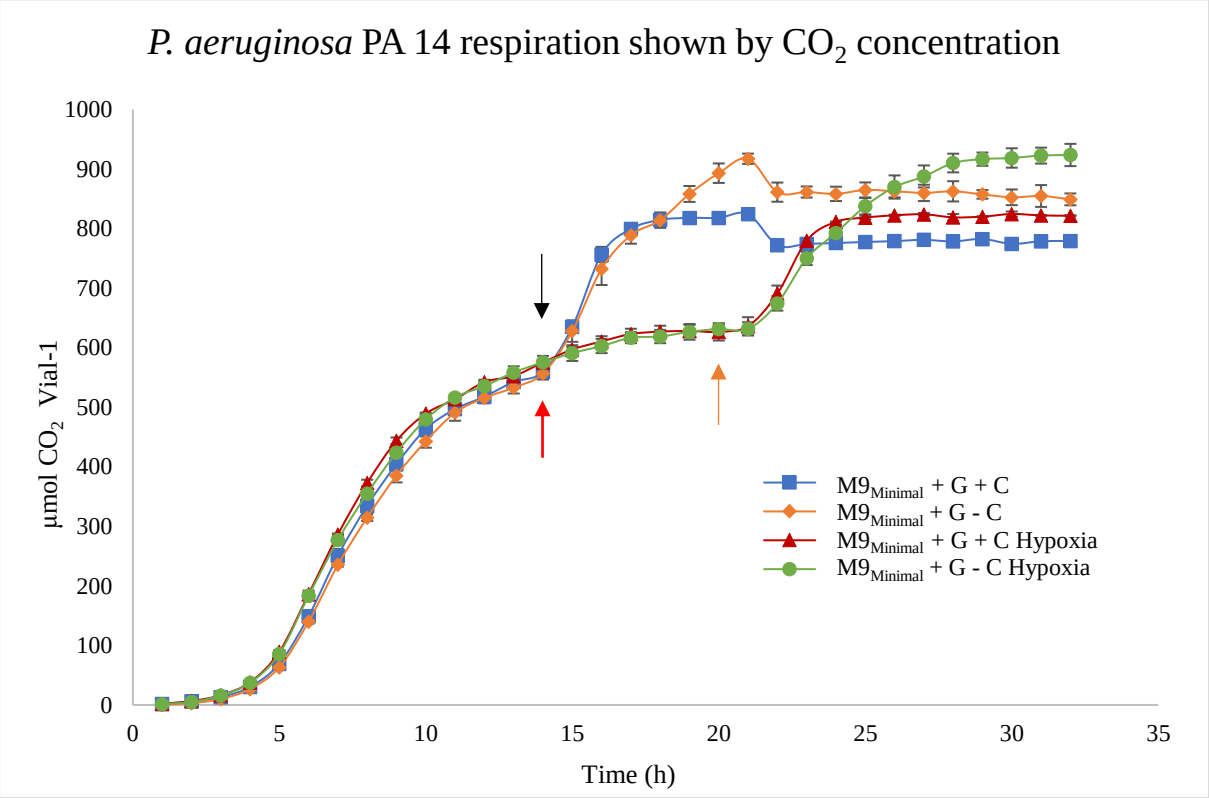

Figure 4-27: Investigating the possible impact of environmental stress factors on chitin utilization. *This graph presents the growth rates of PA14 cultivated in $M9_{minimal}$ supplemented with either chitin (C), glucose (G) or both (G+C). Supplemented medium components are indicated as present (+) or absent (-). One parallel entered hypoxic conditions Samples are colour coded and stated in figure legend. The growth is monitored by measuring CO2 production with gas chromatography coupled with an automatic gas sampling robot. The growth curves for G+C samples are the average of triplicates and the glucose samples are the average of duplicates. The error bars indicate the standard deviation for averages. The x-axis presents the time in hours (h) while the y-axis presents the CO_2 measurements in µmol per vial (µmol CO_2 Vial $^{-1}$). Oxygen was added at the 14 hour mark (black arrow), voiding the 15 hour results for oxidic samples while oxygen was added at the 20 hour mark (orange arrow), voiding the 21 hour results. At the 14 hour mark, 0.2 g/L glucose was added (red arrow) to all samples to expend all oxygen present.*

The experimental setup was designed to keep one parallels in oxidic state and let the other parallel enter anoxic conditions. However, the initial glucose concentration (0.5 g/L) was inadequate to deplete the oxygen. There was still oxygen present when the cultures started to

stagnate, therefore, 0.2 g/L of glucose was added to all samples ensuring total oxygen consumption (**Figure 4-27**; red arrow). The oxidic parallel was supplemented with 5 mL oxygen and increased the carbon dioxide production immediately before stagnating, suggesting the glucose was spent. The anoxic parallel carbon dioxide concentration stagnated when the oxygen was depleted. When oxygen was added to the anoxic parallel (**Figure 4-27**; orange arrow) the carbon dioxide concentrations increased, suggesting that *P. aeruginosa* was not able to utilize the added glucose during low oxygen concentrations.

After the experiment was terminated, supernatant with chitin was retrieved to investigate if CbpD was present and producing oxidized products. The supernatant alone, supernatant with ascorbic acid and supernatant with ascorbic acid and supplemented with $rCbpD_{PA}$, were investigated for the presence of oxidized products. The supernatant alone or the supernatant with ascorbic acid did not show any oxidized products with HILIC analysis. However, the positive control with pure $rCbpD_{PA}$ added to the supernatant with 1 µM ascorbic acid showed a presence of oxidized products (results not shown).

4.9 Mutations of modified lysine residues

Structure prediction aided by the RaptorX server, predicted the 3D model of protein structure when there are no viable homologs in the PDB database (Källberg et al., 2012).

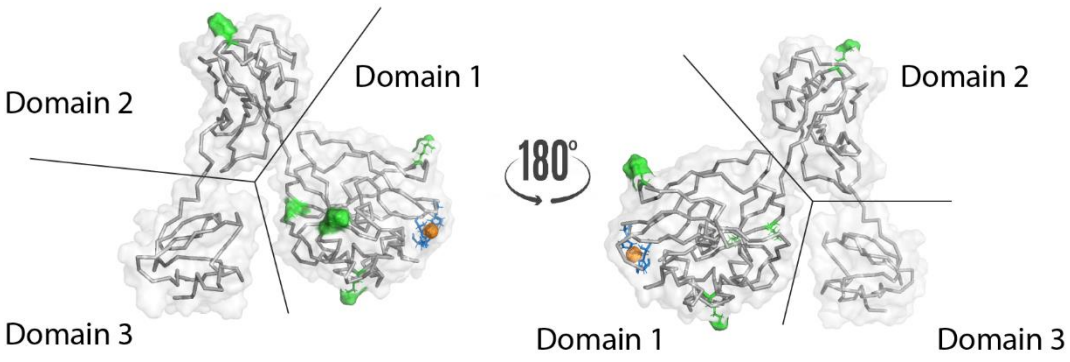

Figure 4-28: 3D homology model of CbpD visualizing the lysine mutations. *The homology model was generated by the Raptor X based on sequence. The image was created in Pymol. The sequence is portrayed as a cartoon model with the surface overlain with low opacity. The lysine residues of interest (green) are shown on the surface of the protein. The active site (blue) with copper molecule (orange) is also indicated on the model. The domain names are placed according to sequence. Both images are taken from the same position only changing the z-axis 180°.*

The previously identified lysine residues K48R, K97R, K185R and K262R (**Figure 4-28**; residues marked in green) that have been shown to contain PTMs (**1.6**) and K166R observed in an unpublished study (Askarian, Pers. comm.) were mutated to arginine. The mutations were performed to investigate if lysine modifications are important for folding, secretion or enzyme activity. The predicted structure shows that the lysine residues are not situated in close proximity to the active site.

4.9.1 PCR of the rCbpD$_{PA}$ Lys -His recombinant gene

In order to investigate the role of lysine modifications, the pGM931 plasmid containing the mutated *cbpD* insert was ordered from Gene script. After electroporating the plasmid into the *P. aeruginosa* PA14ΔCbpD the bacteria were plated on LB 300 µg/mL carbenicillin and incubated overnight. Two colonies were picked, and colony PCR was performed in order to select colonies containing the plasmid. The resulting PCR using AraC-FW-SbfI-Rev (**Figure 4-29**; Lane one and four, expected product size: 2151 bps), AraC-FW-IntC-Rev (**Figure 4-29**; Lane 2 and 5, expected product size: 1320 bps) and OutC-FW-IntC-Rev (**Figure 4-29**; Lane 3 and 6; expected product size: 563 bps)

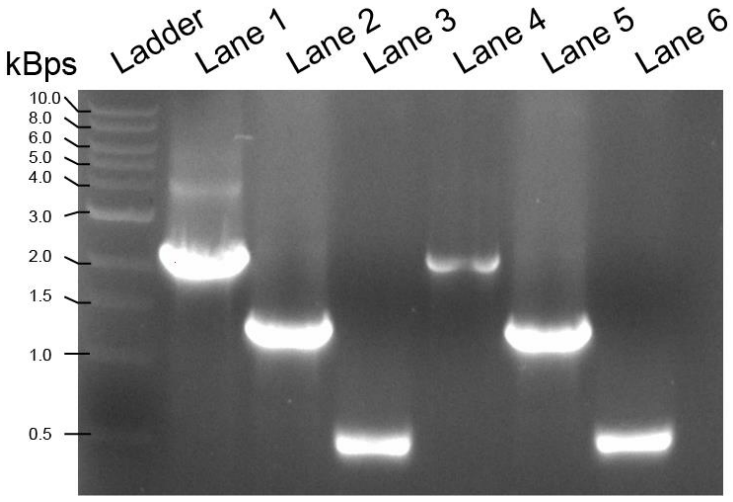

Figure 4-29 Agarose gel analysis of colony PCR for rCbpD$_{PA}$ Lys. *This gel image shows the colony PCR on PA14 cells incorporated with the rCbpD$_{PA}$ Lys variant. The ladder (QuickLoad® 1kb) was placed in the outermost lane on the left. Colony PCR was performed with AraC-FW-SbfI-Rev (Lane 1 and 4), AraC-FW-IntC-Rev (Lane 2 and 5) and OutC-FW-IntC-Rev (Lane 3 and 6). Sample volumes of 20 µL were placed in the wells.*

Purification of the rCbpD$_{PA}$ Lys variant was performed in the same manner as the other full length variants. However, cell culture and protein extract presented a different phenotype rCbpD$_{PA}$ Lys and rCbpD$_{PA.}$ Intriguingly, both the cell culture (**Figure 4-30**; Panel A) and the protein extract (**Figure 4-30**; Panel B) from rCbpD$_{PA}$ exhibited a colour change from green to blue.

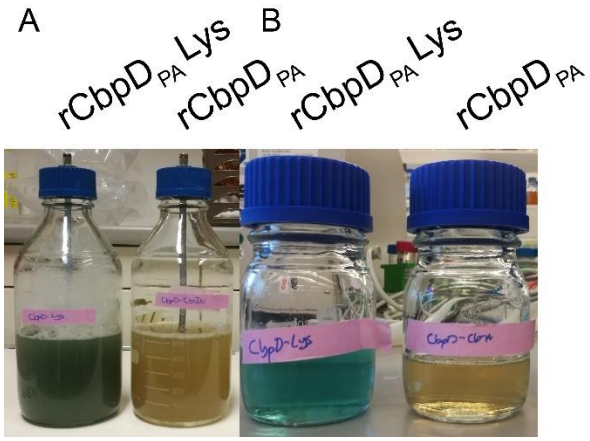

Figure 4-30:Images of cell culture and protein extract comparing rCbpD$_{PA}$ Lys and rCbpD$_{PA}$ full length variant. *(A): Cell cultures after cultivation in Lex-48 bioreactor. (B): Protein extract from the periplasm. The variant names are stated above the images.*

Purification of rCbpD$_{PA}$ Lys (**Figure 4-31**; panel A) does not show any significant differences from the purified rCbpD$_{PA}$ full-length variant (**Figure 4-31**; panel B).

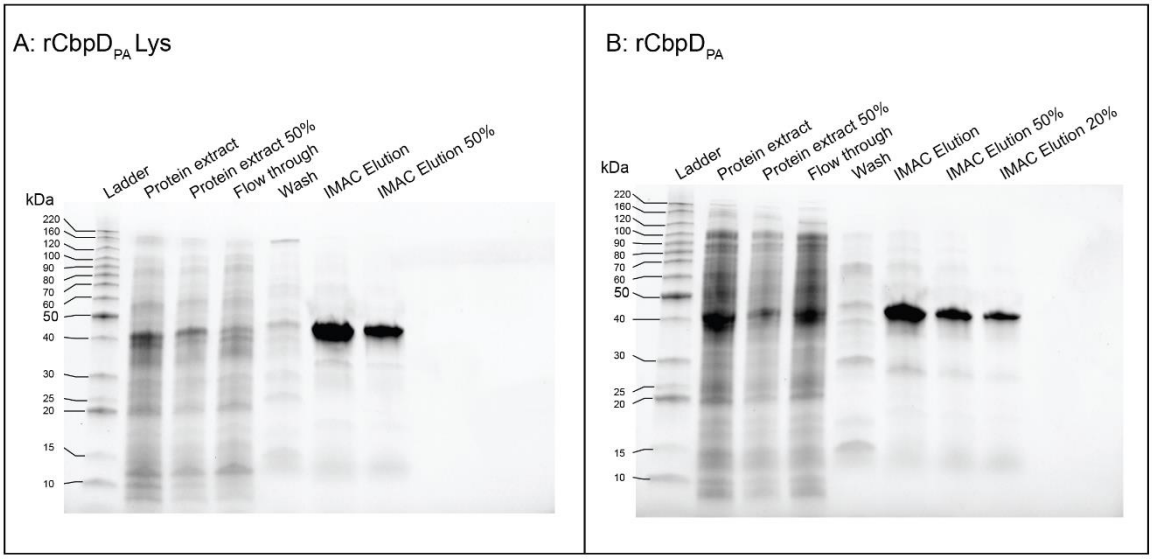

Figure 4-31 SDS-PAGE analysis of rCbpD$_{PA}$ Lys and rCbpD$_{PA}$ variants. *Images of SDS-PAGE gels show analysis of (A): rCbpD$_{PA}$ Lys IMAC purification, (B): rCbpD$_{PA}$ IMAC purification. The sources of the samples are stated above the lanes. The*

protein molecular weight ladder (protein BenchMark™) is placed in the outer left lane of both SDS-PAGE gels. Sample volumes applied were 20 µL of the undiluted sample solution.

4.9.2 Comparison of protein melting point analysis rCbpD$_{PA}$ and rCbpD$_{PA}$ Lys

Protein melting point analysis of the rCbpD$_{PA}$ and rCbpD$_{PA}$ Lys variants was performed to investigate if the mutations alter the melting point of the protein. The absorbance signals were differentialized visualising the highest rate of change for absorbance signals as the lowest point in the graph.

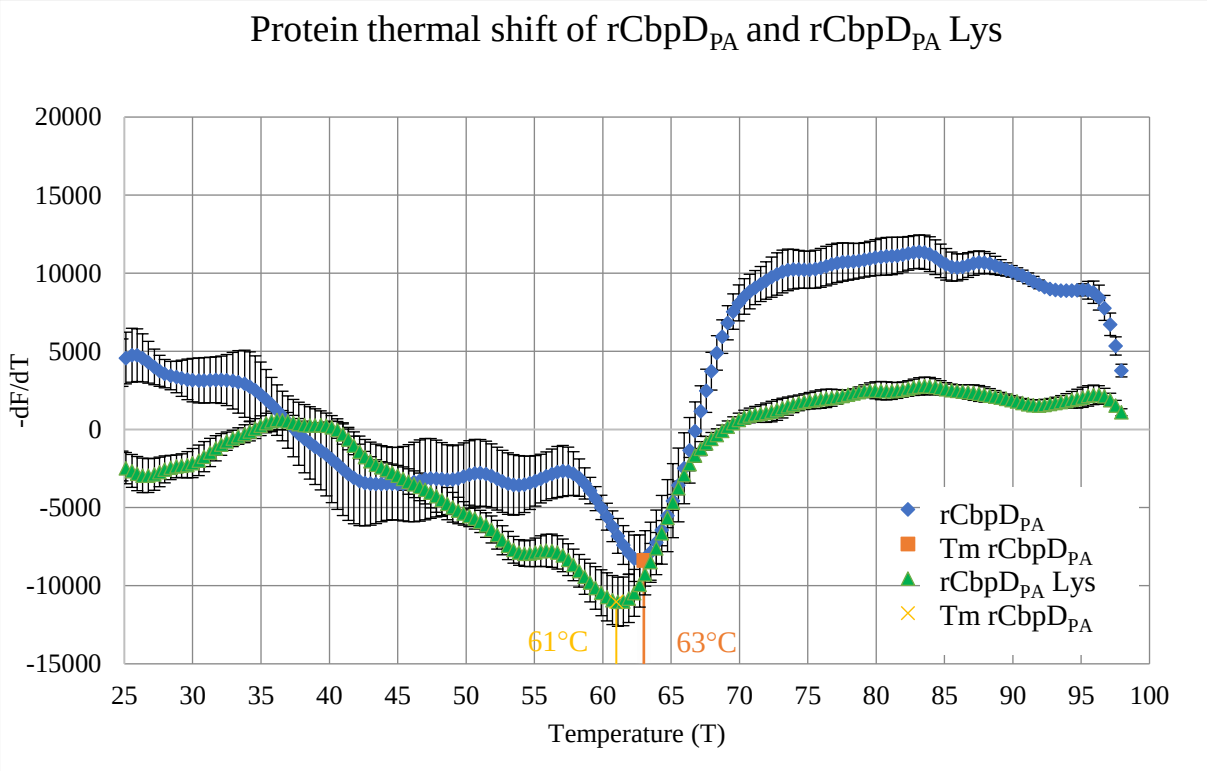

Figure 4-32: Melting point comparison of rCbpD$_{PA}$ and rCbpD$_{PA}$ Lys. *This graph shows the comparison of rCbpD$_{PA}$ (blue) and rCbpD$_{PA}$ Lys (green). The measurements are performed simultaneously with four replicates each. The error bars indicate the standard deviation for the samples. The y-axis shows the derivative of fluorescence (F) with respect to temperature (T) whilst the x-axis shoes the temperature (T). The lowest point in the derivative graph represents the steepest part of the fluorescence measurements, representing the point when the largest amount protein is denatured. The lowest point is indicated in yellow (rCbpD$_{PA}$ Lys) and orange (rCbpD$_{PA}$).*

The mutations from lysine (K) to arginine (R) do not influence the melting temperature significantly as seen in (**Figure 4-32**). Both variants show comparable trends with melting temperatures respectively 61c° and 63c°.

4.9.3 Enzyme activity towards chitin

In order to investigate if the lysine mutations impacted the activity towards chitin, an activity assay with the rCbpD$_{PA}$ Lys variant was performed. The use of MALDI-TOF analysis of chitooligomers is not a quantitative method and only state if there is a presence of activity. The activity assay was performed in the same manner as activity assays performed for other full length variants.

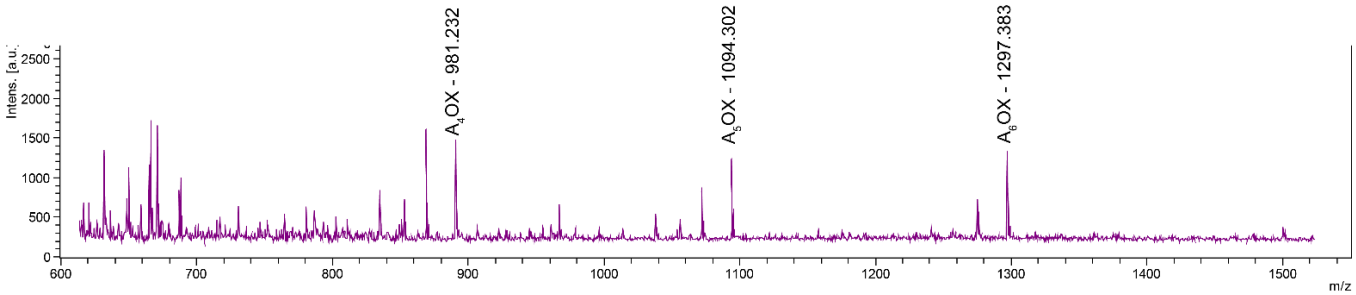

Figure 4-33. Enzyme activity assay of rCbpD$_{PA}$ Lys analysed with MALDI-TOF-MS. *The MALDI-TOF spectrum shows the masses of oxidized chitooligomers (AOX). The degree of polymerization is annotated in subscript. The x-axis is the mass over charge, whilst the y-axis is the intensity measures in absorbance units (a.u).*

The enzyme activity assay show rCbpD$_{PA}$ Lys variant retains the activity towards chitin (**Figure 4-33**). Further investigation of the enzyme activity was performed by quantifying oxidized chitooligomers over time. The enzyme assay was performed simultaneously for both rCbpD$_{PA}$ and rCbpD$_{PA}$ Lys. The supernatant was retrieved from the enzyme assay and relatively quantified using HILIC coupled HPLC.

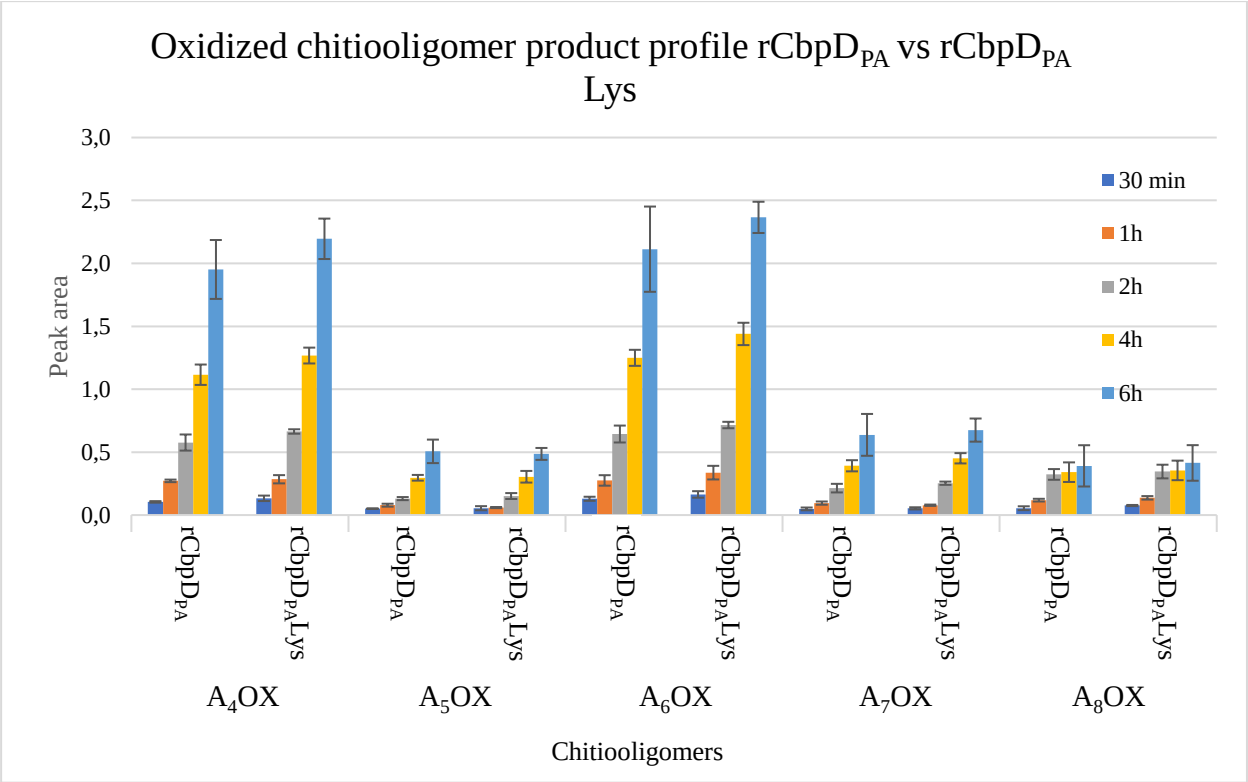

Figure 4-34:Relative quantification of oxidized chitooligosaccharides. *Oxidized product profile of chitin oligomers from both CbpD and CbpD Lys. The analysis is based on relative quantification based on peak area. The analysis performed using a 12 minute HPLC gradient on a HILIC column as described in (3.12.2). The experiment was conducted over 6 hours with sampling at 30 min, 1h, 2h, 4h, and 6h.*

The product profile shows that there are no significant differences in the product profile, oxidized $[GlcNac]_4$ and $[GlcNac]_6$ are present in the highest concentration (**Figure 4-34**). In addition, the product quantity at each time point is comparable for rCbpD$_{PA}$ and rCbpD$_{PA}$ Lys. This indicates that the enzyme activity is comparable for the two protein variants and the mutations have not impacted the enzyme activity significantly.

4.10 Crystallization of CbpD

Since CbpD variants were purified to high purity, crystallization of the protein was attempted. Firstly, crystallization was performed using the mosquito® crystal NanoL robot (SPT Labtech) with rCbpD$_{EC}$. Concentrations 1, ½ and ¼ were screened, respectively 18.9, 9.45 and 4.75 mg/mL. Crystallization buffers in kits JSCG+, Salt RX HT, INDEX, PEG ION (Hampton Research) were screened. No conditions resulted in crystals.

In a second attempt to crystallize (parts of) CbpD, the AA10 module ($rCbpD_{EC}$ M1) was attempted crystallized using the JSCG+ and Wizard™ crystal screens. This screen was set up using 24 well crystallization trays, manually pipetting all solutions. Two protein concentrations were investigated, 18 mg/mL and 43 mg/mL. One well indicated a crystal using 18 mg/mL in 0.1 M Tris-HCl pH 8.5, 0.2 M $MgCl_2$ x $6H_2O$ and 20% PEG 8000. Therefore, a new screen investigating the PEG and $MgCl_2$ x $6H_2O$ concentration by screening 16-26% PEG 8000 increasing by 2% for each well and 0.1, 0.2, 0.25, 0.3 M $MgCl_2$ x $6H_2O$. No crystals were observed in the additional screening.

5 Discussion

The main objective for this study was the biochemical characterization of CbpD and investigating chitin utilization. The secondary objective was the investigation of post-translational modifications on CbpD. Both objectives were made possible by producing CbpD in the native and surrogate organisms.

The use of heterologous protein production in *E. coli* as a surrogate production host is a well-established method within the field of biosciences. The control of induction, high growth rates, high cell densities and ease of cultivation in rich media allows for biochemical characterization of the protein of interest (Rosano & Ceccarelli, 2014). CbpD was purified from *E. coli* as the full-length enzyme and in the form of the truncated variants, $rCbpD_{EC,}$ $rCbpD_{EC}$ M2+M3 and $rCbpD_{EC}$ M1. Production of $rCbpD_{EC}$ presented properly folded, secreted and enzymatically active protein samples which allowed for inexpensive and time efficient production of substantial protein amounts. Because of the general ease of recombinant production of CbpD in *E. coli*, all crystallization attempts were performed with *E. coli* produced rCbpD. However, the use of surrogate hosts will remove several host specific mechanisms which may play a role in the characterization of the protein. Therefore, the establishment of recombinant protein purification protocols in *P. aeruginosa* was performed. Since CbpD is a putative virulence factor, the *P. aeruginosa* PA14 strain was chosen. The strain is a clinical isolate from a burn victim, and is considered a viable strain for the study of pathogenicity (He et al., 2004). In addition, the full genome is sequenced which aids in-depth proteomic analysis.

Initially, cultivation and protein production using *P. aeruginosa* proved more challenging than *E. coli*. Firstly, temperature and growth conditions required optimization. Cultivation in nutrient rich media such as BHI and temperatures of 37°C did not result in a firm pellet after centrifuging, which may indicate cell lysis. By reducing the temperature to room temperature (22-25°C) and utilizing LB as the cultivation media, these issues were solved by both lowering the growth rate and in turn the protein production. During the optimization process different Tryptone suppliers were also tested showing large differences in bacterial growth. Brands may have different production process which most likely interfere with the bacterial growth. Brand differences has been reported by others, showing that different brand components can inhibit the growth or activate stress factors resulting in poor bacterial growth (Spiegeleer et al., 2004).

Purification of rCbpD variants from *E. coli* and *P. aeruginosa* were generally successful except for $rCbpD_{EC}$ M2+M3, where a certain step in the process resulted in proteolysis of the protein in two fragments (**Figure 4-7;** panel A). The proteolysis was most likely caused by improper translation or proteolysis of the heterologous protein. Since other studies have reported truncations caused by improper translations of heterologous protein in *E. coli* (Jennings et al., 2016; Leith et al., 2019). In order to separate the two fragments, HIC purification was performed, resulting in the successful purification of $rCbpD_{EC}$ M2+M3. The fragments were later shown to be a cleavage between the M2 and M3 module, based on both fragments containing an N-terminal His-Tag. Interestingly, the purification method of separating the two fragments illustrated their different physiochemical properties. The M3 module annotated as a CBM73 in Pfam showed great affinity towards the HIC column in addition to chitin as visualized during chitin affinity chromatography (**Figure 4-8**; panel A and B). CBMs show large sequence diversity and present affinity towards different carbohydrates due to a prevalence of aromatic and hydrophobic residues (Shoseyov et al., 2006). The surface bound hydrophobic residues of the CBM73 domain therefore explain the requirement of ddH_2O to elute $rCbpD_{EC}$ M2+M3 and $rCbpD_{PA}$ Native from the HIC column. Several other studies present the great affinity towards carbohydrates and show that CBM affinity can be used in affinity chromatography as a fusion tag in heterologous recombinant purification (Kavoosi et al., 2004).

During full-length rCbpD from *E. coli* and *P. aeruginosa* SEC purification (**Figure 4-13**; panel A and B) the retention profile for *E. coli* purified protein showed two peaks, indicating proteins of different sizes based on SEC elution principals. However, SDS-PAGE analysis presents only one pure band. Possible explanations may be protein aggregation during purification which can be observed with SEC (den Engelsman et al., 2011). However, SDS-PAGE will not show non-covalent protein aggregation excluding disulphide bridges (den Engelsman et al., 2011). Protein aggregation can be caused by several factors, such as temperature, pH, detergents and protein concentration (Cromwell et al., 2006). The retention time phenotype is not observed for $rCbpD_{PA}$ which should exclude the aforementioned factors based on the similar purification and cultivation methods. However, host differences based on the over expression in *E. coli* is a known phenomenon and may explain reversible protein aggregation (Villaverde & Carrió, 2003). Iso-electric focusing performed on $rCbpD_{PA}$ and $rCbpD_{EC}$ both show several bands (**Figure 4-13**; panel C). Separation based on pI may be caused by truncations in the amino acid sequence by removing charged amino acids. Truncations of the His-Tag may also create pI separation as observed for $rCbpD_{PA}$ and $rCbpD_{PA}$ Native (**Figure 4-16**; lane 1 and 2). The

sequence coverage shows peptides from start, middle and end of the protein indicating that large truncations are not wide-spread. Phosphorylation and acetylation have been reported to shift the pI of intact proteins (Zhu et al., 2005). Protein phosphorylation add a negatively charged phosphate group to the protein (Yamagata et al., 2002), while acetylation masks the charged amino groups shifting the acid-base equilibrium (Zhu et al., 2005). A combination of modifications either adding negative groups or shifting the acid-base equilibrium may explain the pI shifts observed for full length enzyme purified in *E. coli* and *P. aeruginosa* as seen in (**Figure 4-15**). Further analysis with mass spectrometry was performed to investigate the possible explanations.

LC-MS analysis identified modifications on both $rCbpD_{PA}$ and $rCbpD_{EC}$, however, the modifications observed deviated from other previously identified modifications on CbpD (Gaviard et al., 2019). Possibly explained by several variables, different cultivation and purification methods may introduce alternate environmental cues which alter regulation. This phenomenon has been observed for the *E. coli* proteome, showing that the PTM distribution is dependent on growth stage and is altered during ethanol stress (Soufi et al., 2015). Furthermore, during this study, PTM mapping utilizing pure protein individually digested with two proteases create a greater sequence coverage and depth which may increase the chance of PTM identification. In addition, no enrichment was performed resulting in an unbiased analysis; however, the issue of low PTM stoichiometry may cause PTMs to remain undetected due to data loss (Mann & Jensen, 2003). The aforementioned explanations are all part of the intrinsic nature of PTM analysis. The PTM analysis of digested $rCbpD_{PA}$ and $rCbpD_{EC}$ showed that different modifications are present, these samples are purified simultaneously, and sample preparation was performed at the same time in an identical manner. Therefore, the same error sources apply for both enzymes, which allows for a comparative analysis of the two proteins. Important questions surrounding why the surrogate host *E. coli,* modifies CbpD remains unanswered. However, both hosts are gram-negative bacteria containing the T2SS which secretes proteins past the outer membrane. Modifications may play a role in protein recruiting or secretion. The T2SS relies on five sub-systems which coordinate the secretion, however, the mechanism is still enigmatic and no common secretion signal in T2SS secreted proteins are observed (Michel-Souzy et al., 2018). More experiments are required to investigate the presence of modifications on $rCbpD_{EC}$ protein and investigate the if the modifications are experimental artefacts. Further LC-MS analysis of the pI separated bands was performed to investigate possible PTM contribution.

In-depth LC-MS analysis of the pI bands (**Figure 4-17**) shows that the bands in fact are CbpD, ruling out impurities. The high sequence coverage confidently identifies the bands as CbpD which was the main goal of the experiment. These results may also explain the difficulties in crystallization, since there are several CbpD protein species present which can hinder the formation of a crystalline structure. Explaining the differences observed in the pI gel may still be truncations in the protein or the presence of PTMs. The IEF separation may have introduced bias during protein handling and have lowered the sequence coverage. In addition, the pI bands are of lower concentration which also results in a lower sequence coverage depth. A variety of modifications are observed in the different fractions. However, PTMs are intrinsically difficult to identify and quantify. The low stichometry of modifications require large amounts of pure protein to enable identification. Furthermore, collision induced fragmentation (CID) during analysis may remove labile modifications increasing the challenges of identifying modifications (Mann et al., 2002). These factors must be considered when analysing the data, the absence of phosphorylations does not alone confidently disprove a phosphorylation-site. The presented data severs as an indication, a larger and directed analysis is required using parallels of enrichment techniques and without. Covalently bound modifications such as methylation, demethylation, acetylation, succinylation and ubiquitination are not as prone to being removed during analysis. However, low stoichiometry and identification challenges still apply. The proteomic results indicate that the presence of different modifications may shift the protein pI and imply that CbpD presents as a heterogenic protein species group. The strict search parameters confidently identify the bands as CbpD, while the PTMs identifications must be further investigated.

In an attempt to understand the biological functions of PTMs, the rCbpD$_{PA}$ Lys mutant was characterized. The lysine to arginine mutations were performed to investigate how known PTM locations may contribute to enzyme function. An interesting observation was made already during the protein purification procedure, where the cell culture and protein extract of the rCbpD$_{PA}$ Lys mutant showed a blue colour compared to the green colour showed by wild type (**Figure 4-30**). Possible explanations may depend on two blue/green pigments secreted by *P. aeruginosa*, pyocyanin (Dietrich et al., 2006) and Azurin (De Rienzo et al., 2000). Altering five lysine residues in CbpD may alter the ability to interact with azurin or pyocyanin which are redox active. Pyocyanin is an active redox phenazine which is blue/green in its reduced form, and colourless in its oxidized form (Price-Whelan et al., 2007). However, more experiments are required to test this hypothesis. The mutations do not affect protein purification, protein melting

temperature, enzyme activity or enzyme product profile. During IEF analysis of $rCbpD_{PA}$ Lys, separation of protein species was observed indicating that lysine acetylation may not affect the protein pI. The lysine to arginine mutations remove the possibilities of some specific modifications such as acetylation. However, phosphorylation which is a main contributor to pI (Zhu et al., 2005) and arginine methylation/ demethylation may still occur. The pI separation can still be explained by truncations of either charged amino acids or the His-Tag.

Activity assays were performed on β-chitin showing LPMO activity by observing oxidized chitooligomers by MALDI-TOF and HILIC analysis. Negative controls showed no oxidized products (**Figure 4-21**) coinciding with other LPMO mechanism reports (Vaaje-Kolstad et al., 2010). Enzyme activity was also shown for $rCbpD_{EC}$, $rCbpD_{PA}$ Native indicating that *E. coli* produced protein and Native protein are also folded correctly. Enzyme characterization of the melting temperature (Tm) was performed for rCbpD and truncated variants. The analysis showed that the full-length enzyme and $rCbpD_{EC}$ M1 variant have comparable melting temperatures, indicating that the LPMO domain is important for the Tm of CbpD. The increased stability of the M1 domain may be explained by the copper binding in the histidine brace, since other studies have reported the importance of Cu binding in LPMO stabilization (Sabbadin et al., 2018). The $rCbpD_{EC}$ M2+M3 variant shows a substantially lower Tm, reaffirming the importance of the LPMO module regarding Tm. The uneven denaturing curve of the full-length protein may be explained by the melting of M2+M3 modules prior to the M1 module. Reports have shown that the LPMO active site has a high binding affinity towards the Cu atom (Frandsen et al., 2016) also the Tm reduces once the LPMO is in apo-form (Sabbadin et al., 2018). The relevance for a chitin active LPMO was further investigated in several experiments.

The presence of a chitin active protein suggests that this versatile bacterium may utilize chitin as a nutrient source. In addition, *P. aeruginosa* contains a chitinase ChiC (Folders et al., 2001).The presence of an LPMO (CbpD) and chitinase (ChiC) may resemble a chitinolytic system. However, a study reported in the literature shows that *P. aeruginosa* is not able to utilize chitin as its sole carbon source (Jagmann et al., 2010). The experimental set up used in the latter study was not complete, as only the sole carbon source was investigated. CbpD and ChiC are both regulated by quorum sensing which requires among other factors, a sufficient cell density (Hentzer et al., 2003). Therefore, in order to produce CbpD and ChiC, the cell density must reach a threshold before regulating the quorum sensing pathways. Therefore, the hypothesis was formed suggesting that the possible chitinolytic system may engage in the utilization of chitin once a sufficient cell density was reached. A study was thus initiated to investigate

whether the bacterium could utilize chitin as a carbon source in the conditions where the growth is firstly sustained by glucose to obtain a high cell density.

Investigating the utilization of chitin proved challenging, since the insoluble nature of chitin interfered with OD measurements. Firstly, light scattering created incorrect measurements and the sedimentation of chitin particles caused challenges in measuring the same distribution of chitin particles. These challenges are exemplified in the OD measurements (**Figure 4-23**). The $M9_{PA}$ medium alone without supplements resulted in higher OD measurements, which is unexpected, the control of media alone should establish the baseline and the supplements should result in increased growth. These observations show that OD_{600} is not a viable method for measuring growth on chitin. A secondary strategy attempted, was plating serial dilutions and counting colony forming units (CFU). However, CFU counting also presented challenges, since visible bacterial clusters forming in the cell culture would not allow a representative sample. With help from the Nitrogen Group at NMBU and guidance from professor Lars Bakken and PhD student Elisabeth Gautefall-Hiis, an automatic gas sampling robot could sample and quantify the amount of carbon dioxide and oxygen present in sealed culture vails (Molstad et al., 2007). The bacterial respiration could be measured rather than visualization of bacterial biomass or bacterial viability. The gas incubation system allowed the establishment of minimal medium containing the minimum requirements of medium components. Initial testing showed that $M9_{Minimal}$ medium alone and $M9_{Minimal}$ supplemented with chitin presented no signs of growth. Only when glucose was added, growth could be monitored. These results show that $M9_{Minimal}$ contains no background nutrients. In addition, the chitin was not laced with any useable carbon source, since no growth was observed.

The investigation of a potential chitinolytic system regulated by quorum sensing was performed by altering the glucose concentrations in the $M9_{Minimal}$. Interestingly, while investigating chitin utilization, one replicate of chitin and glucose supplemented media deviated from the other sample replicates, showing an increase of carbon dioxide whilst the other stagnated. Indicating growth on chitin is initiated after depletion of glucose (**Figure 4-25**). Since only one replicate presented a different phenotype, an error is the obvious explanation. Possible explanations may be, media preparation, stirring, contamination or faulty measurements. However, the growth curves both within the replicates and other samples containing glucose are closely grouped throughout the lag, exponential and start of the potential stationary phase. Only after adding oxygen the one replicate of chitin and glucose supplemented media increased the carbon dioxide concentration. These seemingly similar growth curves should also explain that media

preparation, stirring conditions and contaminations were unviable explanations. The same stock solutions were used for all samples, which excludes contaminations in the stock solutions. However, there is a possibility that the deviation was not based on an error, and in one culture, the *P. aeruginosa* culture was regulated differently. The lack of an obvious error source required further investigation.

P. aeruginosa contains several pathways regulated by quorum sensing which can be influenced by environmental cues. An experiment was initiated on nutrient limitation and hypoxia since reports have shown that the regulatory pathways of CbpD and ChiC may be influenced by the aforementioned conditions (Hentzer et al., 2003; Lee & Zhang, 2015; Pesci et al., 1997).

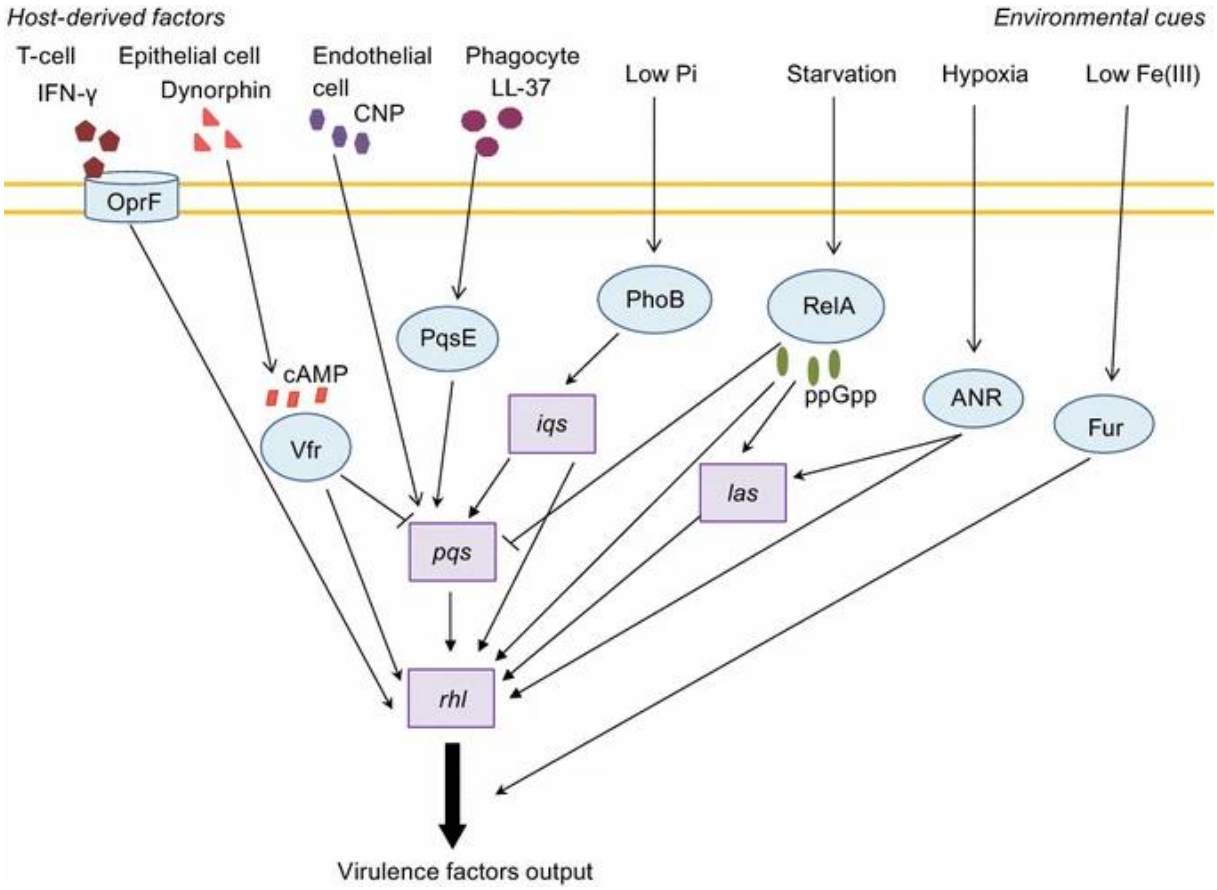

Figure 5-1: Illustration of how some host-derived factors and environmental cue can influence quorum sensing. *The yellow line symbolizes the P. aeruginosa cell membrane. This schematic shows a drastically simplified overview of the environmental cues on the right and host factors on the left that take part in the regulation of the quorum sensing network of P. aeruginosa. The purple boxes are illustrations of quorum sensing systems simplified by only illustrating the name. The blue ovals represent different regulators. ppGpp is a starvation signal which regulates the quorum sensing pathways. Pointed arrows show activation, whilst blunt arrows show inhibition. Figure source: (Lee & Zhang, 2015)*

Nutrient limitation was observed by altering the glucose concentrations. The initial experiment with a deviating replicate was supplemented with 0.5 g/L of glucose. If the deviation was a result of chitin utilization, perhaps the glucose concentration was on a threshold to reach an adequate cell density. However, follow-up experiments by increasing and decreasing glucose

concentrations did not verify this hypothesis. Altering glucose concentration alone did not change the growth curves compared to the controls with only glucose present (**Figure 4-26**). However, as seen in **Figure 5-1**, the quorum sensing pathways are interconnected, and several environmental cues regulate this network. In addition, transcriptional experiments show that CbpD is regulated to the Las and rhI system, while ChiC is regulated by the rhI system (Hentzer et al., 2003). Attempting to create hypoxic and starvation conditions were performed to investigate the effect of several environmental cues. Again, chitin utilization was not observed, however, no controls are present to verify if the quorum sensing systems are regulated. Interestingly, during hypoxic conditions the glucose present could not be utilized indicating that the growth limiting factor was oxygen, and not glucose as first theorized. As seen in **Figure 4-27**, the anoxic parallel is only able to utilize the glucose present, once oxygen is reintroduced into the system. This observation may explain the one replicate deviating in **Figure 4-25**, which most likely contained more glucose in one replicate. The experiments described so far all point in the direction already concluded by (Jagmann et al., 2010; Jindra Folders, 2000) suggesting that *P. aeruginosa* is not able to utilize chitin as a carbon source. Another observation that may provide insight in the CbpD function was the oxygen consumption rates during low oxygen concentrations as observed in the oxygen data **Figure 8-2,** the oxygen consumption slows down. Which suggest a lower oxygen affinity since the culture cannot utilize all the oxygen present. This phenomenon can be explained by biofilm formation. Studies of *P. aeruginosa* biofilms have shown oxygen limitation is present during biofilm formation and that protein regulation changes during these oxygen limiting conditions (Sauer et al., 2002). LPMO mediated colonization has been shown for the LPMO GbpA of *Vibrio cholerae* (Wong et al., 2012). The great substrate affinity towards chitin shown in purification and chitin binding assays may be attributed to a role in biofilm formation on chitin surfaces. MST analysis of binding towards chitin hexose ($GlcNac_6$) oligomers show that CbpD is not able to bind chitooligomers. This indicates that the binding affinity is isolated to crystalline chitin. However, since chitin utilization is not the goal of binding, and the binding affinity towards chitin oligomers is not observed, the substrate affinity must have another biological function or may be an experimental artefact.

Under current testing conditions we have established that CbpD binds chitin and can release chitooligomers from chitin, however, not utilize chitin as a carbon source. Furthermore, the presence of PTMs remain enigmatic and the biological role of CbpD still evades us. *P. aeruginosa* is known for its large genome size containing several small paralogous gene

families, which is concurrent with the phenotype of a highly adaptable pathogen (Stover et al., 2000). Perhaps, *P. aeruginosa* once retained the ability to utilize chitin, however, this ability became redundant as *P. aeruginosa* adapted. Previous literature has shown that cultures of *P. aeruginosa* can utilize the chitin monomer N-acetylglucosamine and parasitically grow in co-cultures with known chitin degrading bacteria (Jagmann et al., 2010). Since the role of CbpD is seemingly not attributed to chitin degradation, a virulence role may more likely. The degradation of CbpD by Elastase when CbpD is not bound to chitin (Jindra Folders, 2000) may serve as mechanism to control the amount of enzyme present when not presenting as virulent. Reports have shown the LPMO GbpA bind to mucins and mediating colonization which is a known virulence factor (Wong et al., 2012). Perhaps, CbpD possesses a role in mediating biofilm formation on chitin surfaces, since biofilm formation is an important virulence factor (Høiby et al., 2010). Furthermore, CbpD is secreted together with other known and characterized virulence factors, the assumption that CbpD also is a virulence factor is near standing, however, evidence linking CbpD as a specific virulence factor is still not available.

6 Conclusion and future work

During this study, we have successfully established purification protocols for recombinant CbpD in *P. aeruginosa*. Biochemical characterization of melting temperature, enzyme activity, structure elucidation and substrate affinity were performed with attempts to understand the biological function of CbpD. Furthermore, PTM analysis was performed in full length enzyme from both *P. aeruginosa* and *E. coli* showing a presence of several modifications. In addition, LC-MS performed on IEF separated protein bands confirm that all the protein species belong to CbpD, indicating that CbpD presents as several protein species. Mutations were performed in an attempt to investigate the function of specific PTMs, resulting in an interesting change of phenotype of culture colour. However, the biological function of PTMs remains enigmatic. Further investigation of a possible function was performed in experiments detailing chitin utilization. Under current testing conditions, CbpD is shown to not degrade chitin as a means of nutrient utilization.

Future projects on CbpD include a directed investigation of regulating the quorum sensing autoinducers and the role of biofilm formation may expand our understanding of the affinity towards chitin. Furthermore, the emerging field of bacteriological PTMs and how CbpD is modified deserves a directed proteomics analysis verifying the modifications observed and the modification ratio. Several studies have annotated PTMs on CbpD and the pI gels show a heterogenic pool of protein species possibly caused by PTMs from both *E. coli* and *P. aeruginosa* produced enzymes. The importance of understanding CbpD is also linked to the LPMO field and understating this conserved protein family and seemingly wide phylogenetic origin. Understanding the role of CbpD will aid in the increasing need for new antimicrobial agents and widen our knowledge of LPMOs. This present study represents a step forward in understanding CbpD.

7 References

Aachmann, F. L., Sørlie, M., Skjåk-Bræk, G., Eijsink, V. G. H. & Vaaje-Kolstad, G. (2012). NMR structure of a lytic polysaccharide monooxygenase provides insight into copper binding, protein dynamics, and substrate interactions. *Proceedings of the National Academy of Sciences*, 109 (46): 18779-18784. doi: 10.1073/pnas.1208822109.

Aebersold, R. & Mann, M. (2003). Mass spectrometry-based proteomics. *Nature*, 422 (6928): 198-207. doi: 10.1038/nature01511.

Allfrey, V. G., Faulkner, R. & Mirsky, A. E. (1964). ACETYLATION AND METHYLATION OF HISTONES AND THEIR POSSIBLE ROLE IN THE REGULATION OF RNA SYNTHESIS. *Proc Natl Acad Sci U S A*, 51: 786-94. doi: 10.1073/pnas.51.5.786.

Alpert, A. J. (1990). Hydrophilic-interaction chromatography for the separation of peptides, nucleic acids and other polar compounds. *Journal of Chromatography A*, 499: 177-196. doi: https://doi.org/10.1016/S0021-9673(00)96972-3.

Beausoleil, S. A., Villén, J., Gerber, S. A., Rush, J. & Gygi, S. P. (2006). A probability-based approach for high-throughput protein phosphorylation analysis and site localization. *Nature Biotechnology*, 24 (10): 1285-1292. doi: 10.1038/nbt1240.

Bejarano, P. A., Langeveld, J. P., Hudson, B. G. & Noelken, M. E. (1989). Degradation of basement membranes by Pseudomonas aeruginosa elastase. *Infect Immun*, 57 (12): 3783-7.

Berthod, A., Chang, S. S. C., Kullman, J. P. S. & Armstrong, D. W. (1998). Practice and mechanism of HPLC oligosaccharide separation with a cyclodextrin bonded phase. *Talanta*, 47 (4): 1001-1012. doi: https://doi.org/10.1016/S0039-9140(98)00179-9.

Bissaro, B., Rohr, A. K., Muller, G., Chylenski, P., Skaugen, M., Forsberg, Z., Horn, S. J., Vaaje-Kolstad, G. & Eijsink, V. G. H. (2017). Oxidative cleavage of polysaccharides by monocopper enzymes depends on H2O2. *Nat Chem Biol*, 13 (10): 1123-1128. doi: 10.1038/nchembio.2470.

Bissaro, B., Várnai, A., Røhr, Å. K. & Eijsink, V. G. H. (2018). Oxidoreductases and Reactive Oxygen Species in Conversion of Lignocellulosic Biomass. *Microbiology and Molecular Biology Reviews*, 82 (4): e00029-18. doi: 10.1128/mmbr.00029-18.

Bjellqvist, B., Ek, K., Giorgio Righetti, P., Gianazza, E., Görg, A., Westermeier, R. & Postel, W. (1982). Isoelectric focusing in immobilized pH gradients: Principle, methodology and some applications. *Journal of Biochemical and Biophysical Methods*, 6 (4): 317-339. doi: https://doi.org/10.1016/0165-022X(82)90013-6.

Bleves, S., Viarre, V., Salacha, R., Michel, G. P. F., Filloux, A. & Voulhoux, R. (2010). Protein secretion systems in Pseudomonas aeruginosa: A wealth of pathogenic weapons. *International Journal of Medical Microbiology*, 300 (8): 534-543. doi: https://doi.org/10.1016/j.ijmm.2010.08.005.

Botzenhart, K. & Döring, G. (1993). Ecology and epidemiology of Pseudomonas aeruginosa. In *Pseudomonas aeruginosa as an Opportunistic Pathogen*, pp. 1-18: Springer.

Bradford, M. M. (1976). A rapid and sensitive method for the quantitation of microgram quantities of protein utilizing the principle of protein-dye binding. *Analytical Biochemistry*, 72 (1): 248-254. doi: https://doi.org/10.1016/0003-2697(76)90527-3.

Burke, M. E. & Pattee, P. A. (1967). Purification and characterization of a staphylolytic enzyme from Pseudomonas aeruginosa. *Journal of bacteriology*, 93 (3): 860-865.

Buszewski, B. & Noga, S. (2012). Hydrophilic interaction liquid chromatography (HILIC)—a powerful separation technique. *Analytical and Bioanalytical Chemistry*, 402 (1): 231-247. doi: 10.1007/s00216-011-5308-5.

Cohen, P. (2002). The origins of protein phosphorylation. *Nature Cell Biology*, 4 (5): E127-E130. doi: 10.1038/ncb0502-e127.
Correa, C. M., Tibana, A. & Gontijo Filho, P. P. (1991). Vegetables as a source of infection with Pseudomonas aeruginosa in a University and Oncology Hospital of Rio de Janeiro. *J Hosp Infect*, 18 (4): 301-6. doi: 10.1016/0195-6701(91)90187-d.
Cox, J. & Mann, M. (2008). MaxQuant enables high peptide identification rates, individualized p.p.b.-range mass accuracies and proteome-wide protein quantification. *Nature Biotechnology*, 26 (12): 1367-1372. doi: 10.1038/nbt.1511.
Cromwell, M. E. M., Hilario, E. & Jacobson, F. (2006). Protein aggregation and bioprocessing. *The AAPS Journal*, 8 (3): E572-E579. doi: 10.1208/aapsj080366.
De Rienzo, F., Gabdoulline, R. R., Menziani, M. C. & Wade, R. C. (2000). Blue copper proteins: a comparative analysis of their molecular interaction properties. *Protein science : a publication of the Protein Society*, 9 (8): 1439-1454. doi: 10.1110/ps.9.8.1439.
Delvillani, F., Sciandrone, B., Peano, C., Petiti, L., Berens, C., Georgi, C., Ferrara, S., Bertoni, G., Pasini, M. E., Dehò, G., et al. (2014). Tet-Trap, a genetic approach to the identification of bacterial RNA thermometers: application to Pseudomonas aeruginosa. *Rna*, 20 (12): 1963-76. doi: 10.1261/rna.044354.114.
den Engelsman, J., Garidel, P., Smulders, R., Koll, H., Smith, B., Bassarab, S., Seidl, A., Hainzl, O. & Jiskoot, W. (2011). Strategies for the assessment of protein aggregates in pharmaceutical biotech product development. *Pharmaceutical research*, 28 (4): 920-933. doi: 10.1007/s11095-010-0297-1.
Dietrich, L. E., Price-Whelan, A., Petersen, A., Whiteley, M. & Newman, D. K. (2006). The phenazine pyocyanin is a terminal signalling factor in the quorum sensing network of Pseudomonas aeruginosa. *Mol Microbiol*, 61 (5): 1308-21. doi: 10.1111/j.1365-2958.2006.05306.x.
Din, N., Damude, H. G., Gilkes, N. R., Miller, R. C., Jr., Warren, R. A. & Kilburn, D. G. (1994). C1-Cx revisited: intramolecular synergism in a cellulase. *Proceedings of the National Academy of Sciences of the United States of America*, 91 (24): 11383-11387. doi: 10.1073/pnas.91.24.11383.
Eijsink, V. G. H., Petrovic, D., Forsberg, Z., Mekasha, S., Røhr, Å. K., Várnai, A., Bissaro, B. & Vaaje-Kolstad, G. (2019). On the functional characterization of lytic polysaccharide monooxygenases (LPMOs). *Biotechnology for biofuels*, 12: 58-58. doi: 10.1186/s13068-019-1392-0.
Favero, M. S., Carson, L. A., Bond, W. W. & Petersen, N. J. (1971). Pseudomonas aeruginosa: Growth in Distilled Water from Hospitals. *Science*, 173 (3999): 836-838. doi: 10.1126/science.173.3999.836.
Filloux, A., Bally, M., Ball, G., Akrim, M., Tommassen, J. & Lazdunski, A. (1990). Protein secretion in gram-negative bacteria: transport across the outer membrane involves common mechanisms in different bacteria. *The EMBO Journal*, 9 (13): 4323-4329. doi: 10.1002/j.1460-2075.1990.tb07881.x.
Folders, J., Algra, J., Roelofs, M. S., van Loon, L. C., Tommassen, J. & Bitter, W. (2001). Characterization of Pseudomonas aeruginosa Chitinase, a Gradually Secreted Protein. *Journal of Bacteriology*, 183 (24): 7044-7052. doi: 10.1128/jb.183.24.7044-7052.2001.
Ford, C. F., Suominen, I. & Glatz, C. E. (1991). Fusion tails for the recovery and purification of recombinant proteins. *Protein Expr Purif*, 2 (2-3): 95-107. doi: 10.1016/1046-5928(91)90057-p.
Forsberg, Z., Vaaje-Kolstad, G., Westereng, B., Bunæs, A. C., Stenstrøm, Y., MacKenzie, A., Sørlie, M., Horn, S. J. & Eijsink, V. G. H. (2011). Cleavage of cellulose by a CBM33 protein. *Protein Science*, 20 (9): 1479-1483. doi: 10.1002/pro.689.
Forsberg, Z., Mackenzie, A. K., Sorlie, M., Rohr, A. K., Helland, R., Arvai, A. S., Vaaje-Kolstad, G. & Eijsink, V. G. (2014). Structural and functional characterization of a conserved pair of bacterial cellulose-oxidizing lytic polysaccharide monooxygenases. *Proc Natl Acad Sci U S A*, 111 (23): 8446-51. doi: 10.1073/pnas.1402771111.

Forsberg, Z., Røhr, Å. K., Mekasha, S., Andersson, K. K., Eijsink, V. G. H., Vaaje-Kolstad, G. & Sørlie, M. (2014). Comparative Study of Two Chitin-Active and Two Cellulose-Active AA10-Type Lytic Polysaccharide Monooxygenases. *Biochemistry*, 53 (10): 1647-1656. doi: 10.1021/bi5000433.

Frandsen, K. E. H., Simmons, T. J., Dupree, P., Poulsen, J.-C. N., Hemsworth, G. R., Ciano, L., Johnston, E. M., Tovborg, M., Johansen, K. S., von Freiesleben, P., et al. (2016). The molecular basis of polysaccharide cleavage by lytic polysaccharide monooxygenases. *Nature Chemical Biology*, 12 (4): 298-303. doi: 10.1038/nchembio.2029.

Gaviard, C., Jouenne, T. & Hardouin, J. (2018). Proteomics of Pseudomonas aeruginosa: the increasing role of post-translational modifications. *Expert Rev Proteomics*, 15 (9): 757-772. doi: 10.1080/14789450.2018.1516550.

Gaviard, C., Cosette, P., Jouenne, T. & Hardouin, J. (2019). LasB and CbpD Virulence Factors of Pseudomonas aeruginosa Carry Multiple Post-Translational Modifications on Their Lysine Residues. *Journal of Proteome Research*, 18 (3): 923-933. doi: 10.1021/acs.jproteome.8b00556.

Gellatly, S. L. & Hancock, R. E. (2013). Pseudomonas aeruginosa: new insights into pathogenesis and host defenses. *Pathog Dis*, 67 (3): 159-73. doi: 10.1111/2049-632x.12033.

Gessard, C. (1984). On the Blue and Green Coloration that Appears on Bandages. *Reviews of Infectious Diseases*, 6 (Supplement_3): S775-S776. doi: 10.1093/clinids/6.Supplement_3.S775.

Graves, J. D. & Krebs, E. G. (1999). Protein Phosphorylation and Signal Transduction. *Pharmacology & Therapeutics*, 82 (2): 111-121. doi: https://doi.org/10.1016/S0163-7258(98)00056-4.

Green, S. K., Schroth, M. N., Cho, J. J., Kominos, S. D. & Vitanza-Jack, V. B. (1974). Agricultural Plants and Soil as a Reservoir for Pseudomonas aeruginosa. *Applied Microbiology*, 28 (6): 987-991.

Han, X., He, L., Xin, L., Shan, B. & Ma, B. (2011). PeaksPTM: Mass spectrometry-based identification of peptides with unspecified modifications. *J Proteome Res*, 10 (7): 2930-6. doi: 10.1021/pr200153k.

Hangasky, J. A., Iavarone, A. T. & Marletta, M. A. (2018). Reactivity of O₂ versus H₂O₂ with polysaccharide monooxygenases. *Proceedings of the National Academy of Sciences*, 115 (19): 4915-4920. doi: 10.1073/pnas.1801153115.

Hardalo, C. & Edberg, S. C. (1997). Pseudomonas aeruginosa: assessment of risk from drinking water. *Crit Rev Microbiol*, 23 (1): 47-75. doi: 10.3109/10408419709115130.

He, J., Baldini, R. L., Déziel, E., Saucier, M., Zhang, Q., Liberati, N. T., Lee, D., Urbach, J., Goodman, H. M. & Rahme, L. G. (2004). The broad host range pathogen Pseudomonas aeruginosa strain PA14 carries two pathogenicity islands harboring plant and animal virulence genes. *Proceedings of the National Academy of Sciences*, 101 (8): 2530-2535.

Hentzer, M., Wu, H., Andersen, J. B., Riedel, K., Rasmussen, T. B., Bagge, N., Kumar, N., Schembri, M. A., Song, Z. & Kristoffersen, P. (2003). Attenuation of Pseudomonas aeruginosa virulence by quorum sensing inhibitors. *The EMBO journal*, 22 (15): 3803-3815.

Horn, S. J., Vaaje-Kolstad, G., Westereng, B. & Eijsink, V. (2012). Novel enzymes for the degradation of cellulose. *Biotechnology for Biofuels*, 5 (1): 45. doi: 10.1186/1754-6834-5-45.

Humphrey, S. J., Karayel, O., James, D. E. & Mann, M. (2018). High-throughput and high-sensitivity phosphoproteomics with the EasyPhos platform. *Nature Protocols*, 13 (9): 1897-1916. doi: 10.1038/s41596-018-0014-9.

Høiby, N., Bjarnsholt, T., Givskov, M., Molin, S. & Ciofu, O. (2010). Antibiotic resistance of bacterial biofilms. *International Journal of Antimicrobial Agents*, 35 (4): 322-332. doi: https://doi.org/10.1016/j.ijantimicag.2009.12.011.

Isaksen, T., Westereng, B., Aachmann, F. L., Agger, J. W., Kracher, D., Kittl, R., Ludwig, R., Haltrich, D., Eijsink, V. G. & Horn, S. J. (2014). A C4-oxidizing lytic polysaccharide monooxygenase cleaving both cellulose and cello-oligosaccharides. *J Biol Chem*, 289 (5): 2632-42. doi: 10.1074/jbc.M113.530196.

Jagmann, N., Brachvogel, H.-P. & Philipp, B. (2010). Parasitic growth of Pseudomonas aeruginosa in co-culture with the chitinolytic bacterium Aeromonas hydrophila. *Environmental Microbiology*, 12 (6): 1787-1802. doi: 10.1111/j.1462-2920.2010.02271.x.

Jeffery, C. J. (2016). Protein species and moonlighting proteins: Very small changes in a protein's covalent structure can change its biochemical function. *Journal of Proteomics*, 134: 19-24. doi: https://doi.org/10.1016/j.jprot.2015.10.003.
Jennings, M. J., Barrios, A. F. & Tan, S. (2016). Elimination of truncated recombinant protein expressed in Escherichia coli by removing cryptic translation initiation site. *Protein expression and purification*, 121: 17-21. doi: 10.1016/j.pep.2015.12.001.
Jindra Folders, J. T., Leendert C. Van Loon, Wilbert Bitter. (2000). Identification of a Chitin-Binding Protein Secreted by P.Aeruginosa. *Journal of Bacteriology*, 182 (5): 1257-1263.
Karas, M. & Hillenkamp, F. (1988). Laser desorption ionization of proteins with molecular masses exceeding 10,000 daltons. *Anal Chem*, 60 (20): 2299-301. doi: 10.1021/ac00171a028.
Kavoosi, M., Meijer, J., Kwan, E., Creagh, A. L., Kilburn, D. G. & Haynes, C. A. (2004). Inexpensive one-step purification of polypeptides expressed in Escherichia coli as fusions with the family 9 carbohydrate-binding module of xylanase 10A from T. maritima. *J Chromatogr B Analyt Technol Biomed Life Sci*, 807 (1): 87-94. doi: 10.1016/j.jchromb.2004.03.031.
Kirn, T. J., Jude, B. A. & Taylor, R. K. (2005). A colonization factor links Vibrio cholerae environmental survival and human infection. *Nature*, 438 (7069): 863-6. doi: 10.1038/nature04249.
Kominos, S. D., Copeland, C. E., Grosiak, B. & Postic, B. (1972). Introduction of Pseudomonas aeruginosa into a hospital via vegetables. *Applied microbiology*, 24 (4): 567-570.
Kopaciewicz, W., Rounds, M. A., Fausnaugh, J. & Regnier, F. E. (1983). Retention model for high-performance ion-exchange chromatography. *Journal of Chromatography A*, 266: 3-21. doi: https://doi.org/10.1016/S0021-9673(01)90875-1.
Kuga, S. (1981). Pore size distribution analysis of gel substances by size exclusion chromatography. *Journal of Chromatography A*, 206 (3): 449-461. doi: https://doi.org/10.1016/S0021-9673(00)88914-1.
Kurita, K. (2001). Controlled functionalization of the polysaccharide chitin. *Progress in Polymer Science*, 26 (9): 1921-1971. doi: https://doi.org/10.1016/S0079-6700(01)00007-7.
Källberg, M., Wang, H., Wang, S., Peng, J., Wang, Z., Lu, H. & Xu, J. (2012). Template-based protein structure modeling using the RaptorX web server. *Nature protocols*, 7 (8): 1511.
Lambert, P. A. (2002). Mechanisms of antibiotic resistance in Pseudomonas aeruginosa. *Journal of the Royal Society of Medicine*, 95 Suppl 41 (Suppl 41): 22-26.
Lee, J. & Zhang, L. (2015). The hierarchy quorum sensing network in Pseudomonas aeruginosa. *Protein Cell*, 6 (1): 26-41. doi: 10.1007/s13238-014-0100-x.
Leith, E. M., O'Dell, W. B., Ke, N., McClung, C., Berkmen, M., Bergonzo, C., Brinson, R. G. & Kelman, Z. (2019). Characterization of the internal translation initiation region in monoclonal antibodies expressed in Escherichia coli. *Journal of Biological Chemistry*, 294 (48): 18046-18056. doi: 10.1074/jbc.RA119.011008.
Levasseur, A., Drula, E., Lombard, V., Coutinho, P. M. & Henrissat, B. (2013). Expansion of the enzymatic repertoire of the CAZy database to integrate auxiliary redox enzymes. *Biotechnology for Biofuels*, 6 (1): 41. doi: 10.1186/1754-6834-6-41.
Liu, P. V. (1974). Extracellular toxins of Pseudomonas aeruginosa. *Journal of Infectious Diseases*, 130 (Supplement): S94-S99.
Lyczak, J. B., Cannon, C. L. & Pier, G. B. (2000). Establishment of Pseudomonas aeruginosa infection: lessons from a versatile opportunist. *Microbes and infection*, 2 (9): 1051-1060.
Ma, B., Zhang, K., Hendrie, C., Liang, C., Li, M., Doherty-Kirby, A. & Lajoie, G. (2003). PEAKS: powerful software for peptide de novo sequencing by tandem mass spectrometry. *Rapid communications in mass spectrometry*, 17 (20): 2337-2342.
Makarov, A. (2000). Electrostatic Axially Harmonic Orbital Trapping: A High-Performance Technique of Mass Analysis. *Analytical Chemistry*, 72 (6): 1156-1162. doi: 10.1021/ac991131p.
Mann, M., Ong, S.-E., Grønborg, M., Steen, H., Jensen, O. N. & Pandey, A. (2002). Analysis of protein phosphorylation using mass spectrometry: deciphering the phosphoproteome. *Trends in Biotechnology*, 20 (6): 261-268. doi: https://doi.org/10.1016/S0167-7799(02)01944-3.
Mann, M. & Jensen, O. N. (2003). Proteomic analysis of post-translational modifications. *Nat Biotechnol*, 21 (3): 255-61. doi: 10.1038/nbt0303-255.

Melander, W. R., Corradini, D. & Horváth, C. (1984). Salt-mediated retention of proteins in hydrophobic-interaction chromatography: Application of solvophobic theory. *Journal of Chromatography A*, 317: 67-85. doi: https://doi.org/10.1016/S0021-9673(01)91648-6.
Michalski, A., Damoc, E., Hauschild, J.-P., Lange, O., Wieghaus, A., Makarov, A., Nagaraj, N., Cox, J., Mann, M. & Horning, S. (2011). Mass Spectrometry-based Proteomics Using Q Exactive, a High-performance Benchtop Quadrupole Orbitrap Mass Spectrometer. *Molecular & cellular proteomics : MCP*, 10: M111.011015. doi: 10.1074/mcp.M111.011015.
Michel-Souzy, S., Douzi, B., Cadoret, F., Raynaud, C., Quinton, L., Ball, G. & Voulhoux, R. (2018). Direct interactions between the secreted effector and the T2SS components GspL and GspM reveal a new effector-sensing step during type 2 secretion. *J Biol Chem*, 293 (50): 19441-19450. doi: 10.1074/jbc.RA117.001127.
Molstad, L., Dorsch, P. & Bakken, L. R. (2007). Robotized incubation system for monitoring gases (O2, NO, N2O N2) in denitrifying cultures. *J Microbiol Methods*, 71 (3): 202-11. doi: 10.1016/j.mimet.2007.08.011.
Muzzarelli, R. A., Jeuniaux, C. & Gooday, G. W. (1986). *Chitin in nature and technology*, vol. 385: Springer.
Nathalie, B. (2016). Production and application of chitin. *Physical Sciences Reviews*, 1 (9): 20160048. doi: https://doi.org/10.1515/psr-2016-0048.
Neu, H. C. & Heppel, L. A. (1965). The release of enzymes from Escherichia coli by osmotic shock and during the formation of spheroplasts. *J Biol Chem*, 240 (9): 3685-92.
Neue, U. D. (2007). CHROMATOGRAPHY: LIQUID | Mechanisms: Reversed Phases. In Wilson, I. D. (ed.) *Encyclopedia of Separation Science*, pp. 1-7. Oxford: Academic Press.
Neumann, E., Schaefer-Ridder, M., Wang, Y. & Hofschneider, P. H. (1982). Gene transfer into mouse lyoma cells by electroporation in high electric fields. *Embo j*, 1 (7): 841-5.
O'Dell, W. B., Agarwal, P. K. & Meilleur, F. (2017). Oxygen Activation at the Active Site of a Fungal Lytic Polysaccharide Monooxygenase. *Angewandte Chemie International Edition*, 56 (3): 767-770. doi: 10.1002/anie.201610502.
Olsen, J., Ong, S.-E. & Mann, M. (2004). Olsen, J. V. , Ong, S. E. & Mann, M. Trypsin cleaves exclusively C-terminal to Arginine and lysine residues. Mol. Cell. Proteomics 6, 608-614. *Molecular & cellular proteomics : MCP*, 3: 608-14. doi: 10.1074/mcp.T400003-MCP200.
Ouidir, T., Jarnier, F., Cosette, P., Jouenne, T. & Hardouin, J. (2014). Extracellular Ser/Thr/Tyr phosphorylated proteins of Pseudomonas aeruginosa PA14 strain. *Proteomics*, 14 (17-18): 2017-30. doi: 10.1002/pmic.201400190.
Ouidir, T., Cosette, P., Jouenne, T. & Hardouin, J. (2015). Proteomic profiling of lysine acetylation in Pseudomonas aeruginosa reveals the diversity of acetylated proteins. *Proteomics*, 15 (13): 2152-7. doi: 10.1002/pmic.201500056.
Pappin, D. J. C., Hojrup, P. & Bleasby, A. J. (1993). Rapid identification of proteins by peptide-mass fingerprinting. *Current Biology*, 3 (6): 327-332. doi: 10.1016/0960-9822(93)90195-T.
Park, S. & Galloway, D. R. (1995). Purification and characterization of LasD: a second staphylolytic proteinase produced by Pseudomonas aeruginosa. *Molecular Microbiology*, 16 (2): 263-270. doi: 10.1111/j.1365-2958.1995.tb02298.x.
Park, S. & Galloway, D. R. (1998). Pseudomonas aeruginosa LasD processes the inactive LasA precursor to the active protease form. *Arch Biochem Biophys*, 357 (1): 8-12. doi: 10.1006/abbi.1998.0787.
Parker, J. (2001). lac Operon. In Brenner, S. & Miller, J. H. (eds) *Encyclopedia of Genetics*, p. 1070. New York: Academic Press.
Perkins, D. N., Pappin, D. J., Creasy, D. M. & Cottrell, J. S. (1999). Probability-based protein identification by searching sequence databases using mass spectrometry data. *Electrophoresis*, 20 (18): 3551-3567. doi: 10.1002/(sici)1522-2683(19991201)20:18<3551::aid-elps3551>3.0.co;2-2.
Pesci, E. C., Pearson, J. P., Seed, P. C. & Iglewski, B. H. (1997). Regulation of las and rhl quorum sensing in Pseudomonas aeruginosa. *Journal of Bacteriology*, 179 (10): 3127-3132. doi: 10.1128/jb.179.10.3127-3132.1997.
Porath, J., Carlsson, J. A. N., Olsson, I. & Belfrage, G. (1975). Metal chelate affinity chromatography, a new approach to protein fractionation. *Nature*, 258 (5536): 598-599. doi: 10.1038/258598a0.

Porath, J. (1992). Immobilized metal ion affinity chromatography. *Protein Expression and Purification*, 3 (4): 263-281. doi: https://doi.org/10.1016/1046-5928(92)90001-D.
Price-Whelan, A., Dietrich, L. E. P. & Newman, D. K. (2007). Pyocyanin Alters Redox Homeostasis and Carbon Flux through Central Metabolic Pathways in Pseudomonas aeruginosa PA14. *Journal of Bacteriology*, 189 (17): 6372-6381. doi: 10.1128/jb.00505-07.
Quinlan, R. J., Sweeney, M. D., Lo Leggio, L., Otten, H., Poulsen, J.-C. N., Johansen, K. S., Krogh, K. B. R. M., Jørgensen, C. I., Tovborg, M., Anthonsen, A., et al. (2011). Insights into the oxidative degradation of cellulose by a copper metalloenzyme that exploits biomass components. *Proceedings of the National Academy of Sciences*, 108 (37): 15079-15084. doi: 10.1073/pnas.1105776108.
Ravichandran, A., Sugiyama, N., Tomita, M., Swarup, S. & Ishihama, Y. (2009). Ser/Thr/Tyr phosphoproteome analysis of pathogenic and non-pathogenic Pseudomonas species. *Proteomics*, 9 (10): 2764-75. doi: 10.1002/pmic.200800655.
Reese, E. T., Siu, R. G. H. & Levinson, H. S. (1950). The biological degradation of soluble cellulose derivatives and its relationship to the mechanism of cellulose hydrolysis. *Journal of bacteriology*, 59 (4): 485-497.
Rinaudo, M. (2006). Chitin and chitosan: Properties and applications. *Progress in Polymer Science*, 31 (7): 603-632. doi: https://doi.org/10.1016/j.progpolymsci.2006.06.001.
Rosano, G. L. & Ceccarelli, E. A. (2014). Recombinant protein expression in Escherichia coli: advances and challenges. *Frontiers in microbiology*, 5: 172.
Sabbadin, F., Hemsworth, G. R., Ciano, L., Henrissat, B., Dupree, P., Tryfona, T., Marques, R. D. S., Sweeney, S. T., Besser, K., Elias, L., et al. (2018). An ancient family of lytic polysaccharide monooxygenases with roles in arthropod development and biomass digestion. *Nature communications*, 9 (1): 756-756. doi: 10.1038/s41467-018-03142-x.
Sauer, K., Camper, A. K., Ehrlich, G. D., Costerton, J. W. & Davies, D. G. (2002). Pseudomonas aeruginosa displays multiple phenotypes during development as a biofilm. *J Bacteriol*, 184 (4): 1140-54. doi: 10.1128/jb.184.4.1140-1154.2002.
Schleif, R. (2010). AraC protein, regulation of the l-arabinose operon in Escherichia coli, and the light switch mechanism of AraC action. *FEMS Microbiol Rev*, 34 (5): 779-96. doi: 10.1111/j.1574-6976.2010.00226.x.
Shepard, C. C. & Tiselius, A. (1949). The chromatography of proteins. The effect of salt concentration and pH on the adsorption of proteins to silica gel. *Discussions of the Faraday Society*, 7 (0): 275-285. doi: 10.1039/DF9490700275.
Shoseyov, O., Shani, Z. & Levy, I. (2006). Carbohydrate binding modules: biochemical properties and novel applications. *Microbiology and molecular biology reviews : MMBR*, 70 (2): 283-295. doi: 10.1128/MMBR.00028-05.
Simonian, M. H. (2002). Spectrophotometric Determination of Protein Concentration. *Current Protocols in Food Analytical Chemistry*, 4 (1): B1.3.1-B1.3.7. doi: 10.1002/0471142913.fab0103s04.
Soufi, B., Krug, K., Harst, A. & Macek, B. (2015). Characterization of the E. coli proteome and its modifications during growth and ethanol stress. *Frontiers in microbiology*, 6: 103.
Spiegeleer, P., Sermon, J., Lietaert, A., Aertsen, A. & Michiels, C. (2004). Source of tryptone in growth medium affects oxidative stress resistance in Escherichia coli. *Journal of applied microbiology*, 97: 124-33. doi: 10.1111/j.1365-2672.2004.02285.x.
Stanley, M. M. (1947). Bacillus pyocyaneus infections: A review, report of cases and discussion of newer therapy including streptomycin (concluded). *The American Journal of Medicine*, 2 (4): 347-367. doi: https://doi.org/10.1016/0002-9343(47)90034-X.
Steen, H. & Mann, M. (2004). The abc's (and xyz's) of peptide sequencing. *Nature Reviews Molecular Cell Biology*, 5 (9): 699-711. doi: 10.1038/nrm1468.
Stover, C., Pham, X., Erwin, A., Mizoguchi, S., Warrener, P., Hickey, M., Brinkman, F., Hufnagle, W., Kowalik, D. & Lagrou, M. (2000). Complete genome sequence of Pseudomonas aeruginosa PAO1, an opportunistic pathogen. *Nature*, 406 (6799): 959.

Tanaka, K., Waki, H., Ido, Y., Akita, S., Yoshida, Y., Yoshida, T. & Matsuo, T. (1988). Protein and polymer analyses up to m/z 100 000 by laser ionization time-of-flight mass spectrometry. *Rapid Communications in Mass Spectrometry*, 2 (8): 151-153. doi: 10.1002/rcm.1290020802.

Turner, B. M. (2000). Histone acetylation and an epigenetic code. *Bioessays*, 22 (9): 836-845.

Vaaje-Kolstad, G., Horn, S. J., van Aalten, D. M., Synstad, B. & Eijsink, V. G. (2005a). The non-catalytic chitin-binding protein CBP21 from Serratia marcescens is essential for chitin degradation. *J Biol Chem*, 280 (31): 28492-7. doi: 10.1074/jbc.M504468200.

Vaaje-Kolstad, G., Houston, D. R., Riemen, A. H., Eijsink, V. G. & van Aalten, D. M. (2005b). Crystal structure and binding properties of the Serratia marcescens chitin-binding protein CBP21. *J Biol Chem*, 280 (12): 11313-9. doi: 10.1074/jbc.M407175200.

Vaaje-Kolstad, G., Westereng, B., Horn, S. J., Liu, Z., Zhai, H., Sørlie, M. & Eijsink, V. G. H. (2010). An Oxidative Enzyme Boosting the Enzymatic Conversion of Recalcitrant Polysaccharides. *Science*, 330 (6001): 219-222. doi: 10.1126/science.1192231.

Vaaje-Kolstad, G., Forsberg, Z., Loose, J. S. M., Bissaro, B. & Eijsink, V. G. H. (2017). Structural diversity of lytic polysaccharide monooxygenases. *Current Opinion in Structural Biology*, 44: 67-76. doi: https://doi.org/10.1016/j.sbi.2016.12.012.

Vebø, H. C., Snipen, L., Nes, I. F. & Brede, D. A. (2009). The transcriptome of the nosocomial pathogen Enterococcus faecalis V583 reveals adaptive responses to growth in blood. *PloS one*, 4 (11).

Villaverde, A. & Carrió, M. M. (2003). Protein aggregation in recombinant bacteria: biological role of inclusion bodies. *Biotechnol Lett*, 25 (17): 1385-95. doi: 10.1023/a:1025024104862.

Villavicencio, R. T. (1998). The history of blue pus. *Journal of the American College of Surgeons*, 187 (2): 212-216. doi: 10.1016/S1072-7515(98)00137-9.

Vorm, O., Roepstorff, P. & Mann, M. (1994). Improved Resolution and Very High Sensitivity in MALDI TOF of Matrix Surfaces Made by Fast Evaporation. *Analytical Chemistry*, 66 (19): 3281-3287. doi: 10.1021/ac00091a044.

Weiner-Lastinger, L. M., Abner, S., Edwards, J. R., Kallen, A. J., Karlsson, M., Magill, S. S., Pollock, D., See, I., Soe, M. M., Walters, M. S., et al. (2020). Antimicrobial-resistant pathogens associated with adult healthcare-associated infections: Summary of data reported to the National Healthcare Safety Network, 2015–2017. *Infection Control & Hospital Epidemiology*, 41 (1): 1-18. doi: 10.1017/ice.2019.296.

WHO. (2017). *WHO publishes list of bacteria for which new antibiotics are urgently needed*. WHO newsletter: WHO. Available at: https://www.who.int/news-room/detail/27-02-2017-who-publishes-list-of-bacteria-for-which-new-antibiotics-are-urgently-needed (accessed: 24.10.2019).

Williams, P. A. & Worsey, M. J. (1976). Ubiquity of plasmids in coding for toluene and xylene metabolism in soil bacteria: evidence for the existence of new TOL plasmids. *Journal of bacteriology*, 125 (3): 818-828.

Wong, E., Vaaje-Kolstad, G., Ghosh, A., Hurtado-Guerrero, R., Konarev, P. V., Ibrahim, A. F., Svergun, D. I., Eijsink, V. G., Chatterjee, N. S. & van Aalten, D. M. (2012). The Vibrio cholerae colonization factor GbpA possesses a modular structure that governs binding to different host surfaces. *PLoS Pathog*, 8 (1): e1002373. doi: 10.1371/journal.ppat.1002373.

Wu, M., Beckham, G. T., Larsson, A. M., Ishida, T., Kim, S., Payne, C. M., Himmel, M. E., Crowley, M. F., Horn, S. J., Westereng, B., et al. (2013). Crystal structure and computational characterization of the lytic polysaccharide monooxygenase GH61D from the Basidiomycota fungus Phanerochaete chrysosporium. *J Biol Chem*, 288 (18): 12828-39. doi: 10.1074/jbc.M113.459396.

Yamagata, A., Kristensen, D. B., Takeda, Y., Miyamoto, Y., Okada, K., Inamatsu, M. & Yoshizato, K. (2002). Mapping of phosphorylated proteins on two-dimensional polyacrylamide gels using protein phosphatase. *Proteomics*, 2 (9): 1267-1276. doi: 10.1002/1615-9861(200209)2:9<1267::aid-prot1267>3.0.co;2-r.

Zhang, J., Xin, L., Shan, B., Chen, W., Xie, M., Yuen, D., Zhang, W., Zhang, Z., Lajoie, G. A. & Ma, B. (2012). PEAKS DB: de novo sequencing assisted database search for sensitive and accurate peptide identification. *Molecular & cellular proteomics : MCP*, 11 (4): M111.010587-M111.010587. doi: 10.1074/mcp.M111.010587.

Zhou, H., Watts, J. D. & Aebersold, R. (2001). A systematic approach to the analysis of protein phosphorylation. *Nature Biotechnology*, 19 (4): 375-378. doi: 10.1038/86777.
Zhu, K., Zhao, J., Lubman, D. M., Miller, F. R. & Barder, T. J. (2005). Protein pI Shifts due to Posttranslational Modifications in the Separation and Characterization of Proteins. *Analytical Chemistry*, 77 (9): 2745-2755. doi: 10.1021/ac048494w.

8 Appendices

8.1 Appendix A

Representative chromatograms for protein purification steps.

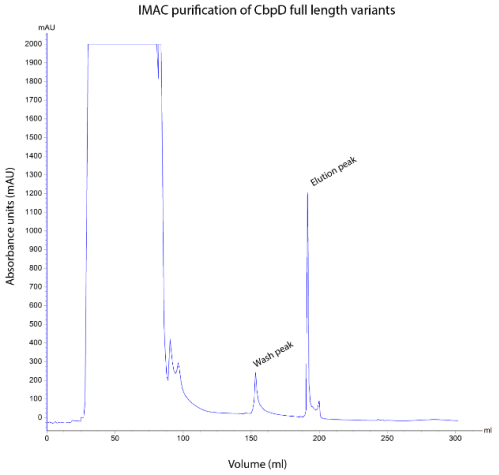

S 1: Chromatogram from IMAC purification, representative of all IMAC purifications. During IMAC purification fractionation was manually performed, and therefore not marked on the graph. The X axis is the volume of buffer. The Y-axis represents milli absorbance units (mAU). The blue line represents the UV signal. The peaks are named depending on which buffer was used.

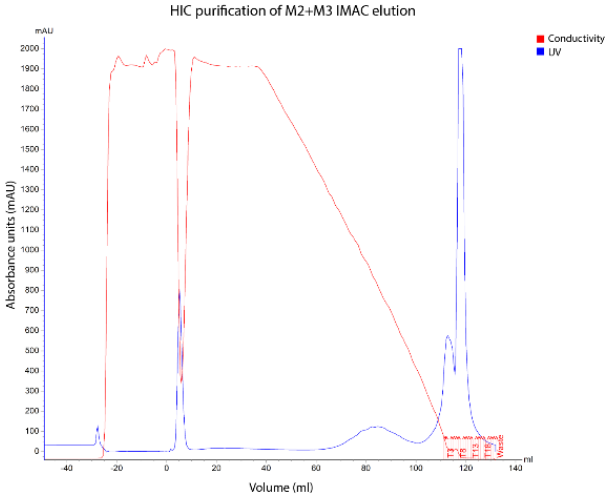

S 2: Chromatogram of HIC purification of the IMAC elution during rCbpD$_{EC}$ M2+M3 purification. The X-axis represents the volume of buffer. While the Y-axis represents milli absorbance units (mAU). The blue line represents the UV signal while the red line is the conductivity measuring salt concentration.

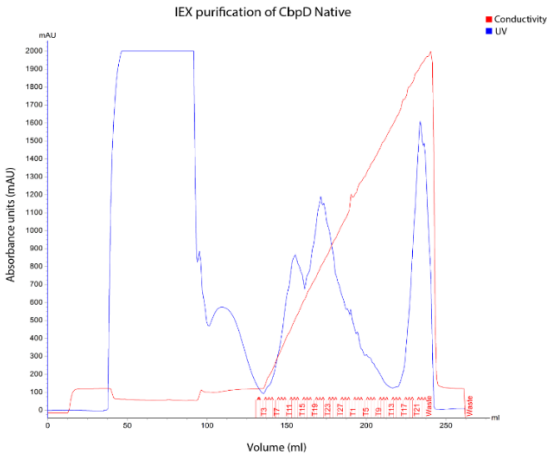

S 3:Chromatogram representing IEX purification of rCbpD$_{PA}$ Native. The X-axis represents the volume of buffer while the Y-axis represents milli absorbance units (mAU). The blue line represents the UV detection while the red line is the conductivity measuring salt concentration. Fractions are marked in red on the x-axis.

8.2 Appendix B

CbpD sequence with signal peptide

MKHYSATLALLPLTLALFLPQAAHAHGSMETPPSRVYGCFLEGPENPKSAACKAAVA
AGGTQALYDWNGVNQGNANGNHQAVVPDGQLCGAGKALFKGLNLARSDWPSTAI
APDASGNFQFVYKASAPHATRYFDFYITKDGYNPEKPLAWSDLEPAPFCSITSVKLEN
GTYRMNCPLPQGKTGKHVIYNVWQRSDSPEAFYACIDVSFSGAVANPWQALGNLRA
QQDLPAGATVTLRLFDAQGRDAQRHSLTLAQGANGAKQWPLALAQKVNQDSTLVN
IGVLDAYGAVSPVASSQDNQVYVRQAGYRFQVDIELPVEGGGEQPGGDGKVDFDYP
QGLQQYDAGTVVRGADGKRYQCKPYPNSGWCKGWDLYYAPGKGMAWQDAWTLL

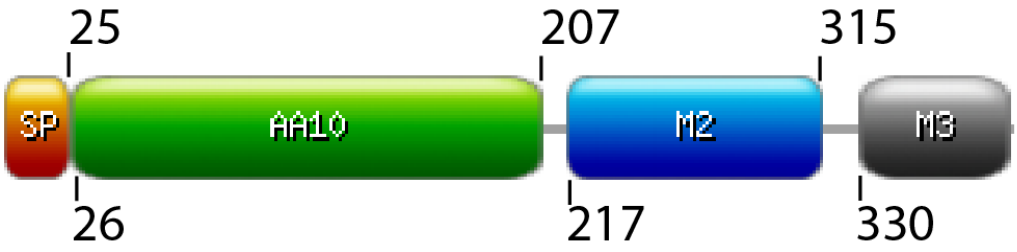

S 4:Illustration of how the CbpD domain structure is predicted. 1-25 is the signal peptide which is cleaved during translocation from the cytoplasm to the periplasm. The AA10 LPMO domain from 26-207 is based on Pfam sequence and M2 domain 217-315 is similarly based on the homology to GbpA. The M3 domain is more uncertain, however the CAZY database annotates the CBM73 domain to M3 330-389.

8.3 Appendix C

PTM identification values of **Figure 4-15**

Table 21: Ascore and -10logP score for the identified PTMs and their position. The modification is stated after the residue and position is annotated as p-phosphorylation, m-methylation, a-acetylation. For Panel A: E. coli and Panel B P. aeruginosa in ***Figure 4-15***

	Panel A *E. coli*		**Panel B *P. aeruginosa***	
	AScore	**-10logP**	**AScore**	**-10logP**
T14p			26.65	36.71
S28p	28.35	45.09	28.35	51.66
R35m	1000.00	59.53		
S49p	100.29	50.69	177.39	66.78
K53m	61.25	58.73	77.52	58.25
K147m	106.58	52.00	131.93	52.86
K166m			93.59	34.94
R173m	46.56	60.47	60.15	71.11
K182m	29.32	44.69	38.15	45.59
K185m	22.45	47.23		
K271m	1000.00	42.04		
K354a			1000.00	36.13
K359a			1000.00	36.13
K368a			1000.00	36.13

PTM identification values of **Figure 4-19**

Table 22 Ascore and -10logP values for the concatenated sequence coverage of excised IEF gel bands. The modification is stated after the residue name and position annotated as p-phosphorylation, m-methylation, a-acetylation and d-demethylation. ***Figure 4-19****.*

	Concatenated sequence coverage of IEF gel bands	
Residue	Best AScore	Best -10logP
Y37p	1000	46.8
K48a	25.58	49.49
K48d	1000	51.85
K97a	1000	36.85
S152p	29.77	64.73
K166d	1000	89.06
K185a	1000	46.22
R238m	1000	57
K262m	83.66	95.38
Y356p	34.23	29.24

8.4 Appendix D

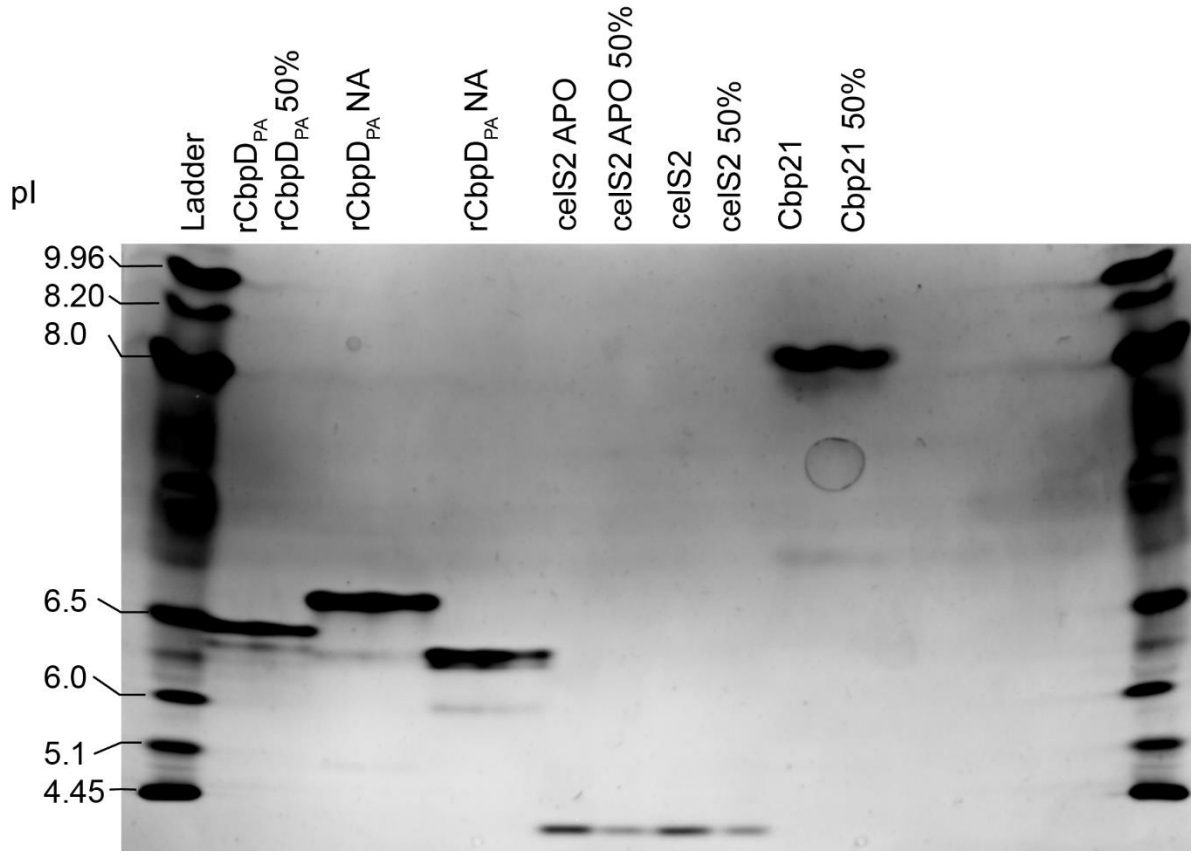

Figure 8-1 Iso-electric focusing gel performed on CbpD, celS2 and Cbp21. This image shows the iso-electric focusing gel performed on three LPMO proteins. The ladder is the IEF Standards pI 4.45-9.96 (Bio-Rad). rCbpD$_{PA}$ presents several but faint bands during separation. Mutants outside the scope of this study are marked as rCbpD$_{PA}$ NA. celS2 an LPMO from *Streptomyces viridosporus* was applied as both APO form and with copper. Cbp21 an LPMO from *Serratia marcescens.*

8.5 Appendix E

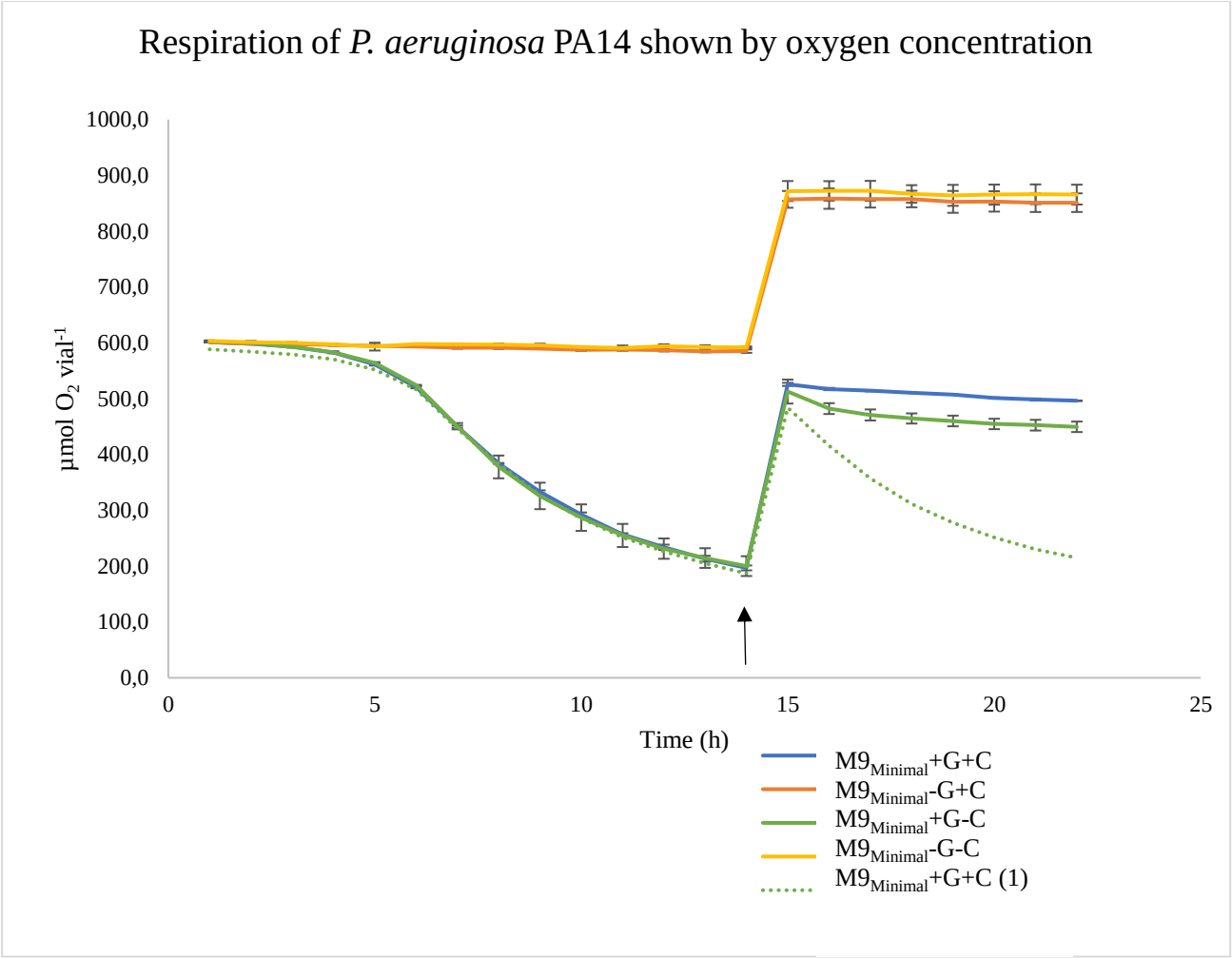

Figure 8-2 ***Investigating the utilization of chitin by monitoring gas metabolism in optimized minimal media.*** *This graph presents the oxygen production of PA14 cultivated in* $M9_{Minimal}$ *supplemented with either chitin (C), glucose (G), both or none. Supplemented medium components are indicated as present (+) or absent (-). The oxygen consumption is monitored by measuring* O_2 *production with gas chromatography coupled with an automatic gas sampling robot. The growth curves are the average of triplicates and the error bars indicate the standard deviation for the triplicates. The x-axis presents the time in hours (h) while the y-axis presents the* CO_2 *measurements in µmol per vial (µmol* O_2 *Vial* $^{-1}$*). Oxygen was added at the 13 hour mark (arrow), voiding the 14 hour results.*

The oxygen consumption rates seen in Figure 8-2 show that $M9_{Minimal}$ and $M9_{Minimal}$ supplemented with chitin does not consume oxygen. However, $M9_{Minimal}$ supplemented with glucose and chitin and glucose alone consume oxygen. The rate of consumption is similar for both, and the rate slows indication that the oxygen diffusion slows down. This phenotype can indicate biofilm formation which has poor diffusion. However, the oxygen rate can also be an artefact introduced by poor vapor diffusion.

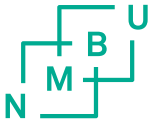

Norges miljø- og biovitenskapelige universitet
Noregs miljø- og biovitskapelege universitet
Norwegian University of Life Sciences

Postboks 5003
NO-1432 Ås
Norway